Exploring a unique vision for heavy ion fusion:

B. Grant Logan, August 6, 2007 Fifth Edition:study of ion two-sided polar direct drive of T-lean targets.

A quest for more efficient beam-to-fuel energy coupling via polar direct drive (30 % overall), to enable:

--> Self-T-breeding, self-neutron-energy-absorbing, large ρr, T-Lean targets @ < 4 MJ driver energies
--> Efficient fusion energy coupling into plasma for direct MHD conversion with moderate yields < 1 GJ
--> Balance-of-plant costs 10X lower than steam cycle (e.g., < 80 $ /kWe instead of 800 $/kWe)
--> CoE low enough (<3 cts/kWehr) for affordable water and H_2 fuel for 10 B people on a hot planet.
--> Enough fissile fuel production for 38 LWR's per GW_{fusion} if uranium gets too expensive meantime.

TABLE OF CONTENTS

Introduction- what we are seeking and why

In 1996 and 1997 two studies of tritium-lean targets [1], [2] showed that large fuel assemblies ($\rho r_f \sim 10$ g/cm^2) with about 1% molar tritium fraction concentrated in a small DT spark plug surrounded by deuterium could achieve fuel energy gains of 500 and 1000 with isobaric [1] and isochoric (fast ignited) [2] hot-spot ignition, respectively, in both cases with sufficient net T breeding by D(d, n)T side reactions to avoid the need for any external T-breeding blankets. Those studies also noted the possibility of such targets providing more extra neutrons that could be used for additional breeding in external blankets, such as for fissile fuel production, and noted larger fractions of fusion yield in charged particles for direct conversion, compared to all-DT targets. A major drawback was the large fuel masses > 20 mg and fuel energies E_f required at stagnation ~ 1 MJ @ adiabat $\alpha = 2$ and 1.5, respectively, which implied very large required driver energies (>10 MJ for = laser direct drive efficiency (beam-to-fuel) $\eta_{df} < 0.1$, and >17 MJ for indirect drive with $\eta_{df} < 0.06$ (0.3 hohlraum coupling x 0.2 x-ray capsule implosion efficiency). Here we seek $\eta_{df} > 0.25$ with ion direct drive.

This MathCAD document presents a numerical implosion model for T-Lean targets driven in the ablative direct drive regime using the same heavy-ion dE/dx deposition model as used in the LLNL HYDRA code. This model explores characteristic beam requirements for such targets, as a guide to motivate hydro code calculations for 2-D polar drive. Thick hydrogen ablators (e.g., 92 mg initial mass) are divided into 30 Lagrangian mass layers, and the model specifies ion ablation of those layers at a rate to achieve a specified drive pulse shape at the peak of rocket efficiency (80% mass ablation fraction by the time the ablation front radius = 50 % of initial ablator radius). Ion beams stop efficiently in hydrogen ablators (most electrons per unit mass) which also have lowest specific ionization energy $<< u^2_{ex}/2$. High ablation velocities in these thick ablator rocket regimes lead to improved stability as well as lower exhaust velocities $u_{ex} = 2\, c_s < 1.9\, 10^7$ cm/s that imply low stagnation $T_e < 30$ eV and low radiation losses. However, ion beams can suffer greater parasitic energy loss passing through ablation corona plasmas compared to laser or x-ray drive photons, despite the dE/dx Bragg peak near the end of the ion range.

An initial ion beam range 0.004 g/cm2 is selected to be 20 % of the initial hydrogen ablator $\rho r_{ho} = 0.02$ g/cm2. If the ion energy were constant, the ions would stop short of the ablation front early into the drive pulse due to rising ablation plasma column density which the model tracks during the drive pulse. Working backwards, the model calculates the higher incident ion beam energy and losses at each time step for ions required to penetrate the rising ablation plasma column density and then stop in the remaining hydrogen ablator shell. An example for a 1 MJ T-lean final fuel assembly finds required incident Argon ion beam energy rising from ~250 to 750 MeV during the pulse (which is actually synergistic with neutralized beam compression and focusing with high compression velocity chirp and time dependent focusing). A total incident ion beam energy of 4 MJ is required (25 % overall drive efficiency assuming zooming), despite 40% loss of ion energy in the ablation corona. Ways to further mitigate the ion beam loss on ablation plasma are discussed for future two-sided (polar) direct drive. Examples for both a small 1 MJ drive DEMO as well as for a 4 MJ drive power plant with 50%-efficient plasma-shell MHD direct conversion [3] are summarized in the table just below and compared with earlier indirect drive heavy ion target designs for DT targets. A summary at the end of this document gives more details for the two selected T-lean IFE examples.

[1] TABAK, M. Nuclear Fusion 36, No 2 (1996)
[2] ATZENI, S., and CIAMPI, C., Nuclear Fusion 37, 1665 (1997)
[3] LOGAN, B. G., Fusion Engineering and Design 22, 151 (1993)
[4] ATZEHI, S. and MEYER-TER-VEHN, J., "The Physics of Inertial Fusion" Clarendon press-Oxford, 2004

T-lean fuel assemblies for MHD direct conversion **Develop and benchmark MCAD model based on Tabak's Case C run[1] for isobaric hot spot ignition (see Fig. 1) with his f = 0.1 tritium parameter (to maximize non-neutron yield for direct conversion with ηG_f>100 for low recirculating power)**

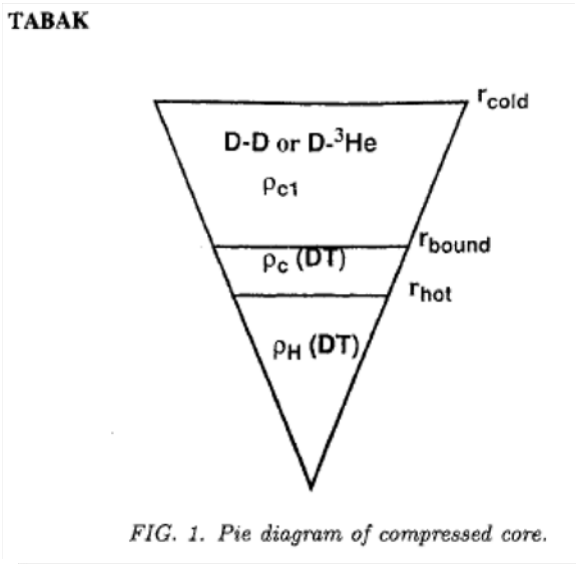

FIG. 1. Pie diagram of compressed core.

Ref [1] Calculates DD burn assuming 10 keV initial DT hot spot. (If needed, a late shock (Betti- Perkins) could be applied to insure ignition at lower implosion velocities and at lower adiabats, say α=1.5 instead of at α=2 as Max assumed). We assume DD main fuel instead of D-^{3}He for reasons Max stated.

Ref [1] calculates burn starting with stagnation with a range fuel energies, both below and above 1 MJ. The compressed core shown in Fig. 1 is representing the fuel assembly at stagnation after whatever ablator has burned off. Lets compare a few examples we will be developing for direct drive with previous heavy ion indirect drive targets, to motivate seeking higher beam-to-fuel coupling efficiencies to enable such T-lean targets.

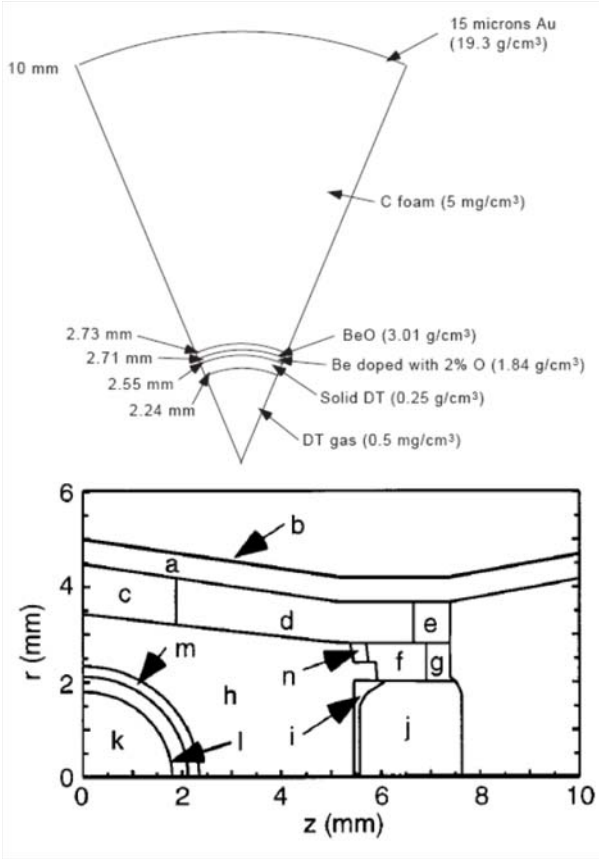

The spherical illumination indirect drive lithium hohlraum target designed by Allshouse and Callahan (Nuclear Fusion, Vol. 39, No.7 (1999). The large case-to-capsule ratio was necessary to provide adequate implosion symmetry by both thermal and geometrical smoothing of x-rays from beam deposition non-uniformities. 16 MJ of total lithium ion drive, with a 100 TW, 40ns foot pulse provided by 32 beams @ 17 to 22 MeV, followed by a 600 TW, 15 ns main pulse provided by 12 beams. (other parameters are in the table below)

A diagram of 1/4 of the capsule and hohlraum for the close-coupled target by Callahan & Tabak (Physics of Plasmas, Vol. 6, No 4, May 2000). This design had a smaller hohlraum for the same capsule size as a previous distributed radiator target (DRT) used for the Robust Point Design. (Callahan and Tabak, Physics of Plasmas, 5, 1895 (1998). See table below. The materials and densities used were as follows: (a) AuGd at 0.1 g/cc, (b) 15 microns layer of AuGd at 13.5 g/cc, (c) Fe at 16 mg/cc, (d)(CD2)0.97Au0.03 at 11 mg/cc, (e) AuGd at 0.11 g/cc, (f) Al at 70 mg/cc, (g) AuGd at 0.26 g/cc, (h) CD2 at 1 mg/cc, (i) Al at 55 mg/cc, (j) AuGd sandwich with densities 0.1 g/cc, 1.0 g/cc, and 0.5 g/cc, (k) DT at 0.3 mg/cc, (l) DT at 0.25 g/cc, (m) Be0.995Br0.005 at 1.845 g/cc, (n) (CD2)0.97Au0.03 at32mg/cc.

Fig. 2. Previous heavy ion indirect-drive target designs (published).

	E_d MJ	T_{rad} (eV)	E_{cap} (kJ)	R_{ho} (mm)	A_{wall} (cm^2)	R_{cap} (mm)	E_{fuel} (kJ)	Yield (MJ)	Target gain	M_{conv} (mg)	η_{df} (%)	$I_{b\text{-}peak}$ W/cm^2
SNL Li hohlraum	16	220	1400	10	12.6	2.7	280	591	37	250	1.8	4.8e13
DRT-Robust point design	6.7	245	1000	5.4	5.0	2.3	200	436	66	80	3.0	3.3e14
DRT Close - coupled	3.3	245	1000	4.0	2.7	2.3	200	436	133	24	6.0	6.2e14
2.5 MJ HI Cannonball	2.5	300	800	3.0	1.1	1.8	160	300	120	40	6.4	6e14
1.5 MJ HI Cannonball	1.5	---	530	2.4	0.72	1.4	100	150	100	25	6.7	8e14
NIF (laser)	1.8	300	175	2.5	1.4	1	35	20	11	na	1.9	1e15leh
HI-dd-direct drive (1.2 GWe)	4	na	2550 ablator	na	na	7.1	1000	494 (Tlean)	123	na	25	2.1e14
HI-dd-direct drive DEMO	0.8	na	490 ablator	na	na	3.7	200	43 (Tlean)	52	na	24	3.1e14

Table 1: The two entries referred to as "Cannonballs" are rough constructs of close-coupled spherical hohlraums using scalings from Lindl's book, not necessarily representing any previous designs. Symmetry is addressed in the three published indirect drive designs above, but symmetry in the close-coupled cannonball examples may be a challenge due to small case-to-capsule ratios. All close-coupled hohlraum examples, cylindrical or spherical, can get beam-to-fuel coupling efficiencies η_{df} ~6 to 7% with DT gains > 100 and higher peak intensity beams incident on target > 600 TW/cm^2 (average of overlapping incident beams -10 x higher than for the SNL Li hohlraum design). The last two rows are numerical calculations for heavy ion ablative direct drive cases for T-lean targets with ~ 25 % coupling (this work). Note that with lower overall coupling efficiencies, indirect drive would require higher driver energies and associated peak beam intensities to create the same fuel energies for the two T-lean cases. *The important thing is that heavy ions with the right range can in principle achieve similar ablation velocities, stability, and rocket efficiency with thick ablators as do x-rays without having to incur the inefficiency of conversion to x-rays.* The analysis below finds that ion beams may suffer more parasitic losses on the ablation corona than x-rays, but that is compensated by using hydrogen ablators that have less ionization energy losses than x-ray ablators require for to be optically thick using atomic Z > 4 to 6 for the hohlraum x-ray temperatures. The incident ion beam smoothness and symmetry will be required as much as with laser direct drive, including in polar direct drive geometry, and we will be investigating techniques to achieve required smoothness and symmetry by twirling arrays of ion beams around the polar axis using upstream R.F. wobblers -those topics will be addressed in a subsequent MathCAD model extension.

.

Why plasma MHD conversion is synergistic with large ρr T-lean targets.

Before beginning the description of the MathCAD model for ion direct drive, lets digress briefly on why we seek forms of fusion energy production into 1 -2 eV plasmas for MHD conversion, and why the consideration now of *T-lean targets* offers a solution to enable efficient capture of fusion yield into that desired form at *reasonable fusion yields < 1 GJ*. Ref. [3] above found that direct MHD conversion could be most efficient (greater than 50%) for dense (10 to 100 bar) plasmas containing an alkali component such as lithium or potassium with optimal temperatures of 1 to 2 eV. Below that optimum temperature, the plasma conductivity decreases strongly with the ionization fraction, and above those temperatures, plasma radiation losses decrease the convertible plasma energy. Following the original idea proposed by Velikhov, the Compact Fusion Advanced Rankine cycle study [3] assumed a solid target shell of chosen working material around each target, where the shell had to be thick enough to stop 14 MeV DT neutrons, and where the fusion yield had to be sufficient (typically several 10's of GJ) to vaporize and ionize the shell mass (typically 100's of kg) into an average 1-2 eV plasma temperature for optimal MHD conversion. Those earlier studies neglected the neutron energy losses within the target ρr, (typically 10 to 20% for DT targets), and the resulting required large target shell masses (to capture most of the 14 MeV neutron energy) forced the requirement of very large fusion yields (10's of GJ) that discouraged further pursuit of the concept. Now, the possibility of creating T-lean fuel assemblies with large ρr~10 g/cm^2 > 2x-average neutron mean-free-paths, *and doing so with higher beam-to-fuel coupling efficiencies to keep the driver energies reasonable*, opens the possibility of *efficient capture of T-lean target fusion yields a hundred times smaller than in the previous CFAR study*, allowing correspondingly smaller fusion yields for efficient MHD conversion. Fig. 3 below provides basic information on plasma MHD conversion for those who may not be familiar with it.

Momentum :

$$\rho u \frac{du}{dx} + \nabla p = j \times B - \rho u^2 \frac{df}{dx}$$

Energy :

$$\rho u \frac{d}{dx}\left[\frac{u^2}{2} + h\right] = j \cdot E - qr$$

Continuity :

$$\rho u A = \text{constant}$$

Load Factor :

$$K = \frac{E}{uB}$$

Electric Power Density :

$$j \cdot E = -\frac{K(1-K)\,\sigma u^2 B^2}{1 + (\omega\tau^2)}$$

Magnet cost, Energy Density :

$$\text{Magnet Cost} / m^3 \sim B^2 / (2\mu_o)$$

where ρ = mass density , u = velocity, x = distance along channel, p = pressure, j = current density, B = magnetic field, E = electric field, σ = electrical conductivity, $\omega\tau$ = Hall parameter, h = specific enthalpy, f = friction due to mass inflow from wall transpiration cooling, qr = heat loss / m^3 due to radiation losses, A = channel area.

➔ MHD Magnet Cost / kWe ~ B^2 / j · E ➔ Figure-of-merit $ / kWe ~ (σu^2)$^{-1}$

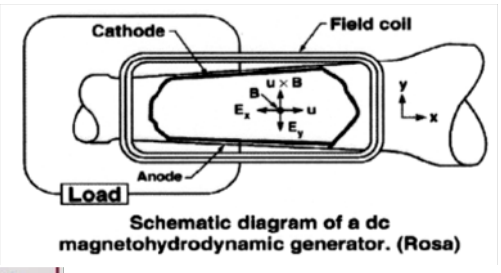

Schematic diagram of a dc magnetohydrodynamic generator. (Rosa)

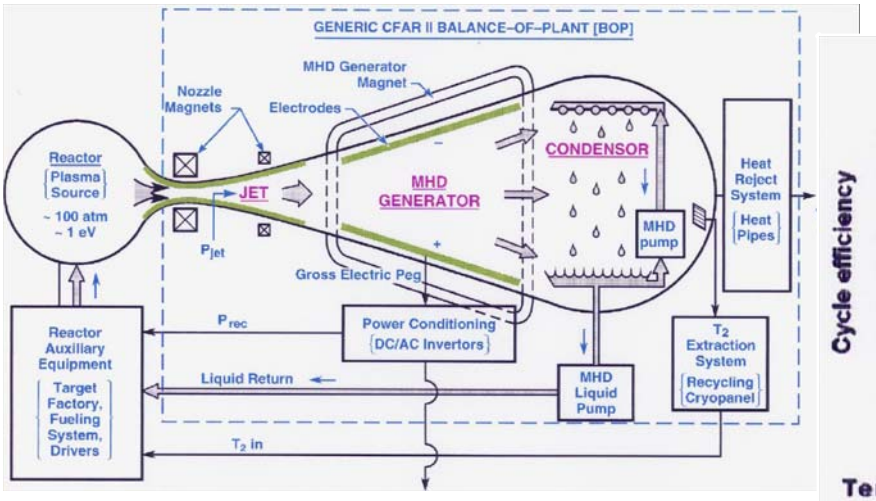

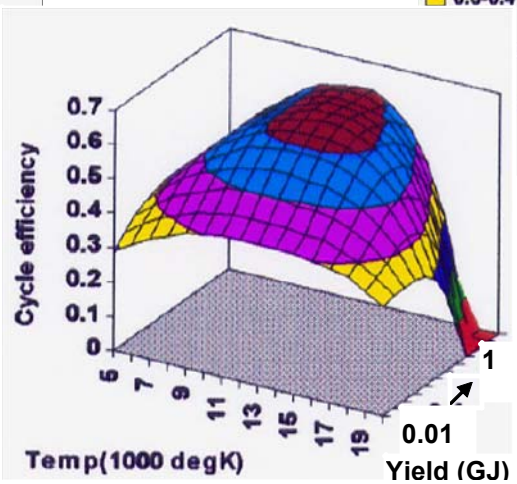

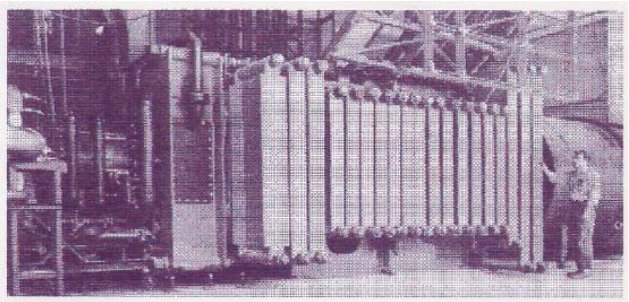

THE AVCO MARK V "ROCKET GENERATOR"
(from Rosa, MHD Energy Conversion, 1968)
Temp ~ 3000 deg K
Conductivity ~ 100 mhos/m
Velocity ~ 1000 m/s
Efficiency ~ 10% (of chemical)
Power (above unit) ~ 20 MWe

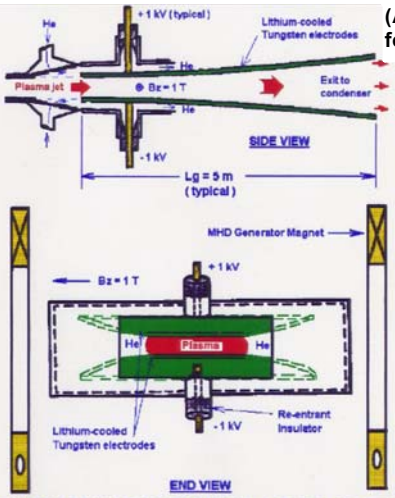

TYPICAL" CFARII MHD GENERATOR
Temp ~ 12000 deg K, Conductivity ~ 500 mho/m
Velocity ~ 10000 m/s, Efficiency ~ 80%(of kinetic)
Power (comparable size to MarkV) ~ 2000 MWe

Fig. 3: Direct fusion yield into working fluids in CFAR MHD [3] -->10 X more energy per kg than chemical combustion --> 10 x higher temperatures --> 100 X more power density ~ σu^2 than "old" MHD, and 30 X more kWe per ton power density than conventional steam balance-of-plant --> 10 X lower costs!

ORIGIN := 1

Model for heavy-ion direct-drive T-Lean targets

Fuel assembly energy (variable), for $i := 1..6$ fuel energy cases, $Ef_i := 0.2 + \sum_{n=1}^{i} [0.2\cdot(n-1) - 0.1]$ MJ

DT radius with minimum T loading $f := 0.1$ $r_{bound}(r_{hot}) := r_{hot}\cdot(1+2\cdot f)$

Nominal implosion adiabat $\alpha := 1.5$ $\zeta := 1-(1+2\cdot f)^{-3}$ DT load parameter

Use Max's formulary[1] for fuel assemblies that optimize gain for given fuel energies:

Cold DD fuel density in g/cm3) $\rho_{cdd}(\alpha, E_f) := 0.8\cdot 1050\cdot\left(\alpha^2\cdot E_f\right)^{-0.3}$ Eq 1

Hot spot fuel density (g/cm3) $\rho_{hdt}(E_f) := 63\cdot E_f^{-0.5}$ Eq 2

Hot spot radius (cm) $r_{hdt}(E_f) := 0.0063\cdot E_f^{0.5}$ Eq 3

Radius of pure DT region (Case C) $r_{bdt}(E_f) := (1+2\cdot f)\cdot r_{hdt}(E_f)$ Eq 4

Outer DD fuel radius (Tabak) (cm) $r_{cdd}(E_f) := \left[\left[\left(3\cdot r_{hdt}(E_f)\right)^3 - r_{bdt}(E_f)^3\right]\cdot 1.25 + r_{bdt}(E_f)^3\right]^{0.333}$ Eq 5

Mass of cold D fuel (g) $M_d(\alpha, E_f) := 4\cdot 3^{-1}\cdot\pi\cdot\left(r_{cdd}(E_f)^3 - r_{hdt}(E_f)^3\right)\cdot\rho_{cdd}(\alpha, E_f)$ Eq 6

Mass of DT hot spot (g) $M_{hdt}(E_f) := 4\cdot 3^{-1}\cdot\pi\cdot r_{hdt}(E_f)^3\cdot\rho_{hdt}(E_f)$ Eq 7

Total initial T fuel mass (g) (Case C) $M_t(\alpha, E_f) := 0.6\cdot\left(M_{hdt}(E_f) + \frac{\zeta}{0.8}\cdot\frac{4}{3}\cdot\pi\cdot r_{bdt}(E_f)^3\cdot\rho_{cdd}(\alpha, E_f)\right)$ Eq 8

Rho-r of total fuel assembly (g/cm^2) $\rho r(\alpha, E_f) := \rho_{hdt}(E_f)\cdot r_{hdt}(E_f) \ldots + 1.25\cdot\rho_{cdd}(\alpha, E_f)\cdot\left(r_{bdt}(E_f) - r_{hdt}(E_f)\right) \ldots + \rho_{cdd}(\alpha, E_f)\cdot\left(r_{cdd}(E_f) - r_{bdt}(E_f)\right)$ Eq 9

Burnup fractions (Fig.2) ~ $\rho r / (\rho r + H_B)$ depend on T which increases with ρr:

f	Main fuel composition	Column density (g/cm^2)	Peak hotspot temperature (keV)	Main fuel temperature (keV)
0.033	D	4.6	40	4
0.033	D	12	100	8
0.166	D	4.6	90	16
0.166	D	12	210	50
0.033	0.01 T/0.5 D	4.6	70	13
0.033	0.01 T/0.5 D	12	210	80
0.033	0.04 T/0.5 D	4.6	180	160
0.033	0.04 T/0.5 D	12	310	160

(Table 2 From Tabak [1]

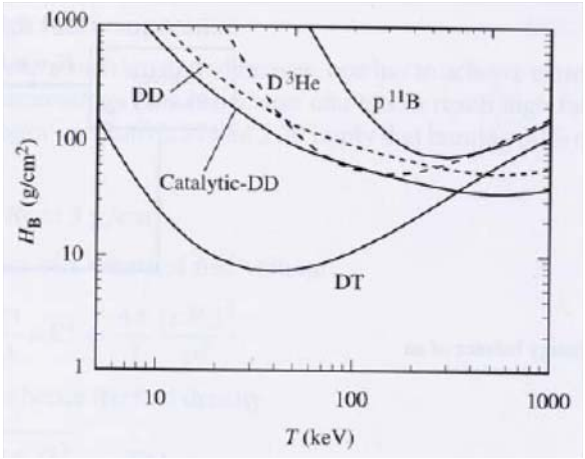

Figure 4: Burnup fractions vs T (from ref. [4])

Model for burnup fractions. Note in Table 1 as ρr increases from 4.6 to 12 g/cm2 (factor of 2.6), temperatures for DT hotspot and DD main fuel increase by a similar factors. Fig. 2 shows those temperature changes raise H_B for DT ~ 2 times, while decreasing H_B for DD by ~3 times. We use this to fit the coefficients for the model H_B terms in Eq. 10 and 11 below.

Est burnup fraction of DD (constant fitted to Tabak's Case C runs).

$$f_{bd}(\alpha, E_f) := \rho r(\alpha, E_f)\cdot\left(\rho r(\alpha, E_f) + 1600\cdot\rho r(\alpha, E_f)^{-1.2}\right)^{-1} \qquad \text{Eq 10}$$

Est burnup fraction of initial DT load

$$f_{bt}(\alpha, E_f) := \rho r(\alpha, E_f)\cdot\left(\rho r(\alpha, E_f) + 2\cdot\rho r(\alpha, E_f)^{0.8}\right)^{-1} \qquad \text{Eq 11}$$

D(d,p)T and D(d,n)3He branching @ 100 keV relative energy $f_p := 0.48 \quad f_n := 0.52$

Est. yield (MJ) = initial T burnup @ f_{bt}

+ D-D burnup yield @ f_{bd}
+ bred T burnup yield @ f_{bt}

+bred 3He burnup yield assuming $fb_{3He} \sim f_{bd}$.

$$Y_f(\alpha, E_f) := 5\cdot 3^{-1}\cdot M_t(\alpha, E_f)\cdot f_{bt}(\alpha, E_f)\cdot\left(3.37\cdot 10^5\right) \ldots + M_d(\alpha, E_f)\cdot f_{bd}(\alpha, E_f)\cdot\begin{pmatrix} 8.85\cdot 10^4 \ldots \\ + 1.25\cdot f_p\cdot f_{bt}(\alpha, E_f)\cdot 3.37\cdot 10^5 \ldots \\ + 1.25\cdot f_n\cdot f_{bd}(\alpha, E_f)\cdot 3.5\cdot 10^5 \end{pmatrix} \qquad \text{Eq 12}$$

Internal (fuel) energy gains

$$G_f(\alpha, E_f) := Y_f(\alpha, E_f)\cdot E_f^{-1} \qquad \text{Eq 13}$$

M.Tabak results[1] for fuel gain G_{mt} for his Case C: $n := 1 .. 7$

$Gmt_1 := 105 \quad Gmt_2 := 160 \quad Gmt_3 := 230 \quad Gmt_4 := 295 \quad Gmt_5 := 360 \quad Gmt_6 := 430 \quad Gmt_7 := 500$

$E_1 := 0.1 \quad E_2 := 0.25 \quad E_3 := 0.5 \quad E_4 := 0.85 \quad E_5 := 1.3 \quad E_6 := 1.85 \quad E_7 := 2.5$

Fig. 5: Comparing fuel gain G_f (model) and in Tabak's Case C vs. fuel energy E_f (At adiabat α=2)

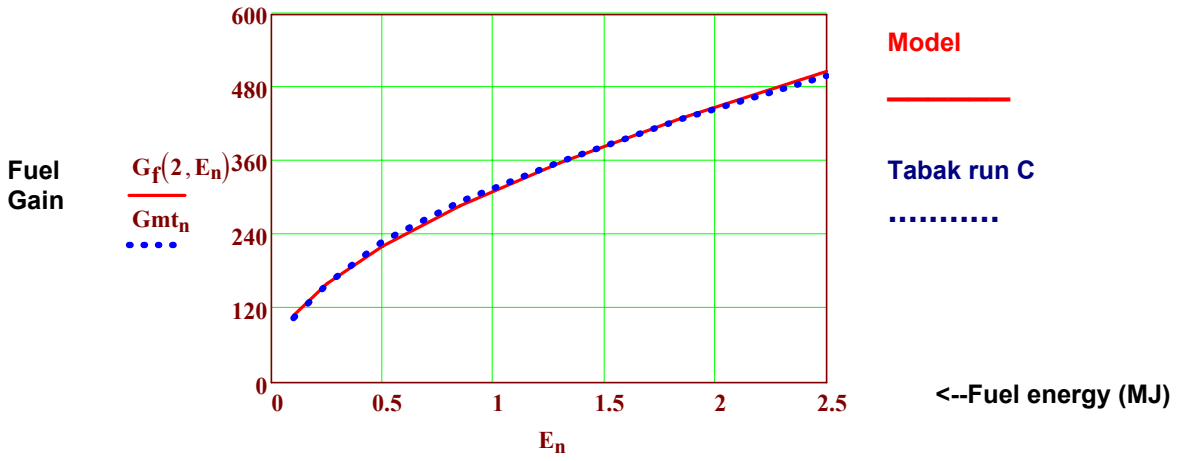

Fig. 5 shows the model and the Case C runs agree well. (Good enough for government work).

Next lets consider T-breeding:

Mass of T-bred in-situ by D+D-->T+p branch (g) $M_{tb}(\alpha, E_f) := 0.75 \cdot f_p \cdot M_d(\alpha, E_f) \cdot f_{bd}(\alpha, E_f)$ Eq 14

Mass of 3He-bred by D+D-->3He+n branch (g) $M_{3Heb}(\alpha, E_f) := 0.75 \cdot f_n \cdot M_d(\alpha, E_f) \cdot f_{bd}(\alpha, E_f)$ Eq 15

Total T consumed by fusion (g) $M_{tc}(\alpha, E_f) := (M_t(\alpha, E_f) + M_{tb}(\alpha, E_f)) \cdot f_{bt}(\alpha, E_f)$ Eq 16

Net T mass gain (loss) (g) $M_{tn}(\alpha, E_f) := M_{tb}(\alpha, E_f) - M_{tc}(\alpha, E_f)$ Eq 17

In-situ Neutrons per Triton burned $N_{ndd}(\alpha, E_f) := (M_{3Heb}(\alpha, E_f) + M_{tc}(\alpha, E_f)) \cdot M_{tc}(\alpha, E_f)^{-1}$ Eq 18

Note if all tritium were burned up, and the DD breeding of T dominated over the initial T load, the maximum N_{nt} max =2. However, about 50 percent of tritium is burned, so the maximum $N_{nt} < 3$, including some initial T load with the parameter f=0.1.

No. of neutrons available (inc. multiplication and minus any needed for T-replacement) per T burned:

For T-lean case $N_{ndda}(\alpha, E_f) := (M_{3Heb}(\alpha, E_f) + 1.4 \cdot M_{tc}(\alpha, E_f)) \cdot M_{tc}(\alpha, E_f)^{-1}$ Eq 19

For DT case $N_{ndta} := 1.4 - 1$ Eq 20

No. of neutrons available for uses other than T replacement, per MeV of fusion yield

For T-lean case $NY_{dd}(\alpha, E_f) := N_{ndda}(\alpha, E_f) \cdot \left(\frac{M_d(2, E_f) \cdot 4.6 + M_t(2, E_f) \cdot 17.6}{M_d(2, E_f) + M_t(2, E_f)} \right)^{-1}$ Eq 21

For DT case $NY_{dt}(\alpha, E_f) := N_{ndta} \cdot 17.6^{-1}$ Eq 22

Ratio of neutrons available T-lean case over DT case, per MeV yield

$NpYR(\alpha, E_f) := NY_{dd}(\alpha, E_f) \cdot NY_{dt}(\alpha, E_f)^{-1}$ Eq 23

Table 3: Model predictions for net tritium production versus fuel energy. (Adiabat α = 1.5)

i =	Fuel energy Ef_i =	Initial T mass $\frac{M_t(1.5, Ef_i)}{10^{-3}}$ =	T-mass bred $\frac{M_{tb}(1.5, Ef_i)}{10^{-3}}$ =	T-mass consumed $\frac{M_{tc}(1.5, Ef_i)}{10^{-3}}$ =	Net T--Mass produced $\frac{M_{tn}(1.5, Ef_i)}{10^{-3}}$ =	Neutrons per T burned $N_{ndd}(1.5, Ef_i)$ =
1	0.1	0.03	0.02	0.02	-0.0011	2.02
2	0.2	0.06	0.06	0.05	0.005	2.19
3	0.5	0.18	0.24	0.18	0.054	2.4
4	1	0.42	0.71	0.5	0.2137	2.55
5	1.7	0.78	1.64	1.08	0.5626	2.65
6	2.6	1.29	3.21	2.03	1.1826	2.72
	(MJ)	(mg)	(mg)	(mg)	(mg)	

Note in Table 3 that net tritium self-breeding sufficiency occurs for fuel energies ~ > 0.2 MJ for these cases with 1.3 % molar fraction of tritium. Thus E_f = 0.2 MJ will be our reference DEMO case.

Table 4 compares the Tabak-based model @ adiabat α=1.5 with the closest Atzeni/Ciampi's T-lean example [2] for marginal net T-sufficiency at adiabat α=1.5, both cases near 1 % molar fraction of tritium, and for 1 MJ fuel assembly energy (which will be our reference case for a CFAR power plant. The Tabak-based model is based on isobaric DT hotspot ignition, while the Atzeni/Ciampi model is based on isochoric fast ignition. We assume the Tabak model would also be consistent with the new Betti-Perkins variant of hot spot ignition with a late shock but without needing a fast igniter pulse (easier for ion beam drive), in case implosions don't quite reach the 10 keV hot spot DT temperatures postulated in the beginning of Max's burn calculations.

Table 4	Atzeni/Ciampi example	Tabak-based MCAD Model
Molar T-fraction	1 %	1.3 %
Adiabat α	1.5	1.5
Fuel energy (MJ)	1	1
Fuel Mass (g)	0.020	$M_d(1.5,1) + M_t(1.5,1) = 0.023$
Fuel density (g/cm^3)	800	$\rho_{cdd}(1.5,1) = 659$
Fuel Rho-r (g/cm^2)	10.7	$\rho r(1.5,1) = 9.9$
Fuel gain G_f *and Fusion Yield* (in MJ)	1050	$G_f(1.5,1) = 494$

Note that despite the difference in the two ignition/burn models, these cases compare reasonably at similar dd fuel masses and fuel energies at comparable seed molar tritium fractions and both at marginal T self-breeding sufficiency. If anything, the Tabak-based model is pessimistic with respect to the Atzeni/Ciampi calculation. We should expect the higher fuel gain for the Atzeni/Ciampi isochoric ignition assumption compared to the isobaric ignition Tabak-based MCAD model. We prefer the latter approach anyway because its easier to drive with mm-spot radius ion beams. Fig. 6 compares neutrons per T burned and extra available neutrons (neutrons produced minus any needed for T breeding) per MeV of fusion yield for the T-lean assembles compared to conventional DT targets, where we assume a typical DT neutron multiplication of 1.4 for FLiBe blankets, but no multiplication for any dd neutrons.

Fig 6: Neutrons produced per T burned and the ratio of available neutrons per MeV yield vs fuel energy.

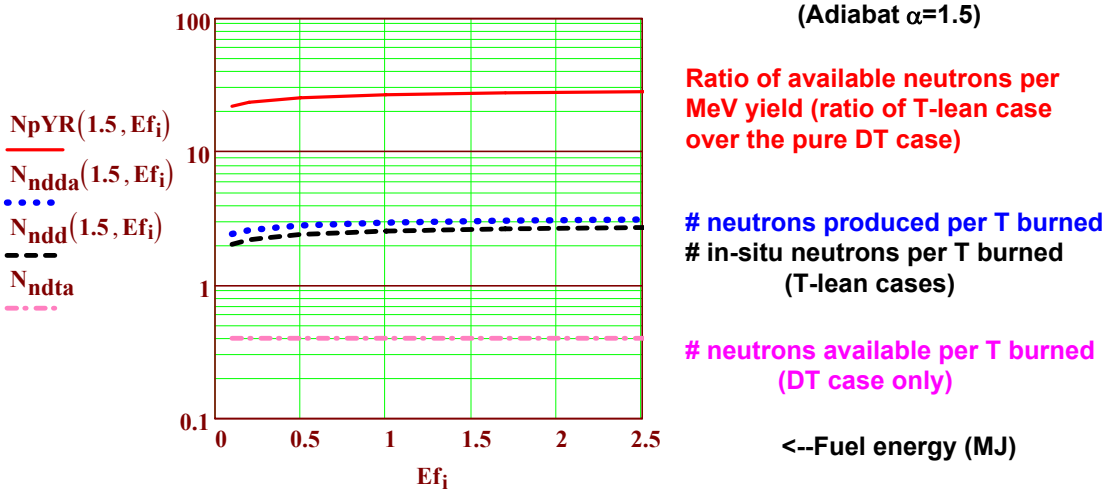

Figure 6 shows that T-lean targets can be 30 times more prolific neutron sources per fusion watt for purposes of various applications in blankets compared to DT targets, besides being tritium self-sufficient (sufficient in-situ breeding so that blanket material options are not restricted to contain lithium).

The copious extra neutrons available with T-lean targets, as pointed out by Tabak[1], can be used in external blankets of different materials, (in some cases without lithium) for several purposes:
(a) generate extra energy for direct conversion through exothermic neutron capture
(b) generate extra tritium for sale to other tritium-deficient reactors like ITER
(c) breed fissile fuel sufficient to support many client fission reactors

Direct MHD conversion. Next, lets look at the potential to use these T-lean cases for low-cost Balance-of-Plant with direct plasma MHD conversion, based on the Compact Fusion Advanced Rankine (CFAR) cycle[2] , in which a small vaporizable/ionizable/recylable shell material is inserted around and simultaneously with each target (See Fig. 8 below).

Scaling of capture fractions of T-lean target outputs into shells for plasmas

Fraction of yield born in neutrons (neglecting inelastic neutron scattering) (un-attenuated neutrons)

$$FY_{no}(\alpha, E_f) := \frac{\begin{aligned} &14.1\cdot 17.6^{-1}\cdot 5\cdot 3^{-1}\cdot M_t(\alpha, E_f)\cdot f_{bt}(\alpha, E_f)\cdot\left(3.37\cdot 10^5\right) \ldots \\ &+ M_d(\alpha, E_f)\cdot f_{bd}(\alpha, E_f)\cdot\left[\begin{aligned} &2.45\cdot 7.31^{-1}\cdot 8.85\cdot 10^4 \ldots \\ &+ 0.625\cdot f_{bt}(\alpha, E_f)\cdot\left(14.1\cdot 17.6^{-1}\right)\cdot 3.37\cdot 10^5 \end{aligned}\right] \end{aligned}}{Y_f(\alpha, E_f)} \qquad \text{Eq 24}$$

Figure 7 Neutron energy loss in hydrogen component of target shells

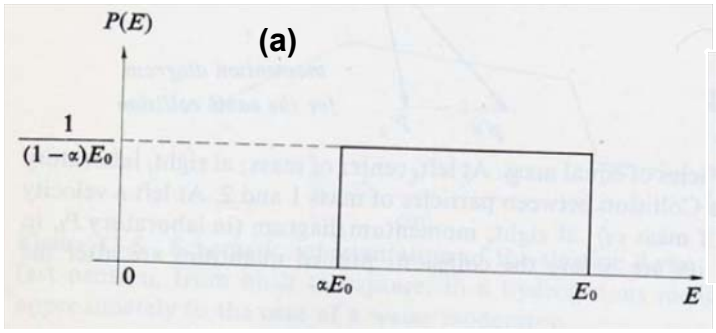

Distribution of the values of the neutron energy E after one collision in the case of isotropic scattering in the center-of-mass system for a neutron of initial energy E_0. The quantity $\alpha = (A-1)^2/(A+1)^2$.

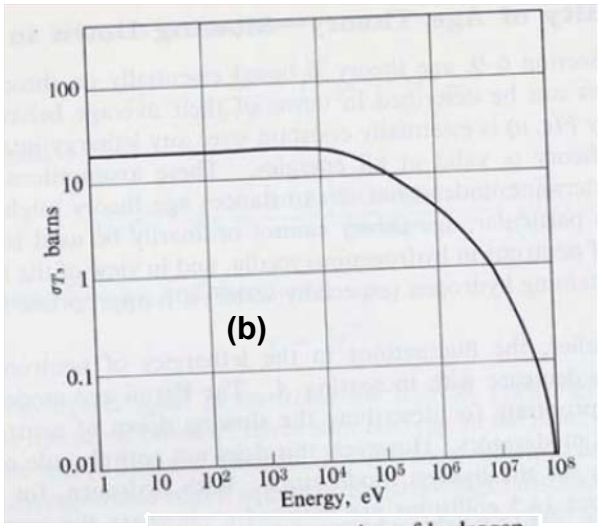

The total cross section of hydrogen.

Note for hydrogen in the target shell, this $\alpha = 0$, for deuterium in the target, $\alpha = 0.11$. For hydrogen/deuterium, neutrons don't diffuse much further from the point they have their first inelastic collision. For 14 MeV neutrons from DT, the efolding ρr in hydrogen is 5 g/cm^2, or 10 g/cm^2 in deuterium, neglecting the neutron's cross section contribution in the deuterium nucleus. For 2.5 MeV neutrons from DD, the e-folding ρr is about 0.7 g/cm^2 in H, or 1.4 g/cm^2 in D. As we will see, the T-lean targets reduce the escaping neutron energy ~50% as in this Fig 5(a), going into the shell.

--->Estimated neutron e-folding ρr's:

$\rho r_{14D} := 10$	$\rho r_{14H} := 5$	$\rho r_{7H} := 2$
$\rho r_{2.5D} := 1.4$	$\rho r_{2.5H} := 0.7$	$\rho r_{1.2H} := 0.4$
in the target	all g/cm^2	in the shell

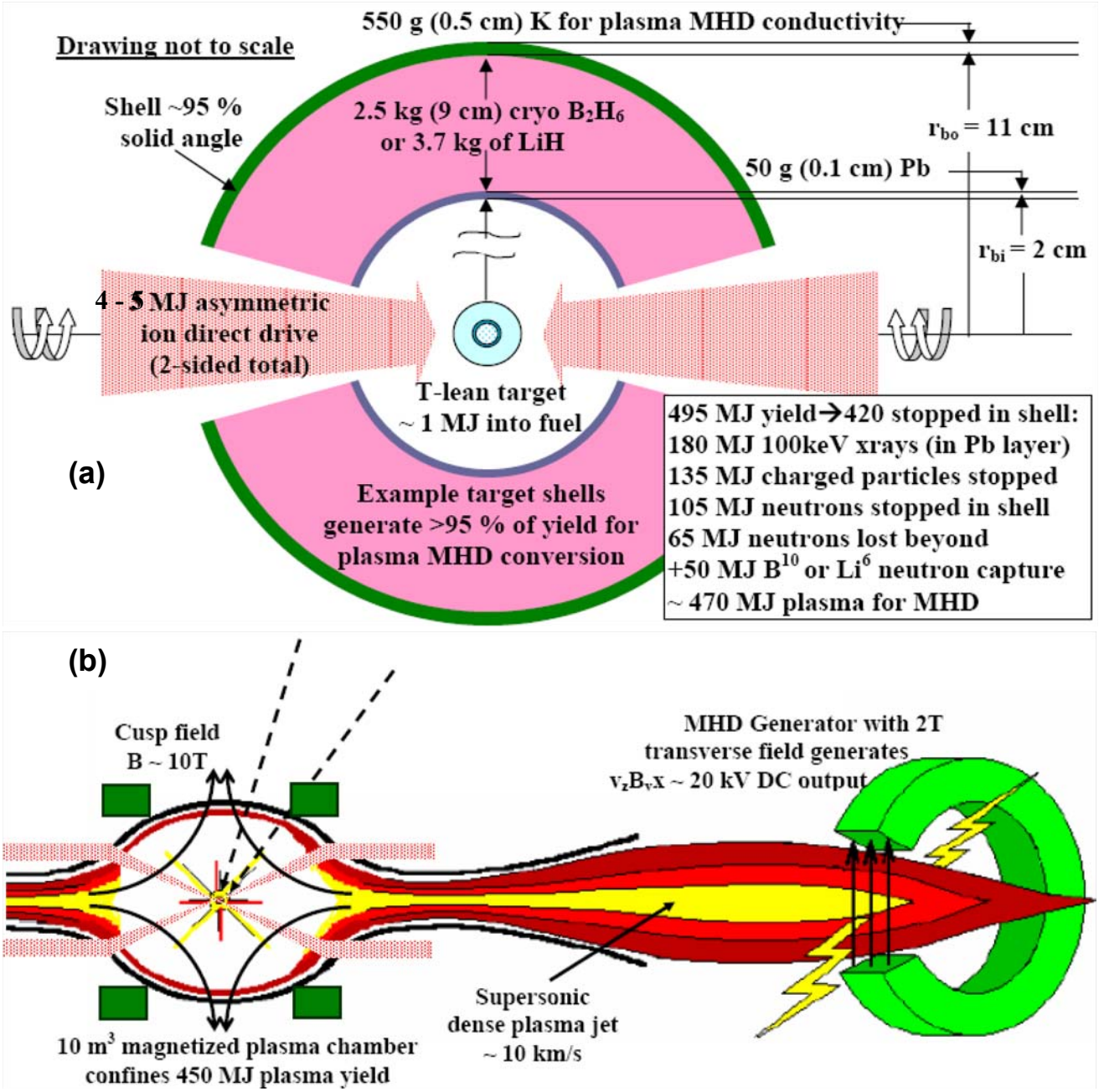

Figure 8: **(a)** Example target shell for efficient conversion of T-lean target output into 1 to 2 eV dense plasma for direct MHD conversion. All shell materials condense and recycle (Rankine cycle).

(b) Schematic of the CFAR MHD scheme (adapting the old 1992 CFAR Logo!)--no detailed design yet.

The shell has 5% solid angle holes for driver beam access, and is used to capture target charged-particle, x-ray, and at least half of the remaining neutron energy *escaping the target* to create 1 to 2 eV dense chamber plasma for direct conversion. (n contrast to ref. 3, most of the neutron energy is internally captured in T-lean cases because the fuel ρr exceeds the neutron mean-free-path. Also, a thin (1 mm) lead layer lines the inner surface of the target shell to capture the 40 % of T-lean target output in the form of 100 keV x-rays. The bulk of the target shell consists of some hydrogen hydride to efficiently absorb neutron energy (which may also provide some energy multiplication through exothermic neutron capture), and is capped by an outer layer of alkali metal such as Potassium to enhance the plasma conductivity of the subsequent mix for efficient (>50 % direct) MHD conversion.

Additional facts about Fig. 8- the marriage of T-lean targets to CFAR energy conversion: A 10 T cusp field on a 2-m vessel/coil radius with a protective 0.6 m-thick Flibe vortex layer inside aids final focusing of ion beams and prevents large shocks to the vessel wall with large yields. The plasma created from the T-lean target shell is conductive enough for the field to confine the 470 MJ plasma until drained out through the MHD generators in ~50 ms. Unlike ref. 3, we assume here < 30 % duty factor for MHD generation to allow the chamber pressure to drop to low values for target insertion. 65 MJ of neutrons + 15 MJ of x-rays not stopped in the target shell act like a small 80 MJ yield in the 10 m^3 Flibe vortex pocket.

Neutron energy attenuation factors A.

The average ρr a neutron has to go to escape in the target depends on where it is born, so we need to define some spatial weighting factors fs when using the total target fuel ρr :

$fsdti := 1$ $\quad A_{nt}(\alpha, E_f) := \exp\left(-fsdti \cdot \rho r(\alpha, E_f) \cdot \rho r_{14D}^{-1}\right)$ for DT neutrons from hot spot Eq 25

$fsddo := 0.2$ $\quad A_{nd}(\alpha, E_f) := \exp\left(-fsddo \cdot \rho r(\alpha, E_f) \cdot \rho r_{2.5D}^{-1}\right)$ outer-born DD neutrons Eq 26

$fsdto := 0.4$ $\quad A_{ndt}(\alpha, E_f) := \exp\left(-fsdto \cdot \rho r(\alpha, E_f) \cdot \rho r_{14D}^{-1}\right)$ outer-born DT neutrons Eq 27

The weighting factor for 2.5 MeV deuterons should be less than the dd-mass weighting 0.33, while the outer-born DT neutrons should be a bit more than 0.33, because the burn wave T increases with r.
Model fraction of fusion energy escaping as neutrons [(1- FY) would be the fraction captured]

$$FY_n(\alpha, E_f) := \frac{\begin{aligned} &14.1 \cdot 17.6^{-1} \cdot 5 \cdot 3^{-1} \cdot M_t(\alpha, E_f) \cdot f_{bt}(\alpha, E_f) \cdot \left(3.37 \cdot 10^5\right) \cdot A_{nt}(\alpha, E_f) \ \ldots \\ &+ M_d(\alpha, E_f) \cdot f_{bd}(\alpha, E_f) \cdot \left[\begin{aligned} &2.45 \cdot 7.31^{-1} \cdot 8.85 \cdot 10^4 \cdot A_{nd}(\alpha, E_f) \ \ldots \\ &+ 0.625 \cdot f_{bt}(\alpha, E_f) \cdot \left(14.1 \cdot 17.6^{-1}\right) \cdot 3.37 \cdot 10^5 \cdot A_{ndt}(\alpha, E_f) \end{aligned}\right] \end{aligned}}{Y_f(\alpha, E_f)}$$ Eq 28

M.Tabak results for escaping neutron fraction of yield for his Case C: $FYmt_1 := 0.45$ $\quad FYmt_2 := 0.4$

$FYmt_3 := 0.35$ $\quad FYmt_4 := 0.33$ $\quad FYmt_5 := 0.31$ $\quad FYmt_6 := 0.30$ $\quad FYmt_7 := 0.29$

Now lets add the additional neutron capture in the target shell. To maintain the optimum shell-produced plasma temperature of 1.5 eV for MHD, we need to scale the shell-blanket mass (see figure 8) proportional to captured fusion yield to keep the average energy deposition in the shell 110 MJ/kg. To simply the estimate, we note that the captured fusion yield is close enough to the fusion yield that we can scale the outer shell-blanket radius r_{bo} simply as:

$$r_{bo}(\alpha, E_f) := 11 \cdot \left(Y_f(\alpha, E_f) \cdot Y_f(1.5, 1)^{-1}\right)^{0.333} \quad \text{(cm)}$$ Eq 29

The resulting additional attenuation (capture) of neutron energy for direct conversion purposes (fraction of yield finally escaping both the target and the shell), estimating attenuation by hydrogen component density in the shell, and augmenting that by 25% to account for Boron/Lithium capture:

$\rho_{Hb} := 0.12$ g/cm^3 density of hydrogen in blanket shell

$A_{ntb}(\alpha, E_f) := \exp\left[-1.25 \cdot \rho_{Hb} \cdot \left(r_{bo}(\alpha, E_f) - 2\right) \cdot \rho r_{7H}^{-1}\right]$ Eq 30

$A_{ndb}(\alpha, E_f) := \exp\left[-1.25 \cdot \rho_{Hb} \cdot \left(r_{bo}(\alpha, E_f) - 2\right) \cdot \rho r_{1.2H}^{-1}\right]$ Eq 31

$$FY_{nb}(\alpha, E_f) := \frac{\begin{aligned} &14.1 \cdot 17.6^{-1} \cdot 5 \cdot 3^{-1} \cdot M_t(\alpha, E_f) \cdot f_{bt}(\alpha, E_f) \cdot \left(3.37 \cdot 10^5\right) \cdot A_{nt}(\alpha, E_f) \cdot A_{ntb}(\alpha, E_f) \ \ldots \\ &+ M_d(\alpha, E_f) \cdot f_{bd}(\alpha, E_f) \cdot \left[\begin{aligned} &2.45 \cdot 7.31^{-1} \cdot 8.85 \cdot 10^4 \cdot A_{nd}(\alpha, E_f) \cdot A_{ndb}(\alpha, E_f) \ \ldots \\ &+ 0.625 \cdot f_{bt}(\alpha, E_f) \cdot \left(\frac{14.1}{17.6}\right) \cdot 3.37 \cdot 10^5 \cdot A_{ndt}(\alpha, E_f) \cdot A_{ntb}(\alpha, E_f) \end{aligned} \right] \end{aligned}}{Y_f(\alpha, E_f)}$$

Eq 32

Table 5: Target shell radius r_{bo} & fusion yield loss fraction FY_{nb} vs fuel energy E_f (Adiabat α = 1.5)

Ef_i =	$\rho r(1.5, Ef_i)$ =	$Y_f(1.5, Ef_i)$ =	$r_{bo}(1.5, Ef_i)$ =	$FY_{nb}(1.5, Ef_i)$ =	$1 - FY_{nb}(1.5, Ef_i)$ =
0.1	6.4	16	3.5	0.34	0.66
0.2	7.3	43	4.9	0.27	0.73
0.5	8.6	171	7.7	0.19	0.81
1	9.9	494	11	0.14	0.86
1.7	10.9	1124	14.5	0.1	0.9
2.6	11.8	2181	18	0.07	0.93
MJ	g/cm²	MJ	cm	Yield fraction lost	Yield fraction captured

Figure 9. Fraction of total T-lean target yield escaping target and shell as neutrons as a function of fuel energy E_f (adiabat α=2). The model (solid red curve), and Max Tabak's case C runs agree well and show significant reduction of lost neutron energy below the un-attenuated neutron yield (blue dotted line) within the large ρr of T-lean targets. The shell captures ~ 50% of remaining neutron energy escaping the target (depending on the fuel ρr- see dashed magenta curve for FY_{nb}).

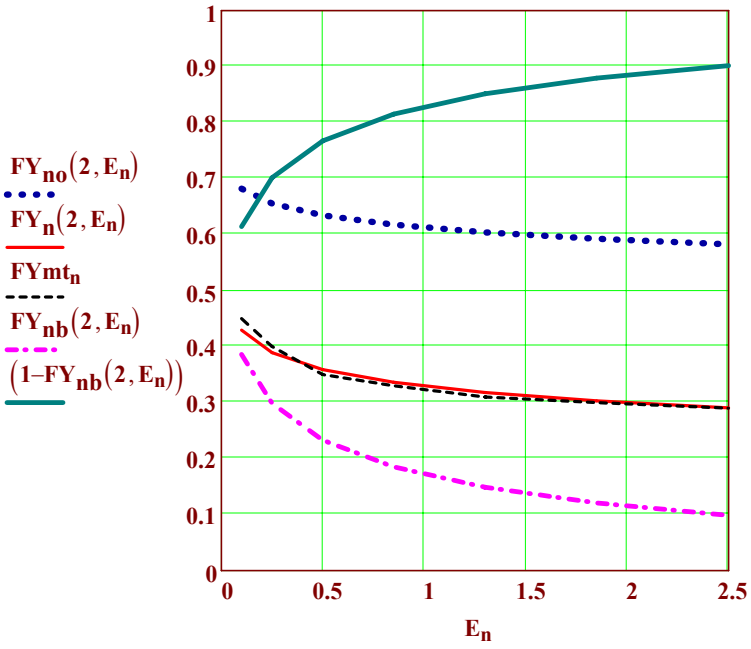

Fraction of yield captured in target + *target shell* (Model)

Un-attenuated neutron energy as a fraction of yield (model)

Max Tabak's Case C neutron energy escaping *the target* as fraction of yield (black dashed) compared to model (red curve).

Fraction of neutron energy escaping both *target and target shell* (model)

<--Fuel energy (MJ)

Rocket efficiency and implosion efficiency with pure H2 ablators.

We assume a pure hydrogen ablator for ion beam direct drive because hydrogen provides the highest exhaust velocity for ablative drive for a given specific energy deposition by short range ions, as well as having the smallest specific ionization energy loss per specific radial kinetic energy of exhaust $0.5 u_{ex}^2$. Working backwards, we will estimate ion beam drive requirements shortly. We assume thin coatings between the DT, DD, and H ablator layers such that the hot spot decay heat gives equilibrium temperatures of 19-->14-->10 deg K for these layers respectively. The DT layer would be filled through the hydrogen layer by a thin fill tube. (see Figure 12 below)

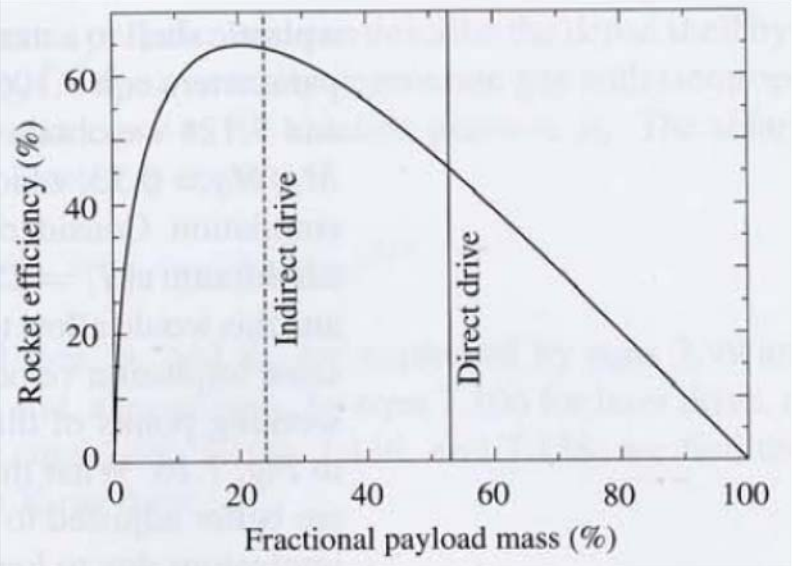

Figure 10: the classic spherical rocket efficiency η_r as a function of the fractional payload mass (Figure from the book by Meyer-ter-Vehn and Atzeni)

An issue is managing space charge in accelerators delivering the energy with short enough range ions to allow pulse shaping for low adiabats. Another factor can be ionization energy losses and radiation losses which can reduce the capsule hydro efficiency η_c below the rocket efficiency η_c. However, pure hydrogen has a small ionization energy of 13.6 eV per atom. So, from Fig. 10, we choose to drive at the peak rocket efficiency $\eta_r := 0.65$

with an associated fractional payload mass $M_1 = 0.2\ M_0$, which requires an H_2 ablator mass M_h:

$$M_h(\alpha, E_f) := 4 \cdot \left(M_d(\alpha, E_f) + M_t(\alpha, E_f)\right) \quad \text{(g).} \qquad \text{Eq 33}$$

The implosion velocity u_{imp} is that required to create the fuel internal energy E_f upon stagnation:

$$u_{imp}(\alpha, E_f) := \left[2 \cdot E_f \cdot 10^{13} \cdot \left(M_d(\alpha, E_f) + M_t(\alpha, E_f)\right)^{-1}\right]^{0.5} \quad \text{(cm/s).} \qquad \text{Eq 34}$$

The ablation exhaust velocity u_{ex} for the chosen peak rocket efficiency is given by

$$u_{ex}(\alpha, E_f) := u_{imp}(\alpha, E_f) \cdot \ln(5)^{-1} \quad \text{(cm/s)} \qquad \text{Eq 35}$$

Radiation losses and avoidance of preheat

$\rho_{Ho} := 0.1$ g/cm^3 for H_2 ablator ρ_0

We estimate the hydrogen ablator compresses by about a factor of 5 during much of the direct drive period, to an average density around 0.5 g/cm^2. The H_2 temperature just behind the ablation front can be estimated by setting $u_{ex} = 2\ c_s$ and solving for T:

$\rho_a := 5 \cdot \rho_{Ho}$ Eq. 36

$m_h := 1.67 \cdot 10^{-24}$ g/H atom

Exhaust temp. $T_{ex}(\alpha, E_f) := 3 \cdot 10^{-4} \cdot m_h \cdot u_{ex}(\alpha, E_f)^2 \cdot 200^{-2} \cdot (1.6 \cdot 10^{-19})^{-1}$ (eV) Eq. 37

For our reference case $T_{ex}(1.5, 1) = 26.3$ eV.

M_o/M_f=5

$u_{imp}(1.5, 1) = 2.95 \times 10^7$ cm/s $\quad \frac{u_{imp}(1.5,1)}{u_{ex}(1.5,1)} = 1.61 \quad \ln(5) = 1.61$

$u_{ex}(1.5, 1) = 1.83 \times 10^7$ cm/s

Figure 11 shows that under these conditions (large ablation fractions at the peak of rocket efficiency), and initial H2 ablator ρr ~ 0.02 g/cm^2 vs κ_R^{-1} = 3 x 10^{-4} g/cm^2, that such ablators are optically thick.

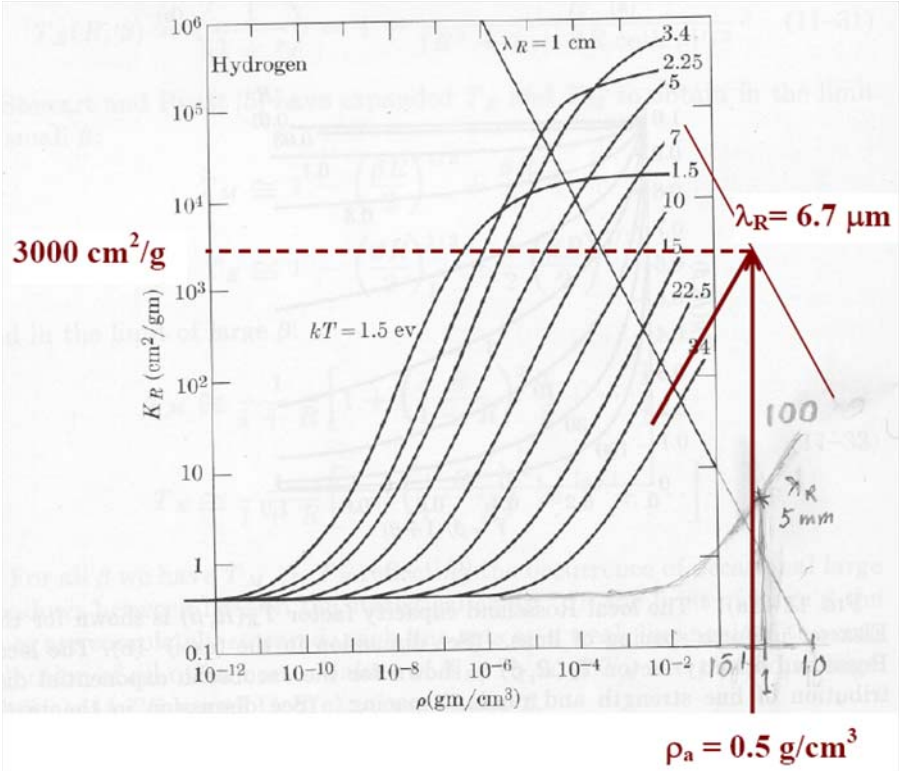

Figure 11: Opacity of H2 ablators are optically thick (marginally) at ~ 30 eV. Note that if local T_e at the ablation front increased for any reason to 100 eV, however, this would no longer be true, and a thin ~ 1 mg/cm^2 plastic CH layer between the outer DD fuel radius and the hydrogen ablator would be required to avoid preheat of the DD. The associated black body radiation loss flux is given by

$\Gamma_{bb}(\alpha, E_f) := 5.67 \cdot 10^{-12} \cdot (T_{ex}(\alpha, E_f) \cdot 11600)^4$ $\quad \Gamma_{bb}(1.5, 1) = 4.91 \times 10^{10}$ W/cm^2 Eq 38

For targets with ~ 1 cm square ablator, this radiation loss can be neglected compared to the 100 TW scale of the PdV work by the ablation pressure, but at 100 eV, it would become significant at 10%.

For good hydrodynamic stability during implosion, we choose a moderate in-flight aspect ratio $A_{if}= \rho_a R_0 /(\rho_0 \Delta R_0)$: (half the "usual" value 30), where ρ_a is the density of the compressed in-flight shell. Typically, $\rho_a \sim 5\ \rho_0$, so the initial aspect ratio $A_{in}=R_0/\Delta R_0 \sim 3$. This initial aspect ratio and the known initial densities and masses of hydrogen and deuterium allows us to find the outer radius r_a of the hydrogen ablator (we can neglect the 1 % DT hotspot mass in this calculation). The initial deuterium layer thickness δD and the outer hydrogen ablator radius r_a are solved:

$A_{if} := 15$ Eq 39

$A_{in} := 3$ $\xi := 1 - A_{in}^{-1}$

$\rho_{Do} := 0.2$ g/cm^3 for D_2 pintail ρ_0

Given Initial guesses $r_{ag} := 0.5$ cm $\delta D := 0.1$ cm

$$\delta D = \left[\left(\frac{3\cdot M_d(\alpha, E_f)}{4\cdot\pi\cdot\rho_{Do}}\right) + \left(\xi\cdot r_{ag}\right)^3\right]^{0.333} - \xi\cdot r_{ag}$$

$$r_{ag} = \left[\left(\frac{3\cdot M_h(\alpha, E_f)}{4\cdot\pi\cdot\rho_{Ho}}\right) + \left(\xi\cdot r_{ag} + \delta D\right)^3\right]^{0.333}$$

$Sol(\alpha, E_f) := Find(\delta D, r_{ag})$

$\delta_D(\alpha, E_f) := Sol(\alpha, E_f)_1$ Initial D2 layer thickness $\delta_D(1.5, 1) = 0.04$ Eq 40

$r_{ao}(\alpha, E_f) := Sol(\alpha, E_f)_2$ Initial outer H2 ablator radius $r_{ao}(1.5, 1) = 0.71$ cm Eq 41

Construct an target pie-sector diagram for a power plant:

$\Delta R_0 := \frac{r_{ao}(1.5, 1)}{A_{in}}$ $\Delta R_0 = 0.24$ $r_{di} := \xi\cdot r_{ao}(1.5, 1)$ $r_{di} = 0.47$ $r_{do} := r_{di} + \delta_D(1.5, 1)$ $r_{do} = 0.51$

$\rho r_{do} := 0.2\cdot(r_{do} - r_{di})$

$\rho r_{do} = 0.008$ g/cm^2

$\rho r_{ho} := 0.1\cdot(r_{ao}(1.5, 1) - r_{do})$

$\rho r_{ho} = 0.0197$ g/cm^2

$M_h(1.5, 1) = 0.092$ g

$M_d(1.5, 1) = 0.023$ g

$M_t(1.5, 1) = 0.0004$ g

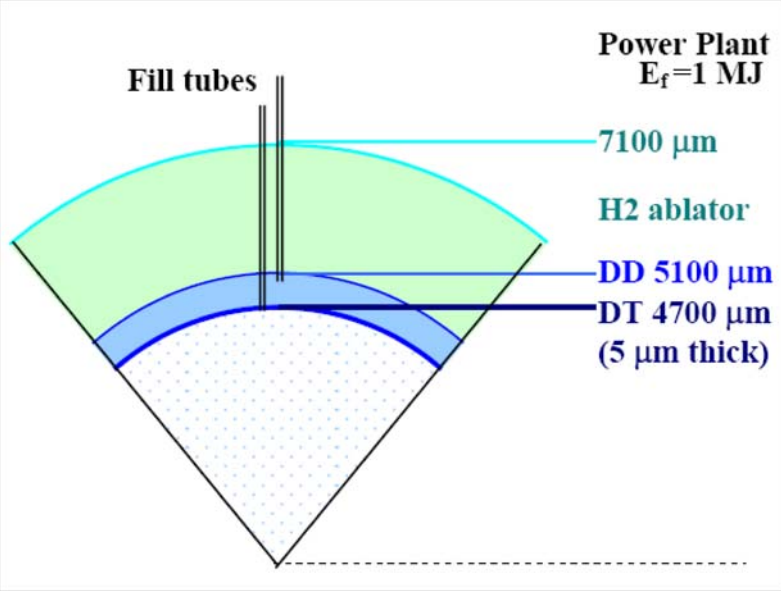

Figure 12: Pie-sector diagram for the CFAR Power Plant reference case (thin mg/cm^2 plastic layers may be used at D_2-H_2 and D_2-DT interfaces).

Construct an initial target pie-sector diagram for a DEMO $r_{ao}(1.5, 0.2) = 0.37$ cm

$\Delta R_0 := \frac{r_{ao}(1.5, 0.2)}{A_{in}}$ $\Delta R_0 = 0.12$ $r_{di} := \xi \cdot r_{ao}(1.5, 0.2)$ $r_{di} = 0.248$ $r_{do} := r_{di} + \delta_D(1.5, 0.2)$ $r_{do} = 0.268$

$\rho r_{do} := 0.2 \cdot (r_{do} - r_{di})$

$\rho r_{do} = 0.004$ g/cm^2

$\rho r_{ho} := 0.1 \cdot (r_{ao}(1.5, 0.2) - r_{do})$

$\rho r_{ho} = 0.0104$ g/cm^2

$M_h(1.5, 0.2) = 0.0134$ g

$M_d(1.5, 0.2) = 0.0033$ g

$M_t(1.5, 0.2) = 0.00006$ g

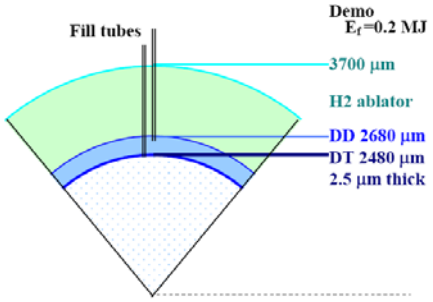

Figure 13: Pie-sector diagram for the CFAR DEMO reference case.

(thin mg/cm^2 plastic layers may be used at D_2-H_2 and D_2-DT interfaces).

Required ion beam power delivered to the ablation front

The total required driver energy E_d input is higher than the radial KE~0.5 M_h u_{ex}^2 because of

(1) hydrogen ionization energy of 13.6 eV/atom x 2 to account for associated line radiation Eq 42

(2) 3T_{ex} temperature-gas energy carried by exhaust plasma implied by $u_{ex}=2c_T=2[2\gamma T/m_h]^{0.5}$

(3) energy E_{cs} required to pre-compress the D+DT payload to the in-flight shell density ρ_a:

Shell compression $E_{cs}(\alpha, E_f) := 0.67 \cdot \alpha \cdot \rho_a^{0.67} \cdot (M_h(\alpha, E_f) + M_d(\alpha, E_f) + M_t(\alpha, E_f))$ (MJ) Eq 43

The resulting required drive energy delivered to the ablation front is then:

$$E_{da}(\alpha, E_f) := 0.5 \cdot 10^{-13} \cdot M_h(\alpha, E_f) \cdot u_{ex}(\alpha, E_f)^2 \ldots + \left(13.6 \cdot 2 + 3 \cdot T_{ex}(\alpha, E_f)\right) \cdot 1.6 \cdot 10^{-25} \cdot M_h(\alpha, E_f) \cdot m_h^{-1} \ldots + E_{cs}(\alpha, E_f)$$

(MJ) Eq. 44

We can define an ion direct drive capsule implosion efficiency that takes these losses into account:

$$\eta_c(\alpha, E_f) := E_f \cdot E_{da}(\alpha, E_f)^{-1}$$

Eq. 45

However, this η_c is still less than the overall drive efficiency η_{df} because of parasitic ion beam losses by dE/dx on outgoing ablation plasma which we will calculate later on in this model. The reason for including the latter losses separately (not in the definition of η_c) is because the parasitic beam losses are less fundamental, depending more on the selected beam ion species (Bragg peak profiles) used and on the beam illumination geometry (including 2-D effects). The fundamental upper limit to direct drive gain based on power deposited usefully at the ablation front (capsule gain, if you will) is

$$G_c(\alpha, E_f) := \eta_c(\alpha, E_f) \cdot G_f(\alpha, E_f)$$

Eq 46

Lower overall direct drive target gains G_t will be evaluated after we include actual beam deposition profiles, but for the next table we can preview overall target gain by using a flat 24% beam-to fuel coupling.

Table 6: Summary of model fuel assembly parameters at stagnation for T-lean fuel assemblies versus fuel energy with T localized near hotspot, D_2 main fuel, H_2 ablators with M_o/M_f=5 (rocket efficiency ηr =0.65), f = 0.1 T-load parameter, and implosion adiabat α=1.5. (Parasitic beam loss NOT included (next section).

Fuel energy Ef_i =	Deuterium density $\rho_{cdd}(1.5, Ef_i)$ =	Hot spot DT radius $\frac{r_{hdt}(Ef_i)}{10^{-4}}$ =	Outer-D radius $\frac{r_{cdd}(Ef_i)}{10^{-4}}$	D-Mass load $\frac{M_d(1.5, Ef_i)}{10^{-3}}$	T-Mass load $\frac{M_t(1.5, Ef_i)}{10^{-3}}$ =	Rho-r total $\rho r(1.5, Ef_i)$	D-burn fraction $f_{bd}(1.5, Ef_i)$	T-burn fraction $f_{bt}(1.5, Ef_i)$ =	
0.1	1314	20	64	1.4	0.03	6.4	0.036	0.42	
0.2	1067	28	91	3.3	0.06	7.3	0.047	0.426	<--DEMO
0.5	811	45	144	9.8	0.18	8.6	0.067	0.435	
1	659	63	204	22.6	0.42	9.9	0.088	0.441	<--Power Plant
1.7	562	82	265	42.6	0.78	10.9	0.107	0.446	
2.6	494	102	328	70.9	1.29	11.8	0.126	0.45	
(MJ)	(g/cm^3)	(μm)	(μm)	(mg)	(mg)	(g/cm^2)			

Fuel energy Ef_i =	Implosion velocity $u_{imp}(1.5, Ef_i)$ =	Exhaust velocity $u_{ex}(1.5, Ef_i)$ =	Exhaust T_e ablation $T_{ex}(1.5, Ef_i)$ =	Outer H2 ablator radius $r_{ao}(1.5, Ef_i)$ =	Energy to Ablator $E_{da}(1.5, Ef_i)$ =	Capsule efficiency $\eta_c(1.5, Ef_i)$	Capsule gain $G_c(1.5, Ef_i)$ =	
0.1	$3.7\cdot10^7$	$2.3\cdot10^7$	41	0.28	0.24	0.41	65	
0.2	$3.5\cdot10^7$	$2.1\cdot10^7$	36	0.37	0.49	0.406	88	<--DEMO
0.5	$3.2\cdot10^7$	$2\cdot10^7$	30	0.54	1.26	0.398	136	
1	$3\cdot10^7$	$1.8\cdot10^7$	26	0.71	2.55	0.392	194	<--Power Plant
1.7	$2.8\cdot10^7$	$1.7\cdot10^7$	24	0.87	4.4	0.387	256	
2.6	$2.7\cdot10^7$	$1.7\cdot10^7$	22	1.03	6.8	0.382	321	
(MJ)	(cm/s)	(cm/s)	(eV)	(cm)	(MJ)			

Fuel energy Ef_i =	Fusion yield $Y_f(1.5, Ef_i)$	Fuel gain $G_f(1.5, Ef_i)$ =	Est. Target gain $\frac{G_f(1.5, Ef_i)}{0.25^{-1}}$ =	Est. Driver energy $\frac{Ef_i}{0.25}$ =	Net T-mass $\frac{M_{tn}(1.5, Ef_i)}{10^{-3}}$ =	# neutrons per T burned $N_{ndd}(1.5, Ef_i)$	Yield fraction for MHD conv. $1 - FY_{nb}(1.5, Ef_i)$ =	
0.1	16	157	39	0.4	-0.0011	2.02	0.66	
0.2	43	217	54	0.8	0.005	2.19	0.73	<--DEMO
0.5	171	342	86	2	0.054	2.4	0.81	
1	494	494	123	4	0.2137	2.55	0.86	<--Power Plant
1.7	1124	661	165	6.8	0.5626	2.65	0.9	
2.6	2181	839	210	10.4	1.1826	2.72	0.93	
(MJ)	(MJ)			(MJ)		(mg)		

Ion beam range and dE/dx profiles versus energy (and rho-r) scaling

This MCAD model is used only as a guide to narrow the parameters to be calculated in detail with hydro codes. We'll use the ion dE/dx model used in HYDRA (Kaiser, Kerbel and Prasad), where for simplicity and the conditions given in Table 6, we can assume full ionization of the hydrogen, set:

$A_t := 1 \quad Z_t := 1 \quad Z_{ta} := 1$

We use the same formulary as in HYDRA ion package documentation[1]-->

$$-\frac{dE}{dx} = \underbrace{\left[\frac{4\pi e^4}{m_e c^2}\right]}_{5.1e-22\ keV\ cm^2}\underbrace{\left[\frac{N_0 \rho_T}{A_T}\right]}_{\frac{6e23}{A}\frac{g}{cm^3}}\left[\frac{Z_{eff}^2}{\beta^2}\right]\left\{(Z_T - \bar{Z})\ \mathrm{Log}\ \Lambda_B + \bar{Z}\ G(\beta/\beta_e)\ \mathrm{Log}\ \Lambda_F\right\}$$

ρ_T = target density in g/cm^3, A_T = target atomic weight

Z_T = target atomic number, $\bar{Z}$ = target ionization state

$\Lambda_B = \frac{2m_e c^2 \beta^2}{\bar{I}}$, $\Lambda_F = \frac{m_e c^2 \beta^2}{\hbar \omega_p}$, $G(x) = erf(x) - x\, erf'(x) \approx 1$ for $x >> 1$

$\bar{I}$ = average ionization potential $\approx .01 Z_T$ keV (Bloch's rule)

ω_p = plasma frequency $= \sqrt{4\pi e^2 n_e / m_e} = 56416\sqrt{n_e}$ /sec

$\hbar\omega_p = (3.7e-14)\sqrt{n_e}$ keV, n_e = electron density in $1/cm^3 = \bar{Z} N_0 \rho_T / A_T$

Ion Beam : $\beta = v/c$, $\gamma = \frac{1}{\sqrt{1-\beta^2}} = 1 + \frac{E}{Mc^2}$

E = Kinetic Energy of Ion Beam in keV,

Mc^2 = Ion Beam Rest Energy = $A_{ionBeam}$ (9.3e5) keV

$m_e c^2$ = Electron Rest Energy = 511 keV

Betz Empirical $Z_{eff} \equiv Z_{ionBeam}\left[1 - \exp(-137\,\beta_{eff} / Z_{ionBeam}^{.69})\right]$

$\beta_{eff}^2 \equiv \beta^2 + \beta_e^2$, with $\gamma_e = \frac{1}{\sqrt{1-\beta_e^2}} = 1 + \frac{kT_e}{m_e c^2}$

[1] LLNL presentation, "Implementing Ion Beams in Kull and Hydra," T. Kaiser, G. Kerbel, M. Prasad

Beam nuclear Z: (nominal-we will keep ion mass dependence) $Z_b := 18$ $A_b := 40$ **(Argon)**

$M_p := 1.67 \cdot 10^{-27}$ (kg), the rest mass of a proton,

$e := 1.6 \cdot 10^{-19}$ (C) electron charge,

$c := 3 \cdot 10^8$ (m/s) the speed of light,

$m_e := 9.1 \cdot 10^{-31}$ (kg), the electron rest mass

$\varepsilon_o := 8.85 \cdot 10^{-12}$ Vacuum permittivity (Farads/m),

$\mu_o := 4 \cdot \pi \cdot 10^{-7}$ Vacuum permeability (Henrys/m)

$I_o := 3.1 \cdot 10^7$ (Amps) -constant in beam perveance)

$\gamma(E_b, A_b) := 1 + \frac{e \cdot E_b}{A_b \cdot M_p \cdot c^2}$ the relativistic gamma factor, with T_b the kinetic energy in eV, A the atomic mass number **Eq 47**

$\beta(E_b, A_b) := \sqrt{1 - \gamma(E_b, A_b)^{-2}}$ the ion velocity normalized to c. $\beta(2 \cdot 10^8, A_b) = 0.1$ **Eq 48**

$\gamma_e(T_e) := 1 + \frac{e \cdot T_e}{m_e \cdot c^2}$ Relativistic gamma for electrons of temperature Te (eV) **Eq 49**

$$\beta_e(T_e) := \sqrt{1 - \gamma_e(T_e)^{-2}} \qquad T_e := 30 \qquad \beta_e(30) = 0.011 \qquad \text{Eq 50}$$

$$\beta_{eff}(E_b, T_e, A_b) := \left(\beta(E_b, A_b)^2 + \beta_e(T_e)^2\right)^{0.5} \qquad \text{Eq 51}$$

The ion beam effective charge while slowing down in the ablator (Betz empirical formula)

$$Z_{eff}(E_b, T_e, A_b, Z_b) := Z_b \cdot \left(1 - \exp\left(-137 \cdot \beta_{eff}(E_b, T_e, A_b) \cdot Z_b^{-0.69}\right)\right) \qquad \text{Eq 52}$$

$$G_v(x) := \operatorname{erf}(x) - x \cdot \left(\frac{d}{dx}\operatorname{erf}(x)\right) \qquad G_v(0) = 0 \qquad G_v(0.5) = 0.08 \qquad G_v(1) = 0.43 \qquad G_v(2) = 0.954$$

$$\Lambda_B(E_b, A_b, I_t) := \left(2 \cdot 511 \cdot \beta(E_b, A_b)^2 \cdot I_t^{-1}\right) + 1 \qquad I_t := 13.6 \cdot 10^{-3} \quad \text{keV, ionization PE for hydrogen} \qquad \text{Eq 53}$$

$$\Lambda_F(E_b, A_b, Z_{ta}, \rho_a) := \left[511 \cdot \beta(E_b, A_b)^2 \cdot \left[3.7 \cdot 10^{-14} \cdot \sqrt{Z_{ta} \cdot \rho_a \cdot \left(1.67 \cdot 10^{-24} \cdot A_t\right)^{-1}}\right]^{-1}\right] + 1 \qquad \text{Eq 54}$$

$$dE_{d\rho x}(\rho_a, E_b, T_e, A_b, A_t, Z_b, Z_t) := \frac{-5.1 \cdot 10^{-19}}{1.67 \cdot 10^{-24} \cdot A_t} \cdot \left(\frac{Z_{eff}(E_b, T_e, A_b, Z_b)}{\beta(E_b, A_b)}\right)^2 \cdot \left[\begin{array}{l} (Z_t - Z_{ta}) \cdot \ln\left(\Lambda_B(E_b, A_b, I_t)\right) \ldots \\ + Z_{ta} \cdot \dfrac{\ln\left(\Lambda_F(E_b, A_b, Z_{ta}, \rho_a)\right)}{G_v\left(\dfrac{\beta(E_b, A_b)}{\beta_e(T_e)}\right)^{-1}} \end{array}\right]$$

dE/d(ρx) in g/cm^2 Eq. 55

Consider DT first example to compare with the Barnard's HYDRA model calculations

$$Ebg := 10^7, 2 \cdot 10^7 .. 10^9 \qquad TOL := 0.001 \qquad A_t := 2.5 \qquad Z_t = 1 \qquad \rho_a := 0.25 \qquad T_e := 500$$

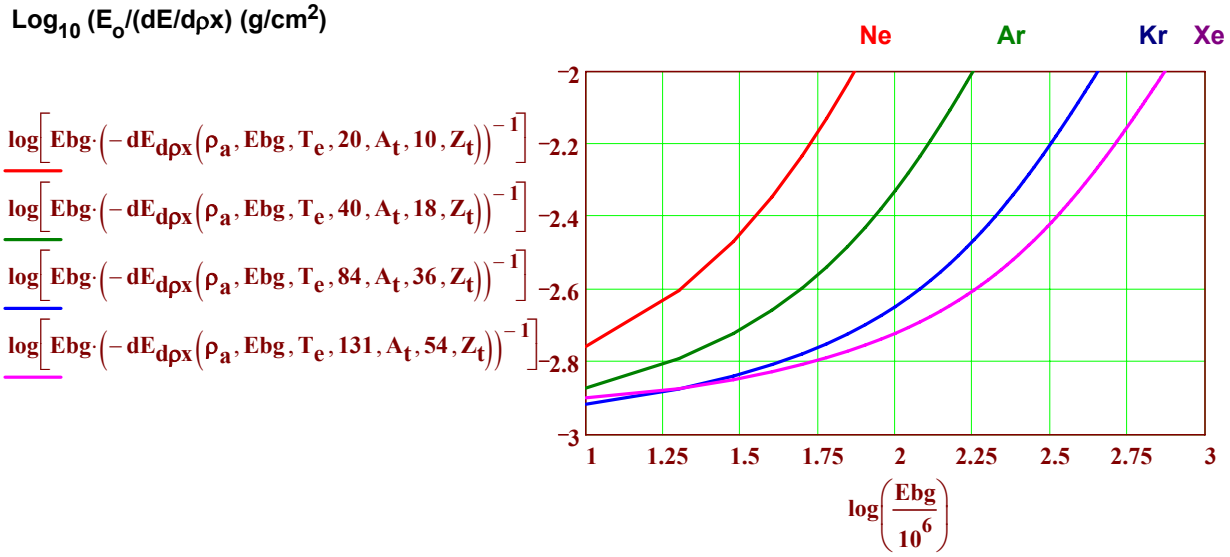

Fig. 14: Beam stopping range versus ion energy for various ions $\text{Log}_{10}(\text{Eb}_o\ (\text{Mev}))$

Now, for a more accurate representation on ion ranges, we should integrate dE/dρx and plot the initial energies required for a specified range as a function of range, ion mass and atomic number:

Initial guess $Eb := 3\cdot 10^8$ $TOL := 0.001$ $T_e := 30$ $A_t := 1$ $\rho_a := 0.5$

$$E_b(\rho_a,\rho rb,T_e,A_b,A_t,Z_b,Z_t) := \text{root}\left(\rho rb - \left(+-\int_{Eb}^{0.02\cdot Eb} dE_{d\rho x}(\rho_a,E,T_e,A_b,A_t,Z_b,Z_t)^{-1}\,dE\right),Eb\right) \quad \text{(eV)} \qquad \text{Eq 56}$$

$E_b(\rho_a,0.01,T_e,40,A_t,18,Z_t) = 3.916\times 10^8$ $\rho rb := 0.001, 0.002 .. 0.03$

Figure 15: Beam range (ρr_b) in Log_{10} (g/cm^2) vs beam energy Log_{10} (MeV), for Ar and Kr

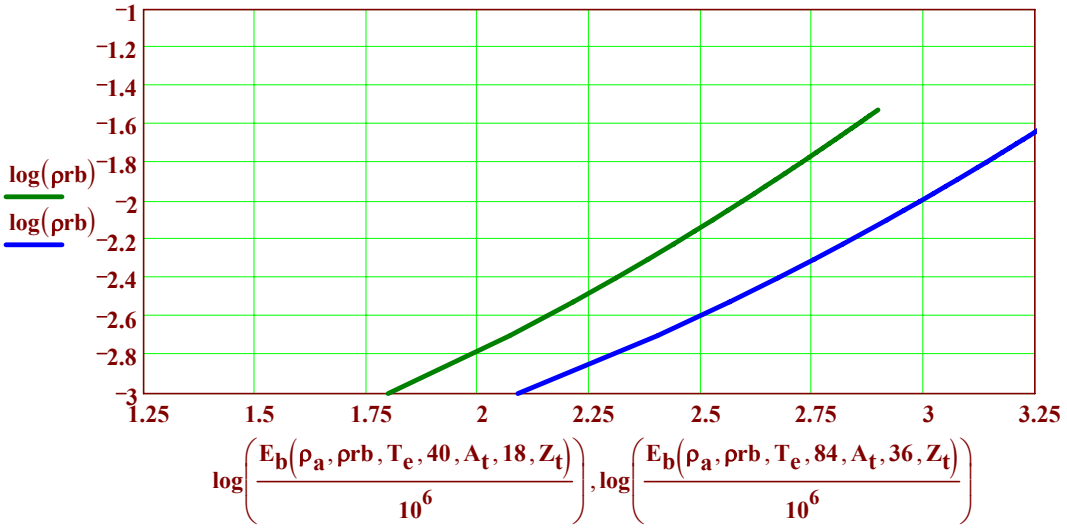

$Ebo_{Ar} := E_b(\rho_a,0.01,T_e,40,A_t,18,Z_t)$ $Ebo_{Kr} := E_b(\rho_a,0.01,T_e,84,A_t,36,Z_t)$ $Ebo_{Ar} = 3.9\times 10^8$ $Ebo_{Kr} = 9.81\times 10^8$

$$\rho r_{bo}(\rho_a,E,Ebo,T_e,A_b,A_t,Z_b,Z_t) := \int_{Ebo}^{E} dE_{d\rho x}(\rho_a,E,T_e,A_b,A_t,Z_b,Z_t)^{-1}\,dE \quad \text{g/cm2} \qquad \text{Eq 57}$$

$T_e = 30$ $A_t = 1$ $\rho_a = 0.5$ $Z_t = 1$

$Ebx_{Ar} := 0.01\cdot Ebo_{Ar}, 0.02\cdot Ebo_{Ar} .. Ebo_{Ar}$

$Ebx_{Kr} := 0.01\cdot Ebo_{Kr}, 0.02\cdot Ebo_{Kr} .. Ebo_{Kr}$

Figure 16: ion energy vs range g/cm^2 for Ar and Kr Bragg peaking (favorable to reduce ion loss in ablated plasma), is not so pronounced at these low ranges.

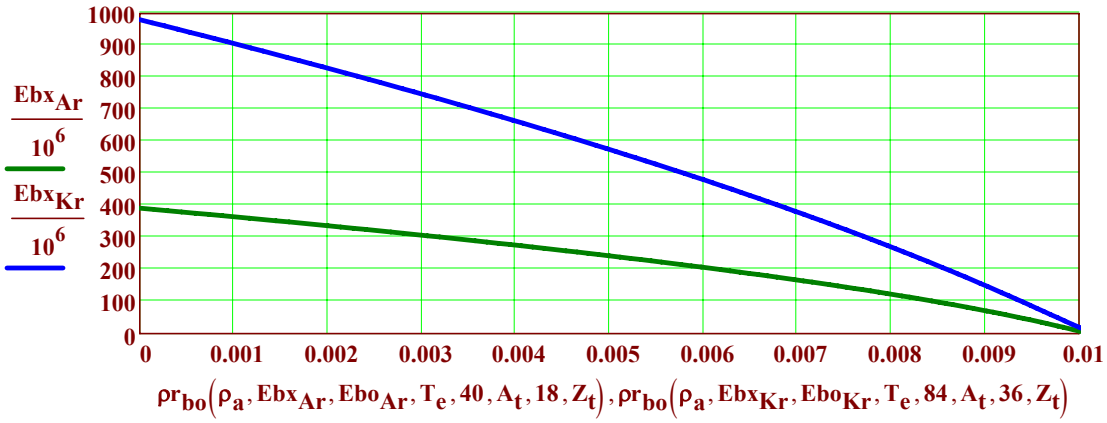

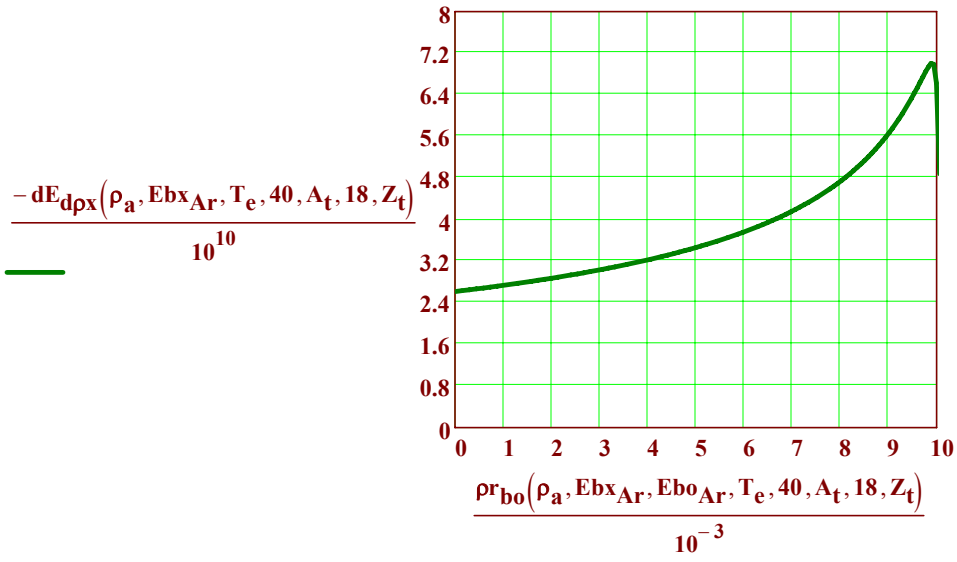

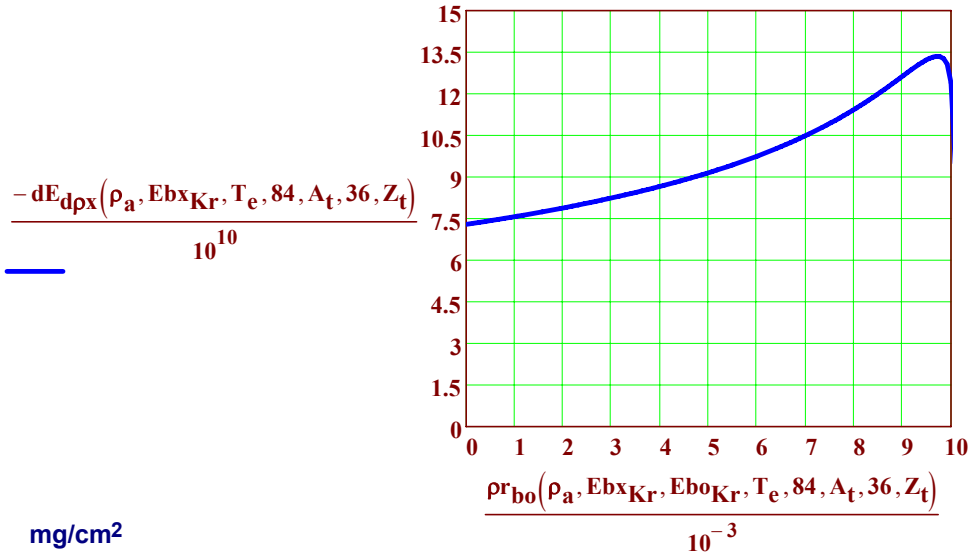

Fig. 17: Ion dE/dρx vs range in (mg/cm²) for Ar (top) and Kr (bottom). Note that Argon Bragg peaking is more pronounced than for Krypton for a given range (and even more so compared to Xenon, which would be less peaked than for Krypton)

Now lets develop a function the ion energy lost in ablation plasma by calculating the reduced ion energy E_{bf} at some specified fraction $f_{\rho r} = \rho r_a/\rho r_b$ of a given required total range $\rho r_b = \rho r_a + \delta\rho r_h$

Reduced ion energy (eV) versus fraction of ion range

$$Ebf := 3 \cdot 10^8$$

$$E_{bf}(\rho_a, \rho rb, f_{\rho r}, T_e, A_b, A_t, Z_b, Z_t) := root\left(f_{\rho r} \cdot \rho rb \ \ldots + -\int_{E_b(\rho_a, \rho rb, T_e, A_b, A_t, Z_b, Z_t)}^{Ebf} dE_{d\rho x}(\rho_a, E, T_e, A_b, A_t, Z_b, Z_t)^{-1}\, dE\right)$$

eV Eq 58

The fraction f_{ba} initial ion beam energy that is lost in the ablated plasma versus fraction of the ablation plasma ρr over total beam ρr_b

$$f_{ba}(\rho_a, \rho rb, f_{\rho r}, T_e, A_b, A_t, Z_b, Z_t) := 1 - \frac{E_{bf}(\rho_a, \rho rb, f_{\rho r}, T_e, A_b, A_t, Z_b, Z_t)}{E_b(\rho_a, \rho rb, T_e, A_b, A_t, Z_b, Z_t)}$$ Eq 59

$$f_{\rho rg} := 0.05, 0.1 .. 1$$

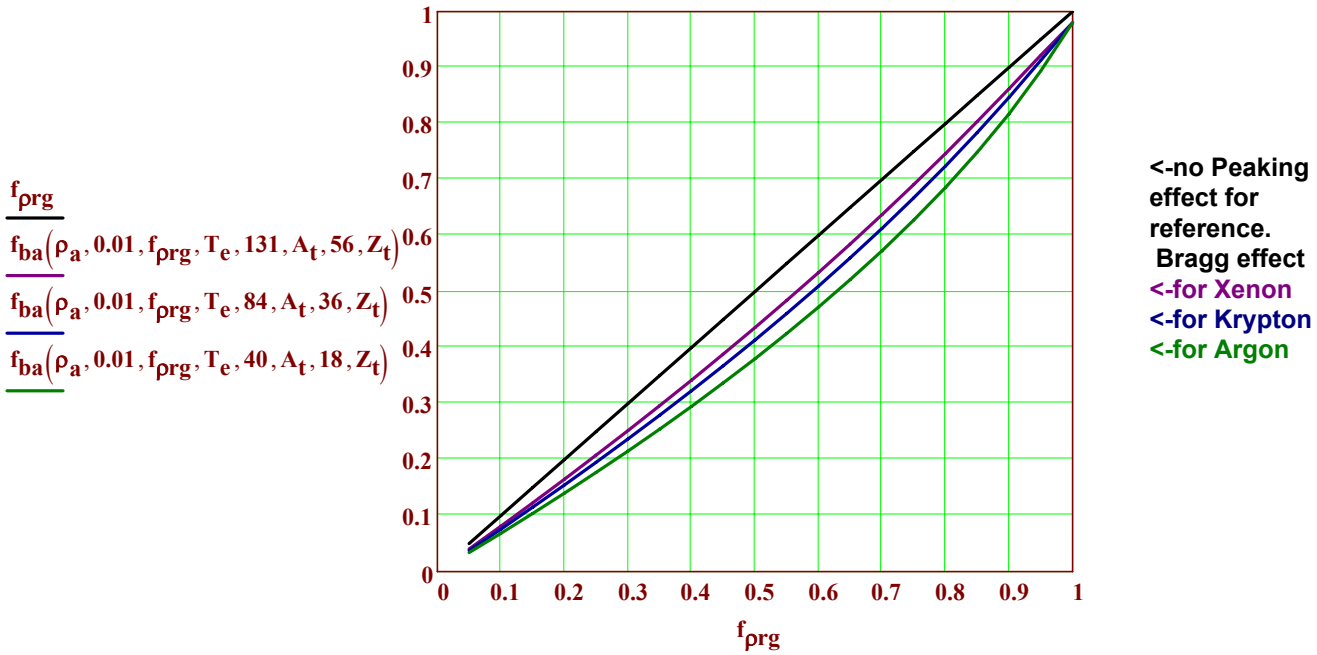

Figure 18. Fractions of ion beam energy loss in prior ablated plasma vs the fraction fρr of the ablated plasma to the total ion range, for Xenon, Krypton, and Argon beams. The black line is for reference if there was no dE/dx Bragg peaking effect at all.

Fig. 18 shows that Bragg peaking can help reduce fractional beam losses in ablated ρr_a = remaining ion range ($f_{\rho r}$ = 0.5) from 50 % (if there were no peaking, i.e. flat dE/dx) down to 35% for A, and down to 39% for Kr, and down to 41 % for Xenon, due to the Bragg peaking profile effect that increases dE/dx above some fractional range to that below. This will be useful when we calculate beam coupling efficiency in implosions with shaped beam pulses below. Since Argon gives the greatest Bragg peaking effect, we will assume Argon for the implosion calculations below. However, if accelerator issues should require it, Krypton and Xenon can be substituted for less beam space charge in the accelerator, if need be, with a small penalty in increased parasitic beam losses due to reduced Bragg peaking profiles.

Implosion Dynamics Case A: at the peak of rocket efficiency = 0.65 (M_o/M_f=5)

In the following example calculation of implosion dynamics we divide the initial hydrogen ablator into 30 Lagrangian mass layers, and calculate shell implosion dynamics by working backwards requiring the mass ablation rates satisfy the rocket equation for the chosen initial/final mass ratio. We make no attempt to calculate exact pulse shaping required for shock timing to produce the desired low α=1.5 adiabat, that requiring actual hydro codes calculations, but we do pick a pulse shape that resembles the desired shapes we know will be required, to get the characteristics. We assume spherical symmetry, even though eventually we want to achieve the same final fuel payload conditions in two-sided asymmetric direct drive. Steve Slutz finds similar large-column density capsules can tolerate P2 asymmetries as large as 20%. Our goal is to explore the implosion characteristics as a guide to later hydro code runs. By working backwards, derive the ion energies and ranges required to produce the ablation rates for the final fuel energy. We track the ablated plasma ρr_a ,increasing during the drive pulse, to estimate the beam losses incurred.

$ORIGIN := 0$ $jm := 31$ $\chi := \frac{0.5 \cdot jm}{(0.5 \cdot jm + 1)^3}$ $\chi = 0.0035$ $\delta to := 240 \cdot 10^{-9}$ s

$j := 0 .. jm$ $k := 0 .. jm - 2$ $\delta t_j := \left[\Phi\left[\frac{j}{(j+1)^3} - \chi\right] \cdot \frac{j}{(j+1)^3} + \Phi\left[\chi - \frac{j}{(j+1)^3}\right] \cdot \chi\right] \cdot \delta to$ $t_j := \sum_{n=0}^{j} \delta t_n$ Eq 60

$jm - 1 = 30$ $M_0 := 1.25 \cdot M_h(1.5, 1)$ $M_0 = 0.1149$ g $\delta M := \frac{0.8}{jm - 1} \cdot M_0$ Eq 61

$(jm - 1) \cdot \delta M = 0.092$ $M_0 := M_0$ $0.8 \cdot M_0 = 0.092$ $M_j := M_0 - j \cdot \delta M$

$M_d(1.5, 1) + M_t(1.5, 1) = 0.023$ $\delta M = 3.06 \times 10^{-3}$ $0.8 \cdot M_0 \cdot (jm - 1)^{-1} = 3.06 \times 10^{-3}$

$uex := u_{ex}(1.5, 1)$ $uex = 1.83 \times 10^7$ $u_j := uex \cdot \ln\left(\frac{M_0}{M_j}\right)$ $u_{imp}(1.5, 1) = 2.95 \times 10^7$ $Ma_0 := 0$

$Ma_j := M_0 - M_j$ $Eex_j := 0.5 \cdot 10^{-13} \cdot Ma_j \cdot uex^2 + 10^{-5}$ $Ep_j := 0.5 \cdot 10^{-13} \cdot M_j \cdot (u_j)^2$ Eq 62

$r_0 := r_{ao}(1.5, 1)$ $r_0 = 0.705$ cm $0.5 \cdot r_0 = 0.353$ $r_0 := r_0$ $\delta r_k := \frac{u_{k+1} + u_k}{2} \cdot \delta t_{k+1}$

$r_k := r_0 - \sum_{n=0}^{k} (\delta r_n)$ $Pex_k := \frac{(Eex_{k+1} - Eex_k) \cdot 10^6}{\delta t_{k+1}}$ $\sum_{n=0}^{jm-2} (Pex_n \cdot \delta t_{n+1}) = 1.54 \times 10^6$ Eq 63

$ua_k := uex - u_k$ $r_{jm-1} := 0.305$ $ra_k := r_k + ua_k \cdot \sum_{n=k}^{jm-2} \delta t_{n+1}$ $\delta \rho a_k := \delta M \cdot \left[4 \cdot \frac{\pi}{3}\left[(ra_k)^3 - (r_{k+1})^3\right]\right]^{-1}$ Eq 64

$\delta \rho ra_k := \delta \rho a_k \cdot (ra_k - r_{k+1})$ $\rho ra_k := \sum_{n=0}^{k} \delta \rho ra_n$ $\rho rh_k := \frac{0.8 \cdot M_0 - k \cdot \delta M}{4 \cdot \pi \cdot (r_k)^2}$ remaining ρr g/cm^2 of ablator vs time t(k) Eq 65

Ablation pressure $pa_k := \frac{10^{-12} \cdot \delta M \cdot uex}{\delta t_{k+1} \cdot \left[4 \cdot \pi \cdot (r_{k+1})^2\right]}$ MBar $\delta Eex := 0.5 \cdot 10^{-13} \cdot \delta M \cdot uex^2$ Eq 66

$\delta Eex = 0.0515$ MJ

Table 7: Parameters during implosion for Case A with parasitic beam loss on uniform ablation plasma

$m := 0, 2 .. 30$ $\quad Pex_{30} := 62 \cdot 10^{12}$ $\quad r_{30} := 0.305$ $\quad ra_{30} := 0.3$ $\quad \rho ra_{30} := 27 \cdot 10^{-3}$ $\quad \rho rh_{30} := 0$ $\quad pa_{30} := 64$

$\frac{t_m}{10^{-9}} =$	$\frac{M_m}{10^{-3}} =$	$\frac{u_m}{10^{7}} =$	$Eex_m =$	$Ep_m =$	$\frac{Ep_m}{Eex_m} =$	$\frac{Pex_m}{10^{12}} =$	$r_m =$	$ra_m =$	$\frac{\rho ra_m}{10^{-3}} =$	$\frac{\rho rh_m}{10^{-3}} =$	$pa_m =$
0.8	115	0	0	0	0	2	0.7	2.62	0.08	15.01	0.3
48.6	109	0.1	0.1	0.005	0.05	5	0.67	1.66	0.38	15.19	0.9
67.5	103	0.21	0.21	0.022	0.11	9	0.64	1.26	0.86	15.31	2
77.3	97	0.32	0.31	0.049	0.16	16	0.62	1.05	1.51	15.23	3.7
83.2	90	0.44	0.41	0.087	0.21	24	0.6	0.91	2.33	14.95	6
87.2	84	0.57	0.51	0.136	0.26	34	0.58	0.81	3.3	14.49	9
90	78	0.71	0.62	0.195	0.32	45	0.56	0.74	4.43	13.86	12.8
92.1	72	0.86	0.72	0.264	0.37	59	0.55	0.68	5.7	13.05	17.5
93.8	66	1.02	0.82	0.342	0.42	62	0.53	0.62	7.14	12.16	19.9
95.5	60	1.2	0.93	0.429	0.46	62	0.51	0.57	8.78	11.25	21.7
97.2	54	1.4	1.03	0.523	0.51	62	0.49	0.52	10.67	10.29	24
98.8	47	1.62	1.13	0.623	0.55	62	0.46	0.47	12.89	9.22	27.3
100.5	41	1.87	1.24	0.725	0.59	62	0.43	0.43	15.54	7.95	31.9
102.1	35	2.17	1.34	0.827	0.62	62	0.39	0.38	18.78	6.32	38.8
103.8	29	2.52	1.44	0.922	0.64	62	0.35	0.34	22.9	3.95	50.2
105.4	23	2.95	1.54	1	0.65	62	0.31	0.3	27	0	64

Figure 19: Case A implosion characteristics at the peak rocket efficiency ($M_o/M_f = 5$) for a fuel payload energy E_f=1MJ, final ρr_f = 10 g/cm^2.

Ablation front radius r(cm)

Exhaust energy E_{ex}(MJ)

Ablation pressure p_a (in100 Mbar units)

Rocket K.E. power P_{ex} (in 100 TW units). (required beam power is roughly 3 X higher)

Time axis in ns

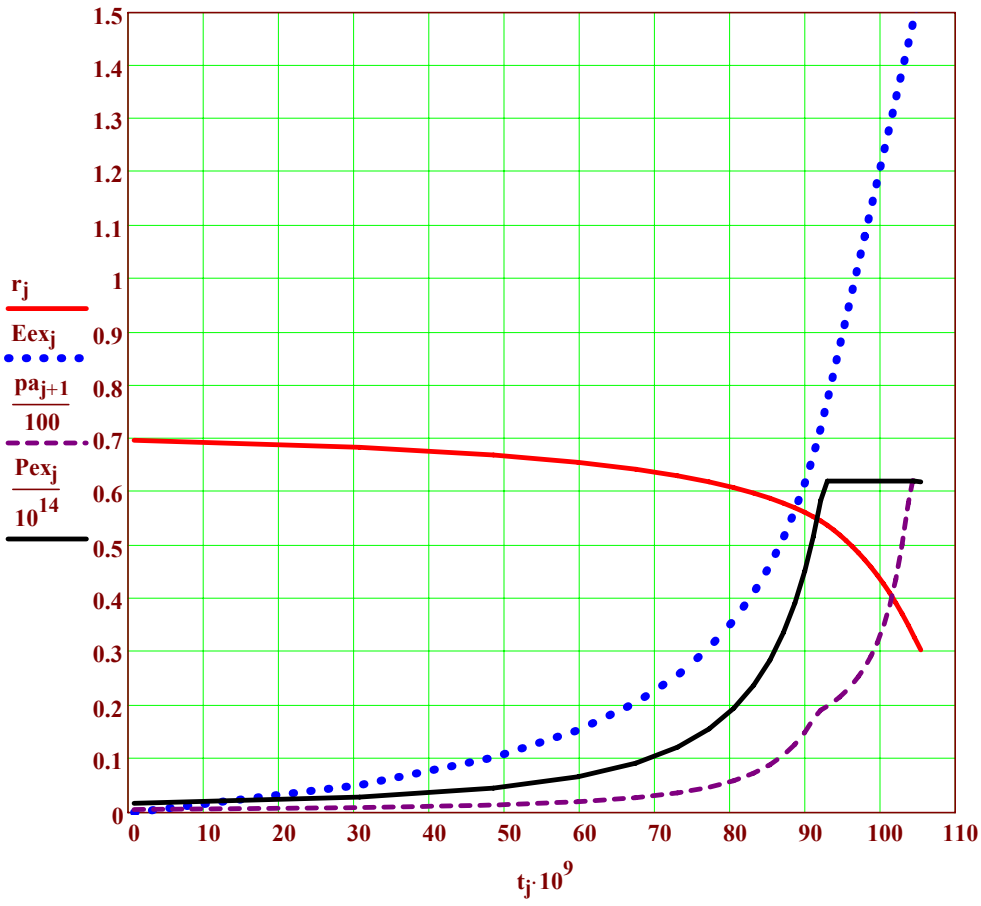

Calculation of ion beam requirements for Case A (Fig. 19) Power Plant, M_o/M_f=5

$\delta M = 0.0031$ $\rho_a = 0.5$ $A_{if} = 15$ $uex = 1.83 \times 10^7$ $A_b = 40$ $Z_b = 18$

Given beam range penetrating ablator $\delta\rho r_{bh} := 0.004$ g/cm^2 = 0.25 of total initial ablator ρr_{ho}

Total incident required beam range ρr $\rho r_b(\rho r_a) := \rho r_a + \delta\rho r_{bh}$ g/cm^2

Required beam range versus t(k) $\rho rb_k := \rho r_b(\rho ra_k)$ g/cm^2

Figure 20: Case A Column densities (ρr)'s: (g/cm^2 units)

Beam range in ablator $\delta\rho r_{bh}$

Ablated plasma ρr_a (dotted) ρra_{j+1}

Total req. beam range incident ρrb_{j+1}

Remaining ablator ρr_h ρrh_{j+1}

Time in ns

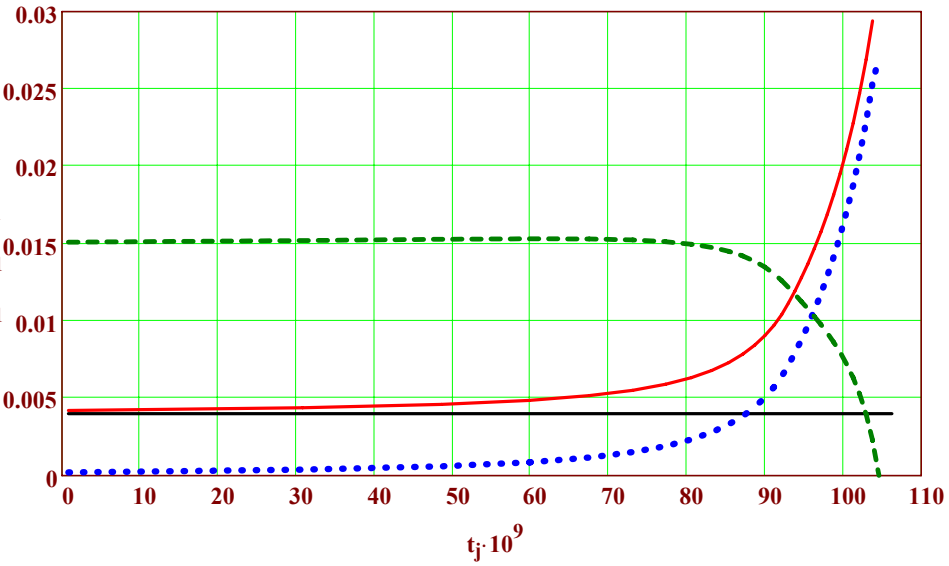

Fraction of ablated ρr in total beam ρr_b $f\rho r_k := \dfrac{\rho ra_k}{\rho r_b(\rho ra_k)}$ Eq 67

Fraction of beam energy in ablated plasma $fba_k := f_{ba}(\rho_a, \rho rb_k, f\rho r_k, T_e, A_b, A_t, Z_b, Z_t)$

Incident beam ion K.E. $Ebo_k := E_{bf}(\rho_a, \rho rb_k, 0.01, T_e, A_b, A_t, Z_b, Z_t)$ MeV

Ratio of exhaust kinetic energy to total exhaust energy $\eta_{ex}(\alpha, E_f) := 0.5 \cdot 10^{-13} \cdot M_h(\alpha, E_f) \cdot u_{ex}(\alpha, E_f)^2 \cdot E_{da}(\alpha, E_f)^{-1}$

Required incident beam energy integrated up to time t_k $Ebinc_k := \sum_{n=0}^{k} \dfrac{\delta Eex}{(1 - fba_n) \cdot \eta_{ex}(1.5, 1)}$ (MJ) Eq 68 Eq 69

$Ebinc_{jm-2} = 5.2$ (MJ) 19 % beam to fuel coupling efficiency

Required incident beam power versus k $Pbinc_k := \dfrac{10^{-6} \cdot \delta Eex}{\delta t_{k+1} \cdot (1 - fba_k) \cdot \eta_{ex}(1.5, 1)}$ TW Eq 70

Incident beam intensity at radius r_k $Ibinc_k := Pbinc_k \cdot \left[4 \cdot \pi \cdot (r_k)^2\right]^{-1}$ TW/cm^2 Eq 71

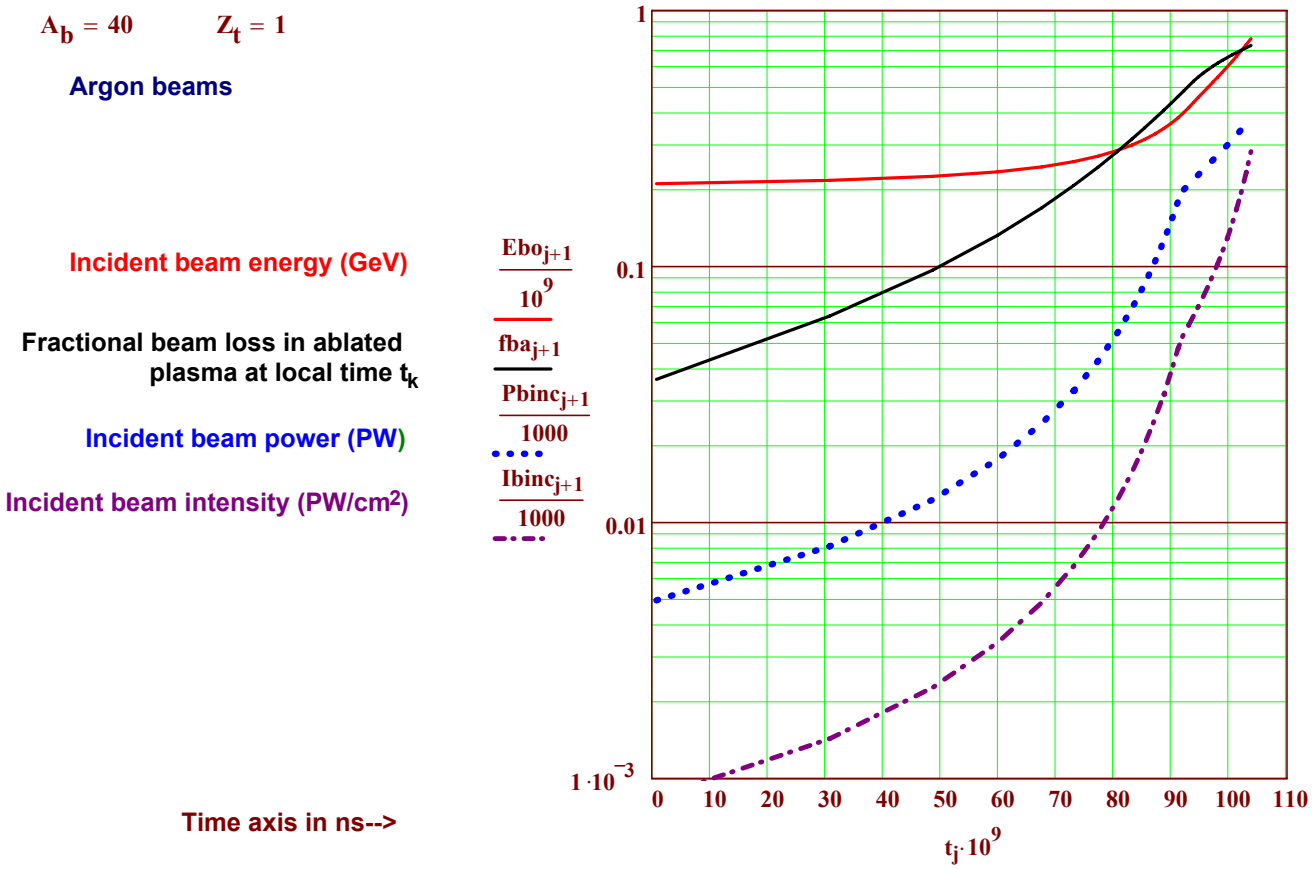

Figure. 21: Ion beam requirements for the Case A (Fig. 19) implosion example for Argon beams, 1 MJ fuel energy at stagnation--> 5.2 MJ total beam deposited , 19% total beam-to-fuel coupling efficiency.

This efficiency is still twice that of laser direct drive and 3 times more than for close-coupled indirect drive hohlraums. This case assumes zooming of the ion beam focus that follows the target ablator radius trajectory from $r_o = 0.7$ cm down to $r_f = 0.35$ cm over the 105 ns shaped pulse. Upstream beam time dependent focusing cab ability is included in the near term NDCX research agenda, because its required to correct for the effect of foot-to-peak velocity ramp with fixed final focus magnets on the focal spot radius. The velocity ramp is needed both to compress the accelerator bunches and here to provide the increasing ion range with time. Further requirements on time dependent upstream beam manipulations for target zooming (see work of Ed Lee in the HIF Skunkworks) will just become part of that same capability. Despite these features, the example shown in Fig. 15 is still not optimized because note the large fractional beam losses f_{ba} in the peak power region (roughly half the incoming beam is wasted on outgoing ablation plasma despite the Bragg peak shapes shown in Fig. 12. There are three possible ways to reduce the parasitic beam losses on ablated plasma, as discussed below:

(1) A final beam energy input in a spike 5 ns before the last ablator burns off would couple peak power with much less than the peak ablation loss fraction, and also, by the way, would launch a final shock, that, with judicious timing, could aid ignition a la Betti-Perkins shock ignition technique.

(2) While this simple numerical model for implosions assumes spherical symmetry, the actual beam geometry we are headed for is two-sided polar as in Fig. 4, where the beam is required to deliver the same pressure to the spherical ablation front, except with a different prescription for beam intensity and ion range as a function of polar angle and time for a symmetric implosion of the fuel payload. In 2-D, the ablated plasma gets heated much more in the beam channel than with spherical beam illumination, and can expand transverse to the beam faster, thus reducing the plasma density in the beam channel. Both effects are very roughly estimated below, in such a fashion that target designers will be motivated (or outraged enough) to get the right answer with 2-D hydro code runs.

(3) Move off the rocket curve peak efficiency towards lower mass ablation fractions like laser fusion, to see if lower mass fractions and higher exhaust velocities reduce parasitic the beam loss see Case C.

(1) Late-spike method of reducing beam losses on ablation plasma. Make beam input spike up at peak intensity before end of ablation: consider inertial time for final beam spike last 5 time steps @ k=25, @ t = 101 ns, 4 ns before the end of ablation @ t = 105 ns: remaining hydrogen ablator mass is 5 δM, and the ablation front is at 0.47 cm radius (about 2/3 of initial radius):

$\delta\rho rh_f := \frac{5\cdot\delta M}{4\cdot\pi\cdot(r_{24})^2}$ $\delta\rho rh_f = 0.0066$ Thickness $\delta rh_f := \frac{\delta\rho rh_f}{\rho_a}$ $\delta rh_f = 0.013$ cm $\rho_a = 0.5$ g/cm^3

Time δt_{hf} to input final beam energy E_{bf}: $\delta\tau h_f := \delta rh_f\cdot 10^{-6}\cdot\left(\frac{5\cdot pa_{24}}{3\cdot\rho_a}\right)^{-0.5}$ $\delta\tau h_f = 1.3\times 10^{-9}$ $pa_{24} = 32$ Mbar

Final beam energy increment $Eb_f := 5\cdot\frac{\delta Eex}{(1-fba_{24})\cdot\eta_{ex}(1.5,1)}$ $Eb_f = 1.23$ MJ $fba_{24} = 0.65$

Total beam energy input = $Ebinc_{23} + Eb_f = 4.76$ $Ebinc_{23} = 3.53$ --> One Petawatt final beam spike

Best case overall coupling efficiency @ 1 MJ fuel energy= $\frac{1}{Ebinc_{23}+Eb_f} = 0.21$ with a spike

Could the spike aid Betti-Perkins-type shock ignition? It might if the timing were adjusted!

Peak pressure in the spike $ps := \frac{10^{12}\cdot 10^{-11}\cdot Eb_f}{\left[4\cdot\pi\cdot(r_{24})^2\right]\cdot\delta rh_f}$ $ps = 402$ Mbar Eq 72

Shock speed $10^6\cdot\left(\frac{5\cdot ps}{3\cdot\rho_a}\right)^{0.5} = 3.66\times 10^7$ $\frac{r_{24}}{10^6\cdot\left(\frac{5\cdot ps}{3\cdot\rho_a}\right)^{0.5} + u_{imp}(1.5,1)} = 6.49\times 10^{-9}$ ns, Eq 73

Time to reach center

Maybe a bit too late, looking at Fig. 14, but can be adjusted to have the shock aid the ignition pressure.

(2) Estimate local reduction of ablated plasma column density in the beam channel for two sided drive.

First check conditions at crossover point when $\rho_a > \rho r_h$ (see Fig. 14) $t_{19} = 9.63\times 10^{-8}$

$M_{19} = 0.0567$ (half initial mass ablated)

In 2-D beam radius ~ ablation front radius: $r_{19} = 0.499$ (Assume beams occupy cylinder =radius r(t))

Beam energy *deposited in ablation plasma* up to that point (assuming the abated plasma doesn't move)

$Ebinc_{19} = 2.65$ $\frac{Eex_{19}}{\eta_{ex}(1.5,1)} = 1.62$ $Ebinc_{19} - \frac{Eex_{19}}{\eta_{ex}(1.5,1)} = 1.03$ MJ Eq 74

Now lets looks at characteristic plasma expansions versus time during the implosion

Beam deposition ΔEba (t,k) $Fbac := 0.5$ $\Delta Eba_k := Fbac\cdot\left(Ebinc_k - \frac{Eex_k}{\eta_{ex}(1.5,1)}\right)$ MJ Eq 75

Note the factor Fbac is inserted to make the net beam energy deposited smaller due to the ablated plasma expansion, it will be iterated to make the plasma expansion and beam deposition approx self consistent.

Mass of ablation plasma in the beam channel $\rho ra_{19} = 0.0097$ $2\cdot\rho ra_{19}\cdot\pi\cdot(r_{19})^2 = 0.0152$ g

$Mba_k := 2\cdot\rho ra_k\cdot\pi\cdot(r_{k+1})^2$ g Eq 76

Mean perpendicular velocity of heated ablation plasma within the channel:

$$v_{aperp}(\Delta E_{ba}, M_{ba}) := 10^2 \cdot \sqrt{\frac{5 \cdot \Delta E_{ba} \cdot 10^6}{3 \cdot M_{ba} \cdot 10^{-3}}} \quad \text{cm/s} \qquad \text{Eq 77}$$

$$vaperp_k := v_{aperp}(\Delta Eba_k, Mba_k) \qquad ta_j := t_j$$

Estimate characteristic reduction factor f_{ar} for ablation plasma density in the beam current channel due to expansion caused by integrated beam heating *prior to time t(k) over the remaining time of the total drive pulse in the beam channel.* (This characteristic method is optimistic in that expansion due to beam heating prior to time t(k) doesn't apply to incremental ablation mass added after time t(k), but is also pessimistic in that expansion after time t(k) doesn't account for additional beam deposition heating after time t(k).

$$far_k := (r_k)^2 \cdot \left[r_k + v_{aperp}(\Delta Eba_k, Mba_k) \cdot \left(\sum_{n=k}^{jm-1} \delta t_{n+1} \right) \right]^{-2} \qquad \text{Eq 78}$$

Now lets reduce all ρra's by the factor far: $\rho rb_k := \rho r_b(\rho ra_k \cdot far_k)$ g/cm^2 **Eq 79**

Fraction of ablated ρr in total beam ρr_b $\quad f\rho rc_k := \dfrac{\rho ra_k \cdot far_k}{\rho r_b(\rho ra_k \cdot far_k)}$ **Eq 80**

Fraction of beam energy in ablated plasma $\quad fbac_k := f_{ba}(\rho_a, \rho rb_k, f\rho rc_k, T_e, A_b, A_t, Z_b, Z_t)$ **Eq 81**

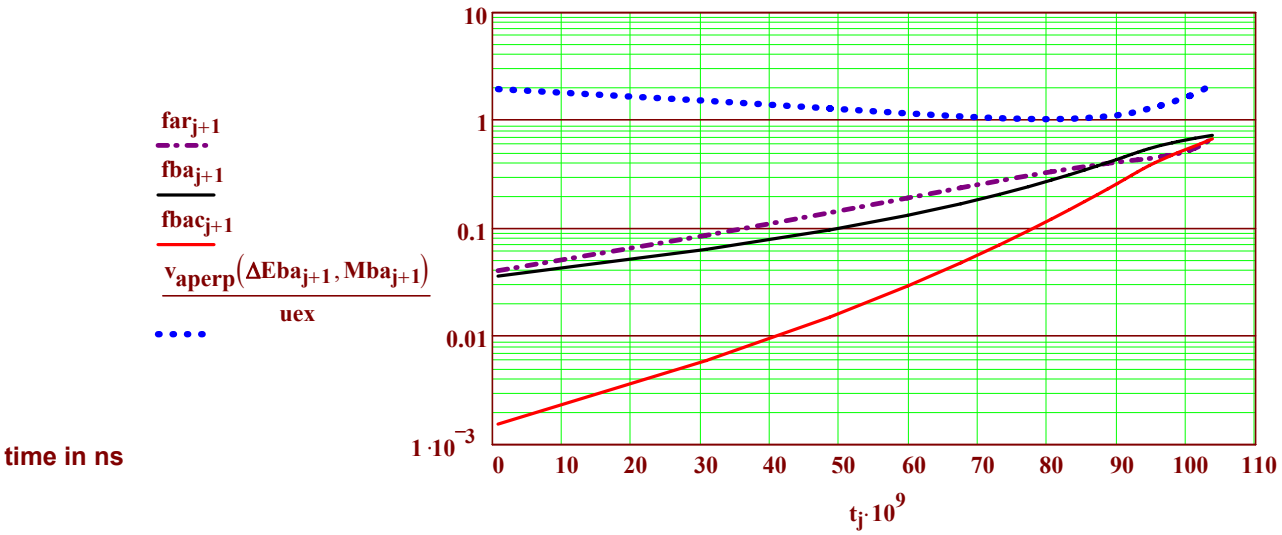

Figure 22: Ablated plasma expansion factors (column density ρr_a reduction factors) f_{ar}, and beam loss fractions without corrections for expansion f_{ba} (as in Fig 21) versus time during implosion and with corrections for expansion f_{bac} (red curve). Note that taking into account ablated plasma heating with expansion in the expected 2-D beam geometry reduces net beam attenuation significantly. The coefficient Fbac=0.5 used in the self consistent beam energy deposition was obtained from the value of fbac at the time of 96 ns when the remaining ablator ρrh equaled the ablated plasma ρra in Fig. 20. Actual 2-D hydro implosion calculations will be needed to get more accurate estimates of beam loss in 2-D. Note the net beam heating is sufficient to give perpendicular plasma expansion velocities comparable to the radial uex.

Now lets recompute Fig. 21 with the corrected (reduced) parasitic beam loss fractions f_{bac}:

Incident beam ion K.E. $Ebo_k := E_{bf}(\rho_a, \rho rb_k, 0.01, T_e, A_b, A_t, Z_b, Z_t)$ MeV

Required incident beam energy integrated up to time t_k $Ebinc_k := \sum_{n=0}^{k} \frac{\delta Eex}{(1 - fbac_n)\cdot \eta_{ex}(1.5, 1)}$ (MJ)

$Ebinc_{jm-2} = 4.06$ $\eta_{dfA} := 1\cdot(Ebinc_{jm-2})^{-1}$ $\eta_{dfA} = 0.25$ <--beam to fuel coupling efficiency!

Required incident beam power versus k $Pbinc_k := \frac{10^{-6}\cdot \delta Eex}{\delta t_{k+1}\cdot(1 - fbac_k)\cdot \eta_{ex}(1.5, 1)}$ TW

Incident beam intensity at radius r_k $Ibinc_k := Pbinc_k\cdot\left[4\cdot\pi\cdot(r_k)^2\right]^{-1}$ TW/cm^2

$A_b = 40$ $Z_t = 1$

Argon beams

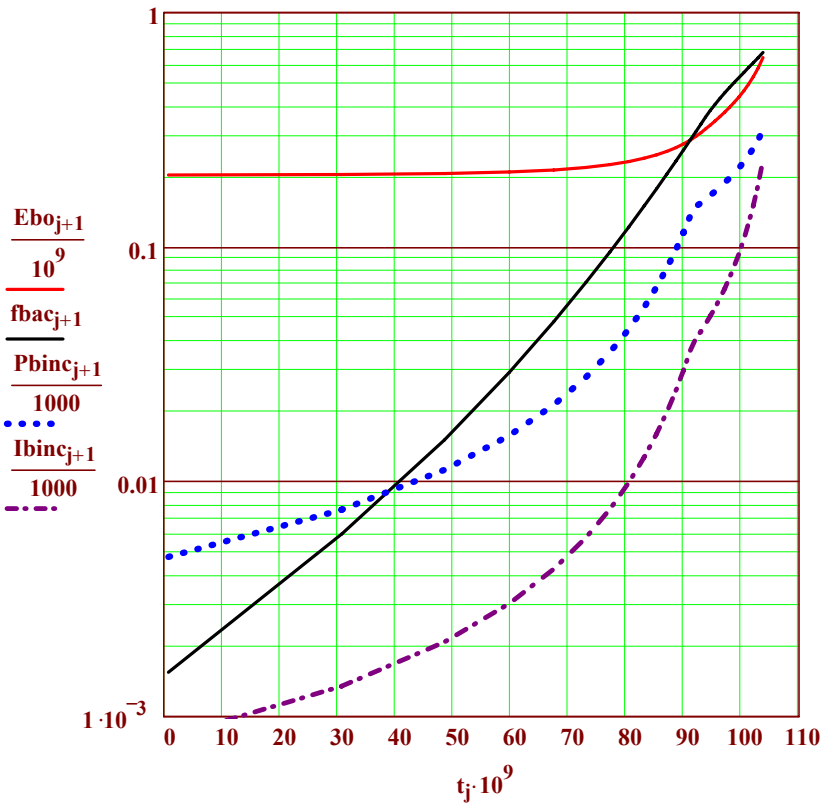

Incident beam energy (GeV)

Fractional beam loss in ablated plasma at local time t_k

Incident beam power (PW)

Incident beam intensity (PW/cm^2)

Time axis in ns-->

Fig. 23: Ion beam requirements for the Case A (Fig. 14) implosion example for Argon beams, 1 MJ fuel energy at stagnation, corrected for 2-D expansion of ablated plasma due to beam heating --> 4 MJ total beam deposited , 25% total beam-to-fuel coupling efficiency. This efficiency is 2.5 X that of laser direct drive and 4 times more than for close-coupled indirect drive hohlraums. This case assumes zooming of the ion beam focus that follows the target ablator radius trajectory from $r_o = 0.7$ cm down to $r_f = 0.35$ cm over the 105 ns shaped pulse.

Upstream beam time dependent focusing capability is included in the near term NDCX research agenda, because its required to correct for the effect of foot-to-peak velocity ramp with fixed final focus magnets on the focal spot radius. The velocity ramp is needed both to compress the accelerator bunches and here to provide the increasing ion range with time. Further requirements on time dependent upstream beam manipulations for target zooming (see work of Ed Lee in the HIF Skunkworks) will just become part of that same capability.

Case B: Small DEMO at the peak of rocket efficiency = 0.65 (M_o/M_f =5)

Fuel energy E_f = 0.2 MJ (nominal driver E_{binc} = 0.8 MJ@ 20% overall coupling efficiency

Compressed D fuel density

$\rho_{cdd}(1.5, 0.2) = 1067$ g/cm^3

Rho-r total at stagnation

$\rho r(1.5, 0.2) = 7.3$ g/cm^2

Net T-mass produced

$M_{tn}(1.5, 0.2)\cdot 10^3 = 0.005$ mg

Hot spot DT radius

$r_{hdt}(0.2)\cdot 10^4 = 28$ microns

D-burn fraction

$f_{bd}(1.5, 0.2) = 0.047$

Neutrons per T burned

$N_{ndd}(1.5, 0.2) = 2.2$

Initial Outer -D radius

$r_{cdd}(0.2)\cdot 10^4 = 91$ microns

T-burn fraction

$f_{bt}(1.5, 0.2) = 0.426$

Outer blanket shell radius

$r_{bo}(1.5, 0.2) = 4.9$ cm

D Mass load

$M_d(1.5, 0.2)\cdot 10^3 = 3.3$ mg

Fusion yield

$Y_f(1.5, 0.2) = 43$ MJ

Fraction of yield captured

$1 - FY_{nb}(1.5, 0.2) = 0.73$

$ORIGIN := 0$ $jm := 31$ $\chi := \frac{0.5\cdot jm}{(0.5\cdot jm + 1)^3}$ $\chi = 0.0035$ $\delta to := 95\cdot 10^{-9}$ s

$j := 0 .. jm$ $k := 0 .. jm - 2$ $\delta t_j := \left[\Phi\left[\frac{j}{(j+1)^3} - \chi\right]\cdot\frac{j}{(j+1)^3} + \Phi\left[\chi - \frac{j}{(j+1)^3}\right]\cdot\chi\right]\cdot\delta to$ $t_j := \sum_{n=0}^{j} \delta t_n$

$jm - 1 = 30$ $M_0 := 1.25\cdot M_h(1.5, 0.2)$ $M_0 = 0.0167$ g $\delta M := \frac{0.8}{jm - 1}\cdot M_0$

$(jm - 1)\cdot\delta M = 0.013$ $M_0 := M_0$ $0.8\cdot M_0 = 0.013$ $M_j := M_0 - j\cdot\delta M$

$M_d(1.5, 0.2) + M_t(1.5, 0.2) = 3.3414\times 10^{-3}$ $\delta M = 4.46\times 10^{-4}$ $0.8\cdot M_0\cdot(jm - 1)^{-1} = 4.46\times 10^{-4}$

$uex := u_{ex}(1.5, 0.2)$ $uex = 2.15\times 10^7$ $u_j := uex\cdot\ln\left(\frac{M_0}{M_j}\right)$ $u_{imp}(1.5, 0.2) = 3.46\times 10^7$ $Ma_0 := 0$

$Ma_j := M_0 - M_j$ $Eex_j := 0.5\cdot 10^{-13}\cdot Ma_j\cdot uex^2 + 10^{-5}$ $Ep_j := 0.5\cdot 10^{-13}\cdot M_j\cdot(u_j)^2$

$r_0 := r_{ao}(1.5, 0.2)$ $r_0 = 0.371$ cm $0.5\cdot r_0 = 0.186$ $r_0 := r_0$ $\delta r_k := \frac{u_{k+1} + u_k}{2}\cdot\delta t_{k+1}$

$r_k := r_0 - \sum_{n=0}^{k}(\delta r_n)$ $Pex_k := \frac{(Eex_{k+1} - Eex_k)\cdot 10^6}{\delta t_{k+1}}$ $\sum_{n=0}^{jm-2}(Pex_n\cdot\delta t_{n+1}) = 3.09\times 10^5$

$ua_k := uex - u_k$ $r_{jm-1} := 0.175$ $ra_k := r_k + ua_k\cdot\sum_{n=k}^{jm-2}\delta t_{n+1}$ $\delta pa_k := \delta M\cdot\left[4\cdot\frac{\pi}{3}\left[(ra_k)^3 - (r_{k+1})^3\right]\right]^{-1}$

$\delta pra_k := \delta pa_k\cdot(ra_k - r_{k+1})$ $pra_k := \sum_{n=0}^{k}\delta pra_n$ $prh_k := \frac{0.8\cdot M_0 - k\cdot\delta M}{4\cdot\pi\cdot(r_k)^2}$ g/cm^2

Ablation pressure $pa_k := \frac{10^{-12}\cdot\delta M\cdot uex}{\delta t_{k+1}\cdot\left[4\cdot\pi\cdot(r_{k+1})^2\right]}$ MBar

$\delta Eex := 0.5\cdot 10^{-13}\cdot\delta M\cdot uex^2$

$\delta Eex = 0.0103$ MJ

Table 8. Parameters during implosion for the small DEMO case B

$Pex_{30} := 31 \cdot 10^{12}$ $r_{30} := 0.186$ $ra_{30} := 0.19$ $\rho ra_{30} := 12.9 \cdot 10^{-3}$ $\rho rh_{30} := 0$ $pa_{30} := 80$

$\frac{t_m}{10^{-9}} =$	$\frac{M_m}{10^{-3}} =$	$\frac{u_m}{10^{7}} =$	$Eex_m =$	$Ep_m =$	$\frac{Ep_m}{Eex_m} =$	$\frac{Pex_m}{10^{12}} =$	$r_m =$	$ra_m =$	$\frac{\rho ra_m}{10^{-3}} =$	$\frac{\rho rh_m}{10^{-3}} =$	$pa_m =$
0.3	16.7	0	0	0	0	1	0.37	1.26	0.05	7.86	0.5
19.2	15.8	0.12	0.02	0.0011	0.05	2	0.36	0.81	0.22	7.87	1.4
26.7	14.9	0.24	0.04	0.0044	0.11	5	0.34	0.63	0.5	7.85	3.1
30.6	14	0.37	0.06	0.0099	0.16	8	0.33	0.53	0.85	7.73	5.5
32.9	13.1	0.52	0.08	0.0175	0.21	12	0.32	0.47	1.29	7.52	8.8
34.5	12.3	0.67	0.1	0.0272	0.26	17	0.31	0.42	1.8	7.23	13.2
35.6	11.4	0.83	0.12	0.039	0.32	23	0.31	0.39	2.38	6.85	18.6
36.5	10.5	1	0.14	0.0528	0.37	30	0.3	0.36	3.03	6.4	25.3
37.1	9.6	1.2	0.16	0.0685	0.42	31	0.29	0.33	3.75	5.91	28.5
37.8	8.7	1.41	0.19	0.0858	0.46	31	0.28	0.31	4.55	5.4	30.6
38.5	7.8	1.64	0.21	0.1046	0.51	31	0.27	0.29	5.46	4.87	33.4
39.1	6.9	1.9	0.23	0.1246	0.55	31	0.26	0.26	6.5	4.28	37.1
39.8	6	2.2	0.25	0.1451	0.59	31	0.24	0.24	7.7	3.6	42.1
40.4	5.1	2.54	0.27	0.1654	0.62	31	0.23	0.22	9.11	2.77	49.4
41.1	4.2	2.95	0.29	0.1844	0.64	31	0.21	0.2	10.82	1.66	60.5
41.7	3.3	3.46	0.31	0.2	0.65	31	0.19	0.19	12.9	0	80

Figure 24: Case B DEMO implosion characteristics at the peak rocket efficiency ($M_o/M_f = 5$) for a fuel payload energy E_f=0.2MJ, final $\rho r_f = 7.3$ g/cm^2.

Ablation front radius r(cm)

Exhaust energy E_{ex}(MJ)

Ablation pressure p_a (in100 Mbar units)

Rocket K.E. power P_{ex} (in 100 TW units). (required beam power is roughly 3 X higher)

Time axis in ns

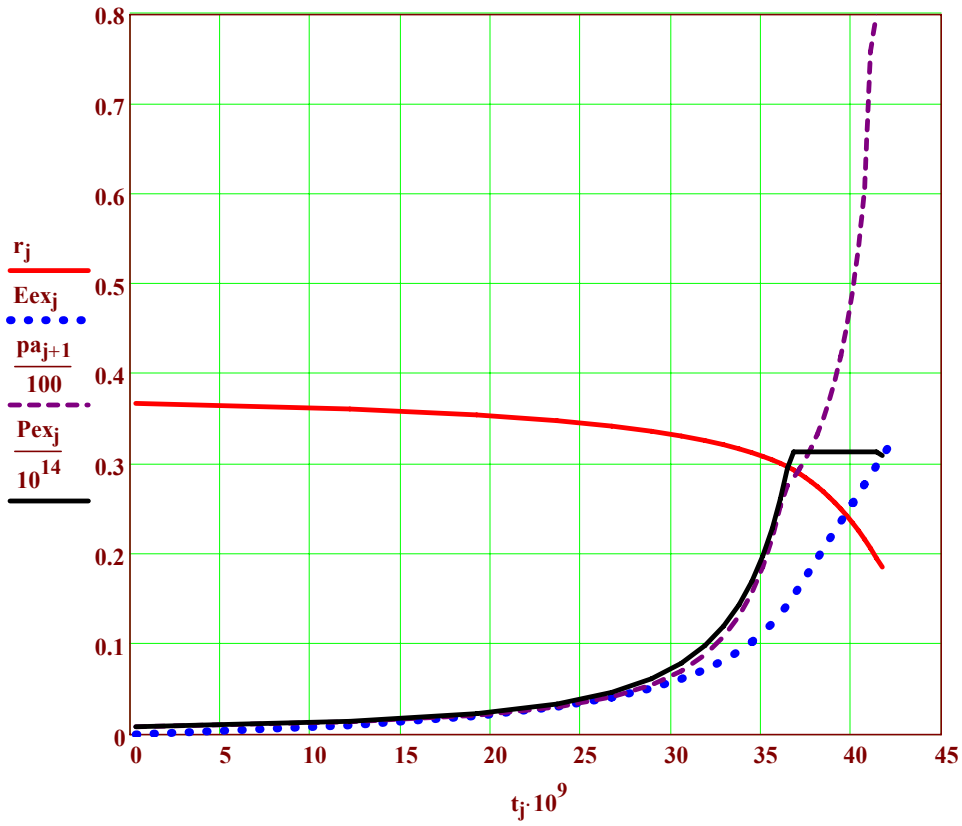

Given beam range penetrating ablator $\delta\rho r_{bh} := 0.002$ g/cm^2 (assumed constant) must be small fraction of total initial ablator ρr_{ho}

Required beam range versus t(k) $\rho r_b(\rho r_a) := \rho r_a + \delta\rho r_{bh}$ $\rho rb_k := \rho r_b(\rho ra_k)$ g/cm^2

Fig. 25: Case B Column densities (ρr)'s: (g/cm^2 units)

Beam range in ablator $\delta\rho r_{bh}$

Ablated plasma ρr_a (dotted)

Total req. beam range incident

Remaining ablator ρr_h

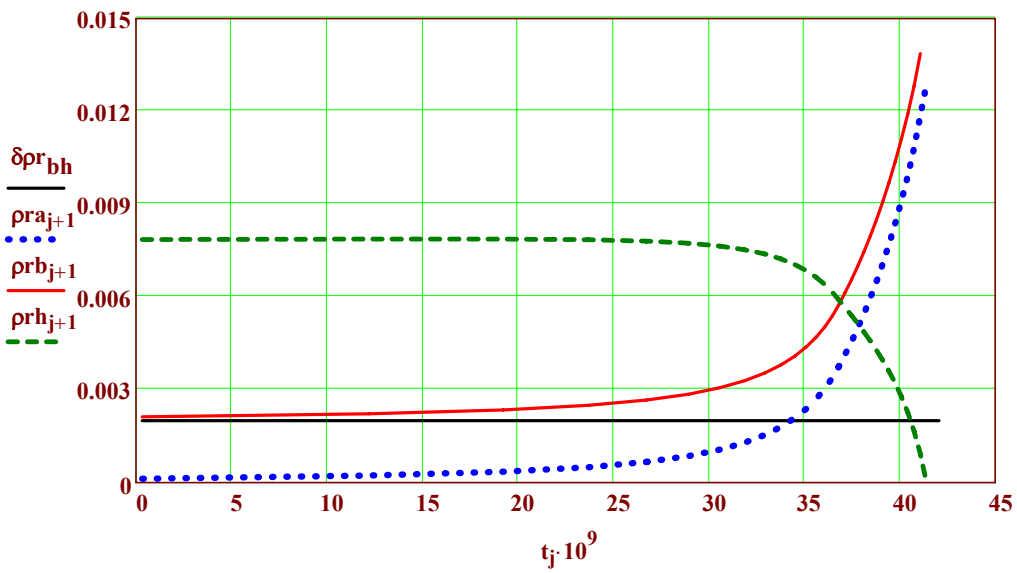

Time in ns

Calculation of ion beam requirements for Case B-DEMO (Fig. 24)

$A_b = 40$

$\delta M = 4.4553 \times 10^{-4}$ $\rho_a = 0.5$ $A_{if} = 15$ $uex = 2.15 \times 10^7$ $Z_b = 18$

Fraction of ablated ρr in total beam ρr_b $f\rho r_k := \dfrac{\rho ra_k}{\rho r_b(\rho ra_k)}$

Fraction of beam energy in ablated plasma $fba_k := f_{ba}(\rho_a, \rho rb_k, f\rho r_k, T_e, A_b, A_t, Z_b, Z_t)$

Required incident beam energy integrated up to time t_k $Ebinc_k := \sum_{n=0}^{k} \dfrac{\delta Eex}{(1 - fba_n)\cdot\eta_{ex}(1.5, 0.2)}$ (MJ)

Beam deposition ΔEba (t,k) $Fbac := 0.5$ $\Delta Eba_k := Fbac\cdot\left(Ebinc_k - \dfrac{Eex_k}{\eta_{ex}(1.5, 1)}\right)$ MJ

Note the factor Fbac is inserted to make the net beam energy deposited smaller due to the ablated plasma expansion, it will be iterated to make the plasma expansion and beam deposition approx self consistent.

Characteristic reduction factor f_{ar} for ablation plasma density in the beam current channel due to expansion caused by integrated beam heating *prior to time t(k) over the remaining time of the total drive pulse in the beam channel.* (This characteristic method is optimistic in that expansion due to beam heating prior to time t(k) doesn't apply to incremental ablation mass added after time t(k), but is also pessimistic in that expansion after time t(k) doesn't account for additional beam deposition heating after time t(k).

$Mba_k := 2 \cdot \rho ra_k \cdot \pi \cdot (r_{k+1})^2$ g

$far_k := (r_k)^2 \cdot \left[r_k + v_{aperp}(\Delta Eba_k, Mba_k) \cdot \left(\sum_{n=k}^{jm-1} \delta t_{n+1} \right) \right]^{-2}$

Now lets reduce all ρra's by the factor far: $\rho rb_k := \rho r_b(\rho ra_k \cdot far_k)$ g/cm²

Fraction of ablated ρr in total beam ρr_b $f\rho rc_k := \dfrac{\rho ra_k \cdot far_k}{\rho r_b(\rho ra_k \cdot far_k)}$

Fraction of beam energy in ablated plasma $fbac_k := f_{ba}(\rho_a, \rho rb_k, f\rho rc_k, T_e, A_b, A_t, Z_b, Z_t)$

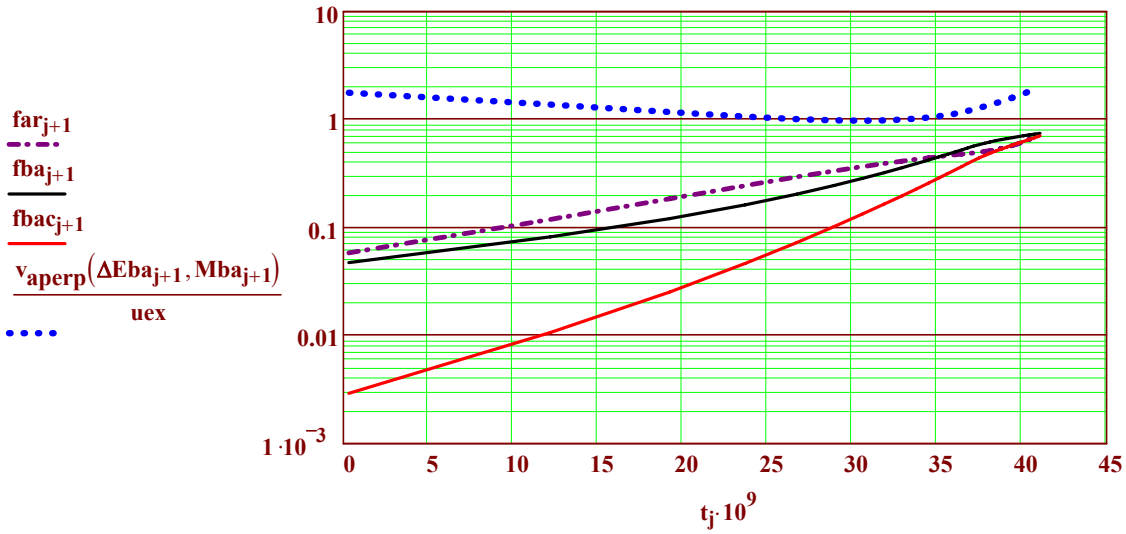

time in ns

Figure 26: Ablated plasma expansion factors (column density ρr_a reduction factors) f_{ar}, and beam loss fractions without corrections for expansion f_{ba} (For Case B as in Fig 24) versus time during implosion and with corrections for expansion f_{bac} (red curve). Note that taking into account ablated plasma heating with expansion in the expected 2-D beam geometry reduces net beam attenuation significantly. The coefficient Fbac=0.5 used in the self consistent beam energy deposition was obtained from the value of fbac at the time of 38 ns when the remaining ablator ρrh equaled the ablated plasma ρr_a in Fig. 25. Actual 2-D hydro implosion calculations will be needed to get more accurate estimates of beam loss in 2-D. Note the net beam heating is sufficient to give perpendicular plasma expansion velocities comparable to the radial uex.

Incident beam ion K.E. $Ebo_k := E_{bf}(\rho_a, \rho rb_k, 0.01, T_e, A_b, A_t, Z_b, Z_t)$ MeV

Required incident beam energy integrated up to time t_k $Ebinc_k := \sum_{n=0}^{k} \dfrac{\delta Eex}{(1 - fbac_n) \cdot \eta_{ex}(1.5, 0.2)}$ (MJ)

$Ebinc_{jm-2} = 0.85$ $\eta_{dfB} := 0.2 \cdot (Ebinc_{jm-2})^{-1}$ $\eta_{dfB} = 0.24$ <--23 % beam to fuel coupling efficiency for DEMO

Required incident beam power versus k $Pbinc_k := \frac{10^{-6} \cdot \delta Eex}{\delta t_{k+1} \cdot (1 - fbac_k) \cdot \eta_{ex}(1.5, 0.2)}$ TW

Incident beam intensity at radius r_k $Ibinc_k := Pbinc_k \cdot \left[4 \cdot \pi \cdot (r_k)^2\right]^{-1}$ TW/cm^2

$A_b = 40$ $Z_t = 1$

Argon beams

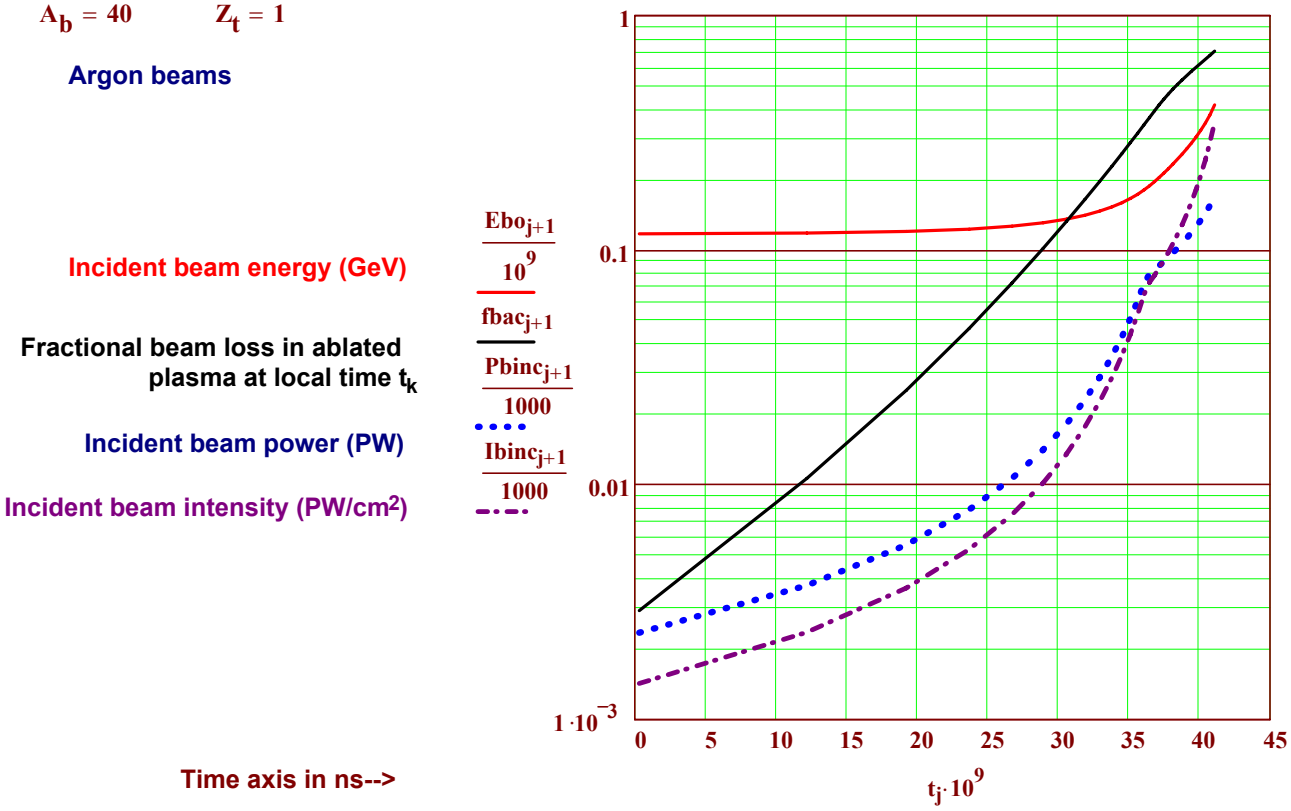

Figure 27. Beam requirements for the Case B -DEMO at the peak of rocket efficiency: 24 % overall beam-to-fuel coupling efficiency.

Implosion Dynamics Case C: at rocket efficiency ~0.5 (M_o/M_f =2 ->more like laser direct drive)

We investigate this case even though the rocket efficiency is lower (see Fig. 10) in hopes that the reduced ablator mass and higher exhaust velocities will reduce incoming ion beam losses on ablated plasma.

$M_h(\alpha, E_f) := M_d(\alpha, E_f) + M_t(\alpha, E_f)$ $M_h(1.5, 1) = 0.023$ $u_{ex}(\alpha, E_f) := u_{imp}(\alpha, E_f) \cdot \ln(2)^{-1}$

Given Initial guesses $r_{ag} := 0.5$ cm $\delta D := 0.1$ cm

$$\delta D = \left[\left(\frac{3 \cdot M_d(\alpha, E_f)}{4 \cdot \pi \cdot \rho_{Do}}\right) + (\xi \cdot r_{ag})^3\right]^{0.333} - \xi \cdot r_{ag} \qquad r_{ag} = \left[\left(\frac{3 \cdot M_h(\alpha, E_f)}{4 \cdot \pi \cdot \rho_{Ho}}\right) + (\xi \cdot r_{ag} + \delta D)^3\right]^{0.333}$$

$Sol(\alpha, E_f) := Find(\delta D, r_{ag})$

$\delta D_0(\alpha, E_f) := Sol(\alpha, E_f)_0$ Initial D2 layer thickness

$r_{ao}(\alpha, E_f) := Sol(\alpha, E_f)_1$ Initial outer H2 ablator radius $r_{ao}(1.5, 1) = 0.489$

ORIGIN := 0 $jm := 31$ $\chi := \frac{0.5 \cdot jm}{(0.5 \cdot jm + 1)^3}$ $\chi = 0$ $\delta to := 130 \cdot 10^{-9}$ s

$j := 0 .. jm$ $k := 0 .. jm - 2$

$$\delta t_j := \left[\Phi\left[\frac{j}{(j+1)^3} - \chi\right] \cdot \frac{j}{(j+1)^3} + \Phi\left[\chi - \frac{j}{(j+1)^3}\right] \cdot \chi\right] \cdot \delta to \qquad t_j := \sum_{n=0}^{j} \delta t_n$$

$jm - 1 = 30$ $M_0 := 2 \cdot M_h(1.5, 1)$ $M_0 = 0.046$ g $\delta M := \frac{0.5}{jm - 1} \cdot M_0$

$(jm - 1) \cdot \delta M = 0.023$ $M_0 := M_0$ $0.5 \cdot M_0 = 0.023$ $M_j := M_0 - j \cdot \delta M$

$M_d(1.5, 1) + M_t(1.5, 1) = 0.023$ $\delta M = 7.6601 \times 10^{-4}$ $0.5 \cdot M_0 \cdot (jm - 1)^{-1} = 7.6601 \times 10^{-4}$

$uex := u_{ex}(1.5, 1)$ $uex = 4.26 \times 10^7$ $u_j := uex \cdot \ln\left(\frac{M_0}{M_j}\right)$ $u_{imp}(1.5, 1) = 2.95 \times 10^7$ $Ma_0 := 0$

$Ma_j := M_0 - M_j$ $Eex_j := 0.5 \cdot 10^{-13} \cdot Ma_j \cdot uex^2 + 10^{-5}$ $Ep_j := 0.5 \cdot 10^{-13} \cdot M_j \cdot (u_j)^2$

$r_0 := r_{ao}(1.5, 1)$ $r_0 = 0.489$ cm $0.5 \cdot r_0 = 0.244$ $r_0 := r_0$ $\delta r_k := \frac{u_{k+1} + u_k}{2} \cdot \delta t_{k+1}$

$$r_k := r_0 - \sum_{n=0}^{k} (\delta r_n) \qquad Pex_k := \frac{(Eex_{k+1} - Eex_k) \cdot 10^6}{\delta t_{k+1}} \qquad \sum_{n=0}^{jm-2} (Pex_n \cdot \delta t_{n+1}) = 2.08 \times 10^6$$

$ua_k := uex - u_k$ $r_{jm-1} := 0.22$ $ra_k := r_k + ua_k \cdot \sum_{n=k}^{jm-2} \delta t_{n+1}$ $\delta pa_k := \delta M \cdot \left[4 \cdot \frac{\pi}{3}\left[(ra_k)^3 - (r_{k+1})^3\right]\right]^{-1}$

$\delta pra_k := \delta pa_k \cdot (ra_k - r_{k+1})$ $pra_k := \sum_{n=0}^{k} \delta pra_n$ $prh_k := \frac{0.5 \cdot M_0 - k \cdot \delta M}{4 \cdot \pi \cdot (r_k)^2}$ g/cm²

Ablation pressure $pa_k := \frac{10^{-12} \cdot \delta M \cdot uex}{\delta t_{k+1} \cdot \left[4 \cdot \pi \cdot (r_{k+1})^2\right]}$ MBar $\delta Eex := 0.5 \cdot 10^{-13} \cdot \delta M \cdot uex^2$

Table 9. Parameters during implosion for the Mo/Mf =2 case C

$Pex_{30} := 155 \cdot 10^{12}$ $r_{30} := 0.21$ $ra_{30} := 0.22$ $\rho ra_{30} := 12 \cdot 10^{-3}$ $\rho rh_{30} := 0$ $pa_{30} := 130$

$\frac{t_m}{10^{-9}} =$	$\frac{M_m}{10^{-3}} =$	$\frac{u_m}{10^{7}} =$	$Eex_m =$	$Ep_m =$	$\frac{Ep_m}{Eex_m} =$	$\frac{Pex_m}{10^{12}} =$	$r_m =$	$ra_m =$	$\frac{\rho ra_m}{10^{-3}} =$	$\frac{\rho rh_m}{10^{-3}} =$	$pa_m =$
0.4	46	0	0	0	0	4	0.48	2.89	0.02	7.8	0.7
26.3	44	0.14	0.14	0.005	0.03	11	0.46	1.73	0.1	8	2.1
36.6	43	0.29	0.28	0.018	0.07	23	0.44	1.25	0.24	8.2	4.6
41.9	41	0.45	0.42	0.042	0.1	39	0.42	1	0.45	8.2	8.5
45.1	40	0.61	0.56	0.074	0.13	59	0.41	0.85	0.73	8.1	13.9
47.2	38	0.78	0.69	0.115	0.17	84	0.39	0.74	1.09	7.9	20.9
48.8	37	0.95	0.83	0.166	0.2	113	0.38	0.66	1.52	7.6	30
49.9	35	1.13	0.97	0.225	0.23	146	0.37	0.59	2.02	7.2	41.2
50.8	34	1.32	1.11	0.294	0.26	155	0.36	0.54	2.6	6.7	47
51.7	32	1.52	1.25	0.371	0.3	155	0.34	0.49	3.28	6.2	51.1
52.6	31	1.73	1.39	0.456	0.33	155	0.33	0.44	4.08	5.7	56.5
53.5	29	1.94	1.53	0.55	0.36	155	0.31	0.39	5.03	5	63.7
54.4	28	2.17	1.67	0.652	0.39	155	0.29	0.35	6.2	4.3	73.3
55.3	26	2.42	1.8	0.761	0.42	155	0.27	0.3	7.66	3.4	86.9
56.2	25	2.68	1.94	0.877	0.45	155	0.25	0.26	9.55	2	106.8
57.1	23	2.95	2.08	1	0.48	155	0.21	0.22	12	0	130

Fig. 28: Case C
E_f = 1 MJ implosion dynamics for lower mass ablator case M_o/M_f = 2 (more laser-like rocket)

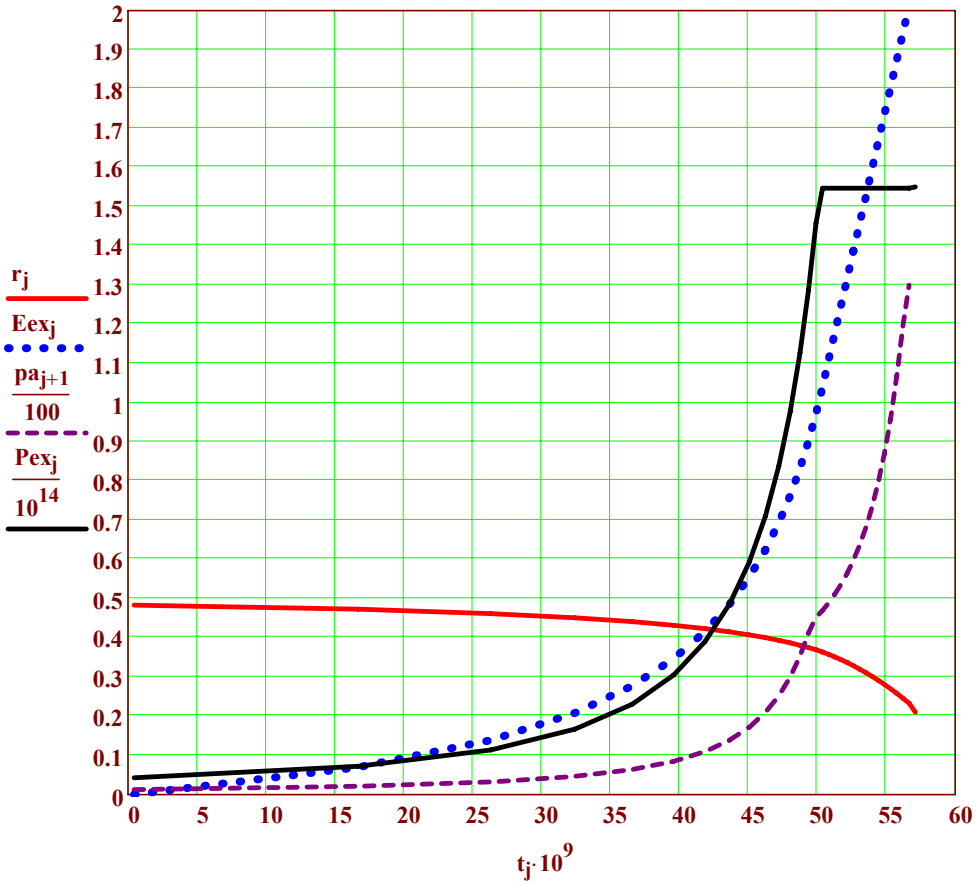

Ablation front radius r(cm)

Exhaust energy E_{ex}(MJ)
Ablation pressure p_a (in100 Mbar units)

Rocket K.E. power P_{ex} (in 100 TW units). (required beam power is roughly 3 X higher)

Time axis in ns

Given beam range penetrating ablator $\delta\rho r_{bh} := 0.002$ g/cm^2 (assumed constant) must be small fraction of total initial ablator ρr_{ho}

Required beam range versus t(k) for case C $\rho r_b(\rho r_a) := \rho r_a + \delta\rho r_{bh}$ $\rho rb_k := \rho r_b(\rho ra_k)$ g/cm^2

Fig. 29: Case B Column densities (ρr)'s: (g/cm^2 units)

Beam range in ablator $\delta\rho r_{bh}$

Ablated plasma ρr_a (dotted)

Total req. beam range incident

Remaining ablator ρr_h

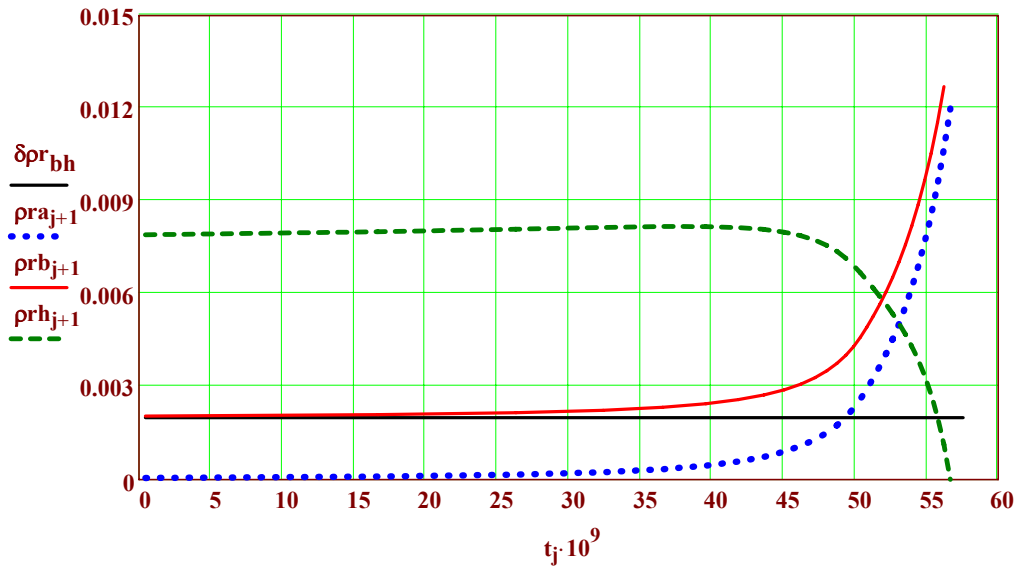

Time in ns

Calculation of ion beam requirements for Case C Power Plant M_o/M_f = 2 (Fig. 28)

$\delta M = 7.66\times10^{-4}$ $\rho_a = 0.5$ $A_{if} = 15$ $uex = 4.26\times10^{7}$ $A_b = 40$

$T_{ex}(\alpha, E_f) := 3\cdot10^{-4}\cdot m_h\cdot u_{ex}(\alpha, E_f)^2\cdot200^{-2}\cdot(1.6\cdot10^{-19})^{-1}$ $T_{ex}(1.5, 1) = 142$ eV

$E_{da}(\alpha, E_f) := 0.5\cdot10^{-13}\cdot M_h(\alpha, E_f)\cdot u_{ex}(\alpha, E_f)^2 \ldots$
$+ (13.6\cdot2 + 3\cdot T_{ex}(\alpha, E_f))\cdot1.6\cdot10^{-25}\cdot M_h(\alpha, E_f)\cdot m_h^{-1} \ldots$
$+ E_{cs}(\alpha, E_f)$

$\eta_{ex}(\alpha, E_f) := 0.5\cdot10^{-13}\cdot M_h(\alpha, E_f)\cdot u_{ex}(\alpha, E_f)^2\cdot E_{da}(\alpha, E_f)^{-1}$

Fraction of ablated ρr in total beam ρr_b $f\rho r_k := \dfrac{\rho ra_k}{\rho r_b(\rho ra_k)}$ $Z_b = 18$

Fraction of beam energy in ablated plasma $fba_k := f_{ba}(\rho_a, \rho rb_k, f\rho r_k, T_e, A_b, A_t, Z_b, Z_t)$

Required incident beam energy integrated up to time t_k $Ebinc_k := \sum_{n=0}^{k} \dfrac{\delta Eex}{(1 - fba_n)\cdot\eta_{ex}(1.5, 1)}$ (MJ)

Beam deposition ΔEba (t,k) $Fbac := 0.4$ $\Delta Eba_k := Fbac\cdot\left(Ebinc_k - \dfrac{Eex_k}{\eta_{ex}(1.5, 1)}\right)$ MJ

$Mba_k := 2 \cdot \rho ra_k \cdot \pi \cdot (r_{k+1})^2$ g

$far_k := (r_k)^2 \cdot \left[r_k + v_{aperp}(\Delta Eba_k, Mba_k) \cdot \left(\sum_{n=k}^{jm-1} \delta t_{n+1} \right) \right]^{-2}$

Now lets reduce all ρra's by the factor far: $\rho rb_k := \rho r_b(\rho ra_k \cdot far_k)$ g/cm²

Fraction of ablated ρr in total beam ρr_b $f\rho rc_k := \frac{\rho ra_k \cdot far_k}{\rho r_b(\rho ra_k \cdot far_k)}$

Fraction of beam energy in ablated plasma $fbac_k := f_{ba}(\rho_a, \rho rb_k, f\rho rc_k, T_e, A_b, A_t, Z_b, Z_t)$

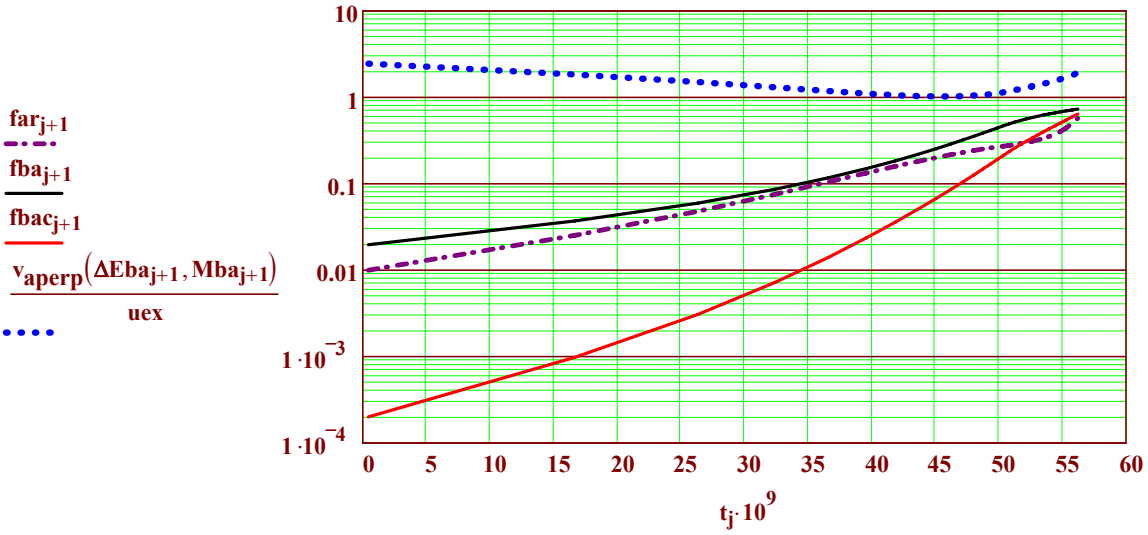

Figure 30: Ablated plasma expansion factors (column density ρr_a reduction factors) f_{ar}, and beam loss fractions without corrections for expansion f_{ba} (For case C as in Fig 28) versus time during implosion and with corrections for expansion f_{bac} (red curve). Note that taking into account ablated plasma heating with expansion in the expected 2-D beam geometry reduces net beam attenuation significantly. The coefficient Fbac=0.4 used in the self consistent beam energy deposition was obtained from the value of fbac at the time of 53 ns when the remaining ablator ρrh equaled the ablated plasma ρra in Fig. 29. Actual 2-D hydro implosion calculations will be needed to get more accurate estimates of beam loss in 2-D. Note the net beam heating is sufficient to give perpendicular plasma expansion velocities comparable to the radial uex.

Incident beam ion K.E. $Ebo_k := E_{bf}(\rho_a, \rho rb_k, 0.01, T_e, A_b, A_t, Z_b, Z_t)$ MeV

Required incident beam energy integrated up to time t_k $Ebinc_k := \sum_{n=0}^{k} \frac{\delta Eex}{(1 - fbac_n) \cdot \eta_{ex}(1.5, 1)}$ (MJ)

$Ebinc_{jm-2} = 4.39$ <--23 % beam to fuel coupling efficiency- 2 % less than for M_o/M_f =5 Case A

Required incident beam power versus k $Pbinc_k := \frac{10^{-6} \cdot \delta Eex}{\delta t_{k+1} \cdot (1 - fbac_k) \cdot \eta_{ex}(1.5, 1)}$ TW

Incident beam intensity at radius r_k $Ibinc_k := Pbinc_k \cdot \left[4 \cdot \pi \cdot (r_k)^2 \right]^{-1}$ TW/cm²

$A_b = 40$ $Z_t = 1$

Argon beams

Incident beam energy (GeV)

Fractional beam loss in ablated plasma at local time t_k

Incident beam power (PW)

Incident beam intensity (PW/cm^2)

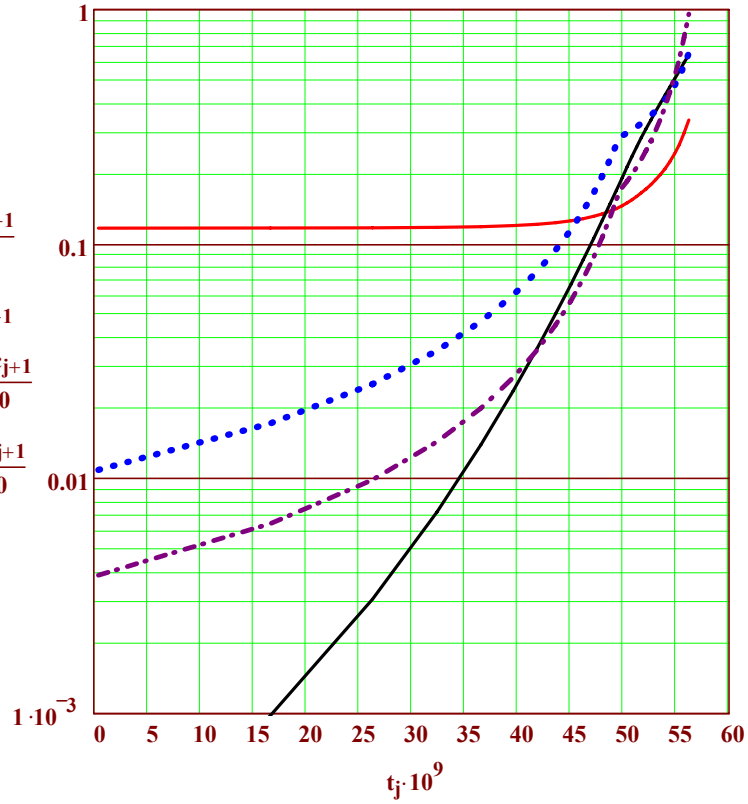

Time axis in ns-->

Figure 31. Beam requirements for the Case C -M_o/M_f =2 laser-like ablation regime. This case gives 2 % less coupling efficiency than Case A -M_o/M_f =5, and has considerably more difficult beam requirements (~three times the peak beam power and intensity, 40% smaller focal spot radius, and at half the beam ion kinetic energy --much much higher combined difficulty for the modular induction driver to deliver. In addition, the ablator energy density and ablation front stagnation temperature ~ 100 eV is no longer optically thick to bremstrahlung radiation, so that preheat cannot be neglected in this case as it can be in Case A, or one must a small amount of carbon (plastic) to increase opacity.

Lets now change back to the M_o/M_f = 5 case with higher rocket efficiency for the 2-D calculations.

$$M_h(\alpha, E_f) := 4\cdot\left(M_d(\alpha, E_f) + M_t(\alpha, E_f)\right) \qquad M_h(1.5, 1) = 0.092$$

$$u_{ex}(\alpha, E_f) := u_{imp}(\alpha, E_f)\cdot \ln(5)^{-1} \qquad u_{ex}(1.5, 1) = 1.83\times 10^7$$

$$T_{ex}(\alpha, E_f) := 3\cdot 10^{-4}\cdot m_h\cdot u_{ex}(\alpha, E_f)^2\cdot 200^{-2}\cdot\left(1.6\cdot 10^{-19}\right)^{-1} \qquad T_{ex}(1.5, 1) = 26 \text{ eV}$$

$$E_{da}(\alpha, E_f) := 0.5\cdot 10^{-13}\cdot M_h(\alpha, E_f)\cdot u_{ex}(\alpha, E_f)^2 \ldots + \left(13.6\cdot 2 + 3\cdot T_{ex}(\alpha, E_f)\right)\cdot 1.6\cdot 10^{-25}\cdot M_h(\alpha, E_f)\cdot m_h^{-1} \ldots + E_{cs}(\alpha, E_f) \qquad E_{da}(1.5, 1) = 2.55 \text{ MJ}$$

$$\eta_{ex}(\alpha, E_f) := 0.5\cdot 10^{-13}\cdot M_h(\alpha, E_f)\cdot u_{ex}(\alpha, E_f)^2\cdot E_{da}(\alpha, E_f)^{-1} \qquad \eta_{ex}(1.5, 1) = 0.61$$

Rough power plant parameters and cost model

We will consider both cases with CHFAR MHD Balance of Plant only, and cases with an added steam bottoming cycle. in the latter case the steam bottoming cycle will add 35% of the unconverted plasma power exiting the MHD generator, but the cost per kilowatt for the steam cycle is much higher, and the optimum choice we will see depends on the target gain, which is the biggest factor that determines the relative importance of the driver cost vs the balance of plant cost. We will adopt the cost scalings for both cases given in reference 5, more or less reproduced below. To account for the scale lengths of chamber size with yield, we assign somewhat arbitrarily the following pulse repetition rates RR as a function of fuel energy E_f:

8 Hz for 0.2 MJ, 6Hz for 1 MJ, and 5 Hz for 2.6 MJ.

[5] B. G. Logan, Lawrence Livermore National Laboratory Report UCRL-ID-110129 (July 1992)

Gross electric output per pulse

$$W_e(\eta_{con},\alpha,E_f) := \eta_{con}\cdot\left(1 - FY_{nb}(\alpha,E_f)\right)\cdot Y_f(\alpha,E_f)$$ MJ_e/pulse Eq 82

Net electric output per pulse

$$W_{net}(\eta_{con},\eta_{df},\eta_d,\alpha,E_f) := \eta_{con}\cdot 0.95\cdot\left(1 - FY_{nb}(\alpha,E_f)\right)\cdot Y_f(\alpha,E_f) - E_f\cdot\eta_{df}^{-1}\cdot\eta_d^{-1}$$ MJ_e/pulse Eq 83

We will provide most detail for two cases A (the reference CFAR Power Plant with E_f = 1 MJ fuel energy and case B (a CFAR demo with E_f = 0.2 MJ, the net T-breeding breakeven point), and just a bit at the end for a very large plant with E_f = 2.6 MJ fuel energy (ultimate low CoE). For the demo case we will find that the lowest CoE occurs with a steam bottoming plant included, as so for DEMO we use an estimated η_{con} = (η_{MHD} = 0.4) + (η_{steam} =0.35*(1-η_{MHD})) =0.65, the same as the efficiency with MHD conversion alone at the larger yield power plant case A (see Fig. 3 efficiency plot). Powers in MW, costs in M$ of direct costs , to be multiplied by 2.8, indirect cost + assembly multiplier in CoE.

$$W_{netA} := W_{net}(0.65,\eta_{dfA},0.4,1.5,1) \qquad W_{netB} := W_{net}(0.65,\eta_{dfB},0.2,1.5,0.2)$$ MJ_e/pulse

Net electric power

$$P_{net}(RR,\eta_{con},\eta_{df},\eta_d,\alpha,E_f) := RR\cdot W_{net}(\eta_{con},\eta_{df},\eta_d,\alpha,E_f)$$ MWe Eq. 84

$$P_{netA} := P_{net}(6,0.65,\eta_{dfA},0.4,1.5,1) \qquad P_{netB} := P_{net}(8,0.65,\eta_{dfB},0.2,1.5,0.2)$$ MWe

Modular solenoid driver (+driver bldg cost). Here we use last years study, ref
[6] B. G. Logan, "Small Modular Driver Study" Lawrence Berkeley National Lab Report May 2006. See web site www.osti.gov/servlets/purl/902800-eyJKrw/) $/J beam direct cost.
We take the driver cost to be linear with driver energy because of high modularity. $UDC_{driver} := 130$

$$C_{driver}(\eta_{df},E_f) := UDC_{driver}\cdot\frac{E_f}{\eta_{df}}$$ M$ direct (Factory built modules-less on site fabrication/assembly Eq 85

$$C_{driver}(\eta_{dfA},1) = 527 \qquad C_{driver}(\eta_{dfB},0.2) = 111$$ M$ direct cost

Cost of reactor vessel inc vessel magnet (twice the HYLIFE-II vessel cost because of the magnets)

$$C_{vessel}(\alpha,E_f) := 60\cdot\left(\frac{Y_f(\alpha,E_f)}{500}\right)^{0.8}$$ M$ (assumes magnet cost scales with magnetic stored energy ~plasma yield) Eq 86

$$C_{vessel}(1.5,1) = 59 \qquad C_{vessel}(1.5,0.2) = 8$$ M$, direct cost

Balance of Plant costs (MHD only and MHD+steam bottoming)

$$C_{mhdBoP}(Pnet) := 0.07 \cdot Pnet \cdot \left(\frac{1400}{Pnet}\right)^{0.27} \qquad C_{steamBoP}(Pnet) := 0.57 \cdot \frac{Pnet}{2} \cdot \left(\frac{1400}{0.5 \cdot Pnet}\right)^{0.1}$$

M$ direct Eq 87

$C_{mhdBoP}(1500) = 103$ $C_{steamBoP}(1500) = 455$ M$, direct

$C_{mhdBoP}(120) = 16$ $C_{steamBoP}(120) = 47$ M$ direct

Other costs: aux pumps security bldgs, maintenance equip, rad waste

$$C_{other}(Pnet) := 100 \cdot \left(\frac{Pnet}{1400}\right)^{0.4}$$

M$ direct Eq 88

$C_{other}(1500) = 103$ $C_{other}(120) = 37$

Operating costs-here we treat operation fuel costs OT_{fuel} (target and target-shell factory on site with recycled materials in the Rankine cycle, and regular O&M costs

Cost per target+target shell

$$C_{target}(RR, \alpha, E_f) := \left[0.15 + 6 \cdot \left(0.002 \cdot \frac{Y_f(\alpha, E_f) \cdot 3.7}{500}\right)^{0.8}\right] \cdot \left(\frac{6}{RR}\right)^{0.4}$$

$/target Eq 89

$C_{target}(6, 1.5, 1) = 0.27$ $C_{target}(8, 1.5, 0.2) = 0.15$

Operating charge for fueling (target and target-shell factory)

$$OT_{fuel}(RR, \eta_{con}, \eta_{df}, \eta_d, \alpha, E_f) := C_{target}(RR, \alpha, E_f) \cdot \frac{3600 \cdot RR}{P_{net}(RR, \eta_{con}, \eta_{df}, \eta_d, \alpha, E_f)}$$

mills/kW$_e$hr Eq 90

$OT_{fuel}(6, 0.65, \eta_{dfA}, 0.4, 1.5, 1) = 3.8$ $OT_{fuel}(8, 0.65, \eta_{dfB}, 0.2, 1.5, 0.2) = 35$ mills/kW$_e$hr

$$OM(RR, \eta_{con}, \eta_{df}, \eta_d, \alpha, E_f) := 8 \cdot \left(\frac{1200}{P_{net}(RR, \eta_{con}, \eta_{df}, \eta_d, \alpha, E_f)}\right)^{0.5}$$

mills/kW$_e$hr Eq 91

Cost of Electricity: Fixed charge rate $FCR := 0.1$ **Indirect cost** $IND := 2.8$ **Capacity factor** $CF := 0.9$

$$CoE_{cfar}(RR, \eta_{con}, \eta_{df}, \eta_d, \alpha, E_f) := 114 \cdot FCR \cdot IND \cdot \frac{\left(\begin{array}{l} C_{driver}(\eta_{df}, E_f) + C_{vessel}(\alpha, E_f) \ldots \\ + C_{mhdBoP}(P_{net}(RR, \eta_{con}, \eta_{df}, \eta_d, \alpha, E_f)) \end{array}\right) \ldots}{+ C_{other}(P_{net}(RR, \eta_{con}, \eta_{df}, \eta_d, \alpha, E_f))} \ldots$$
$$P_{net}(RR, \eta_{con}, \eta_{df}, \eta_d, \alpha, E_f) \cdot CF$$
$$+ OT_{fuel}(RR, \eta_{con}, \eta_{df}, \eta_d, \alpha, E_f) \ldots$$
$$+ OM(RR, \eta_{con}, \eta_{df}, \eta_d, \alpha, E_f)$$

mills/kW$_e$hr Eq 92

$$CoE_{mhdsteam}(RR, \eta_{con}, \eta_{df}, \eta_d, \alpha, E_f) := 114 \cdot FCR \cdot IND \cdot \frac{\left(\begin{array}{l} C_{driver}(\eta_{df}, E_f) + C_{vessel}(\alpha, E_f) \ldots \\ + C_{mhdBoP}(P_{net}(RR, \eta_{con}, \eta_{df}, \eta_d, \alpha, E_f)) \ldots \\ + C_{steamBoP}(P_{net}(RR, \eta_{con}, \eta_{df}, \eta_d, \alpha, E_f)) \end{array}\right) \ldots}{+ C_{other}(P_{net}(RR, \eta_{con}, \eta_{df}, \eta_d, \alpha, E_f))} \ldots$$
$$P_{net}(RR, \eta_{con}, \eta_{df}, \eta_d, \alpha, E_f) \cdot CF$$
$$+ OT_{fuel}(RR, \eta_{con}, \eta_{df}, \eta_d, \alpha, E_f) \ldots$$
$$+ OM(RR, \eta_{con}, \eta_{df}, \eta_d, \alpha, E_f)$$

mills/kW$_e$hr Eq 93

$CoE_A := CoE_{cfar}(6, 0.65, \eta_{dfA}, 0.4, 1.5, 1)$ $\overline{CoE_A = 29.4}$ $CoE_{cfar}(8, 0.4, \eta_{dfB}, 0.2, 1.5, 0.2) = 195$

$CoE_{mhdsteam}(6, 0.77, \eta_{dfA}, 0.4, 1.5, 1) = 36.2$ $CoE_B := CoE_{mhdsteam}(8, 0.65, \eta_{dfB}, 0.2, 1.5, 0.2)$ $\overline{CoE_B = 125}$

TABLE 10: SUMMARY

	POWER PLANT	DEMO	
T-lean fuel energy at ignition	1 MJ	0.2 MJ	
Energy delivered to ablation front	$E_{da}(1.5,1) = 2.55$	$E_{da}(1.5,0.2) = 0.49$	MJ
Capsule implosion efficiency	$\eta_c(1.5,1) = 0.39$	$\eta_c(1.5,0.2) = 0.41$	
Overall coupling efficiency beam-to-fuel corrected for parasitic loss on ablation plasma	$\eta_{dfA} = 0.25$	$\eta_{dfB} = 0.24$	
H_2 ablation front temperature	$T_{ex}(1.5,1) = 26.3$	$T_{ex}(1.5,0.2) = 36$	eV
Fusion yield	$Y_f(1.5,1) = 494$	$Y_f(1.5,0.2) = 43$	MJ
Driver energy	$1 \cdot \eta_{dfA}^{-1} = 4.06$	$0.2 \cdot \eta_{dfB}^{-1} = 0.85$	MJ
Driver efficiency	$\eta_{dA} := 0.4$	$\eta_{dB} := 0.2$	
Driver electric input energy/pulse	$1 \cdot \eta_{dA}^{-1} \cdot \eta_{dfA}^{-1} = 10.1$	$0.2 \cdot \eta_{dB}^{-1} \cdot \eta_{dfB}^{-1} = 4.3$	MJ_e
Target gain	$Y_f(1.5,1) \cdot \eta_{dfA} \cdot 1^{-1} = 122$	$Y_f(1.5,0.2) \cdot \eta_{dfB} \cdot 0.2^{-1} = 51$	MJ_f
Fusion energy conversion eff. (lowest CoE for Demo requires 35% steam bottoming cycle to get 0.65 conversion overall)	$\eta_{MHD} := 0.65$ ^| lowest CoE this case	$\eta_{MHD} := 0.4$ $\eta_{MHDsteam} := 0.65$	(see Fig 3)
Gross electric output (per pulse)	$W_e(0.65,1.5,1) = 278$	$W_e(0.65,1.5,0.2) = 20.5$	MJ_e
Net electric output per pulse, inc 5 % aux	$W_{netA} = 254$	$W_{netB} = 15.21$	MJ_e
Pulse repetition rate	$RR_A := 6$	$RR_B := 8$	Hz
Net electric power	$P_{netA} = 1522$	$P_{netB} = 122$	MW_e
Driver direct cost	$C_{driver}(\eta_{dfA},1) = 527$	$C_{driver}(\eta_{dfB},0.2) = 111$	M$
Vessel direct cost	$C_{vessel}(1.5,1) = 59$	$C_{vessel}(1.5,0.2) = 8.5$	M$
Balance-of-Plant direct cost	$C_{mhdBoP}(1522) = 104$	$C_{mhdBoP}(122) + C_{steamBoP}(122) = 64$	M$
Other direct costs	$C_{other}(1522) = 103$	$C_{other}(122) = 38$	M$
Cost of Electricity, inc. targets and O&M	$CoE_A = 29.4$	$CoE_B = 125$	mills/kW_ehr
	-->may meet affordable CoE goal for 10 billion people	--> total capital < 1 B$ for DEMO for net power and tritium production	

As a final teaser, peek at largest T-lean 2.6 MJ fuel case: $2.6 \cdot 0.26^{-1} = 10$ MJ driver,

$Y_f(1.5,2.6) = 2181$ MJ yield (3m radius, 10 T plasma chamber), $P_{net}(5,0.7,0.26,0.5,1.5,2.6) = 6651$ MW_e

$CoE_{cfar}(5,0.7,0.26,0.5,1.5,2.6) = 16$ mills/kW_ehr!

2-D time-dependent polar (two-sided) beam requirements $I_{binc}(r,t)$ and $\rho r_b(r,t)$ for symmetric implosions

In this section we examine more closely how the goal of two-sided beam illumination might be met, and the time-dependant beam requirements, including zooming and parasitical beam loss on ablated plasma, taking into account the 2-D geometery shown in Fig. 32 below. Recent implosion calculations by John Perkins at LLNL (June 2007) indicates that one important self-consistent effect of parasitical beam heating of outgoing ablation plasma is increases in ion range (for constant ion incident energy) with increased beam intensity, and we show below this is likely the result of the electron thermal speed increased by heating beyond the ion beam speed. In the calculations on pages 28 and 29, and equation 78, we already found one beneficial effect of beam heating in reducing ablated plasma density in the beam channel in two -sided illumination geometry (see Fig 32 below) and this is a 2-D effect for ablated plasma density reduction, but neglects range lengthening due to increases in electron temperature. On the other hand, the 2-D effect of ablated plasma expansion in a beam channel doesn't apply to Perkins' case of symmetric 1-D radial beam geometry, and moreover, beam heating of Te in a beam channel would be more concentrated in 2-D geometry. So, now we will construct a model for ion parasitic loss on ablated plasma with both Te increasing and density decreasing due to beam heating, as a guide to future HIF direct drive 2-D (two-sided) implosion calculations.

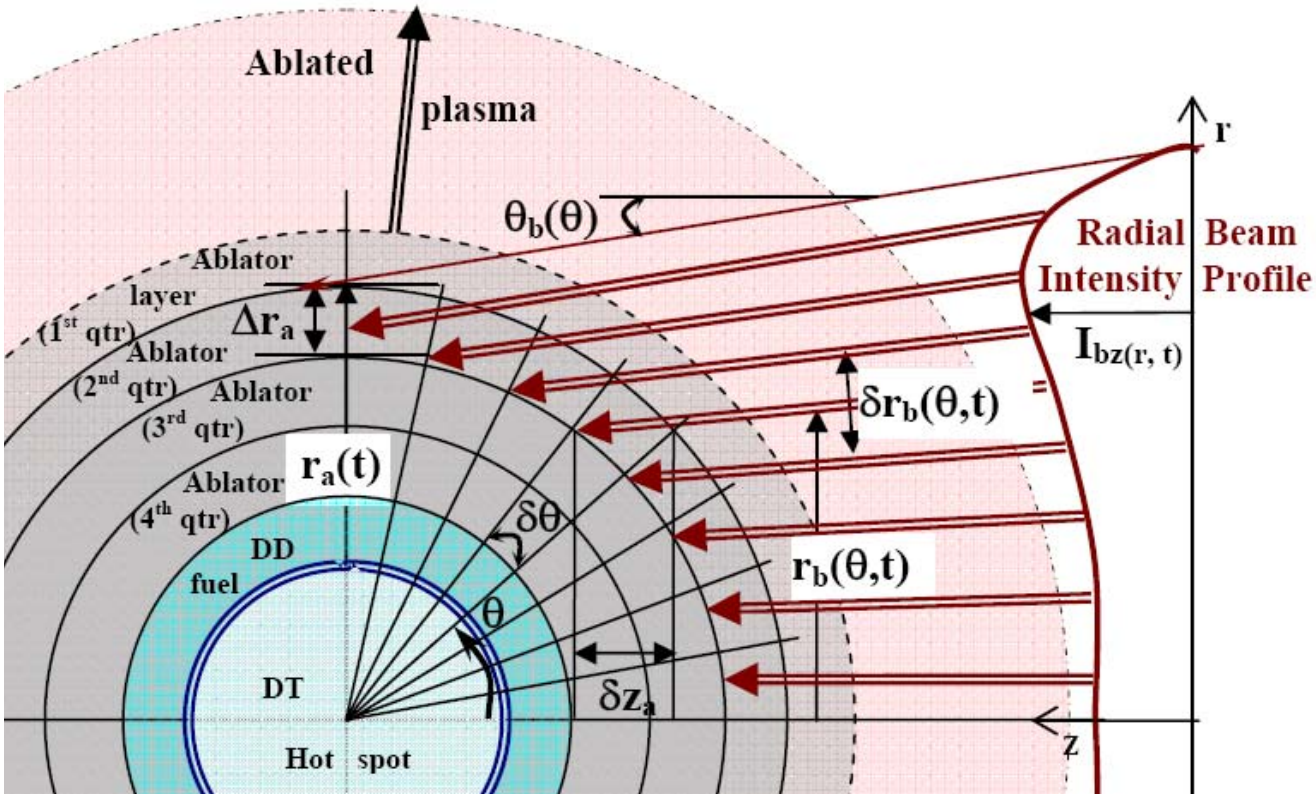

Figure 32: Geometry for two sided beam illumination of a direct drive target (only one beam side is shown). Ion range is initally set = 0.25 of initial ablator ρr. The model derives beam intensity and range profiles required for spherically symmetric beam energy deposition in four layers of the ablator at four different times during the implosion. The incident beam energy is calculated to penetrate the ablation plasma in the beam channel at each time, and deposit the energy required in each ablator layer around the sphere uniformly to match the spherically symmetric ablation pressure (t) calculated for a shaped drive pulse for a low adiabat from 1-D implosion calculations.

Effect of beam heating on ion range in ablated plasma for John Perkins DT ablator 1 MJ capsule example @ 50 MeV Argon ion energy (fixed)

$uex_{dt} := 4\cdot\frac{10^7}{\ln(2)}$ $\quad uex_{dt} = 5.8\times10^7$ cm/s exhaust velocity necessary to get John's implosion v

$Tex_{dt} := 3\cdot10^{-4}\cdot2.5\cdot m_h\cdot1.4\cdot uex_{dt}^{\,2}\cdot200^{-2}\cdot\left(1.6\cdot10^{-19}\right)^{-1}$ $\quad Tex_{dt} = 912$ eV. Note bremsstrahlung at this Te penetrated DT or H ablators without some carbon opacity!

$0.25\cdot0.11\cdot0.25 = 0.007$ g/cm2 nominal initial ion range $\quad TOL = 0.001$

$\rho_a := 0.25$ for DT $\quad A_b = 40 \quad Z_b = 18 \quad A_t = 1 \quad Z_t = 1 \quad T_e = 30$

$R_b\left(Eb,\rho_a,T_e,A_b,A_t,Z_b,Z_t\right) := \rho_a^{-1}\cdot\int_{Eb}^{0.02\cdot Eb} dE_{d\rho x}\left(\rho_a,E,T_e,A_b,A_t,Z_b,Z_t\right)^{-1}\,dE$ range, cm Eq. 94

$R_b\left(5\cdot10^7,\rho_a,30,A_b,2.5,Z_b,1\right) = 0.007$ cm-close agreement with John's inital ion range

$\rho_a\cdot R_b\left(5\cdot10^7,\rho_a,30,A_b,2.5,Z_b,1\right) = 0.002$ rho-r range in g/cm2

Table 11: Range vs temperature. Note how the ion beam range can increase with temperature as beam intensity increases Te during the pulse in this table!

$it := 1..12 \qquad Te_{it} := 2^{it-1}$

Te_{it} =	$\rho_a\cdot R_b\left(5\cdot10^7,\rho_a,Te_{it},A_b,2.5,Z_b,Z_t\right)$ =	$R_b\left(5\cdot10^7,\rho_a,Te_{it},A_b,2.5,Z_b,Z_t\right)\cdot10^4$ =
1	0.00184	74
2	0.00183	73
4	0.00182	73
8	0.0018	72
16	0.00178	71
32	0.00181	72
64	0.00194	78
128	0.00236	94
256	0.00341	136
512	0.00568	227
1024	0.01054	422
2048	0.02148	859

eV $\qquad$ g/cm^2 $\qquad$ range in microns

$\rho_a := 0.5$ (change back to Hyrodogen) $\quad A_t = 1 \quad Z_t = 1 \quad A_b = 40 \quad Z_b = 18$

$E_{bf}\left(\rho_a,0.0008,0.01,30,A_b,A_t,Z_b,Z_t\right) = 4.94\times10^7$ Small 1 MJ DT case (Perkins)

$E_{bf}\left(\rho_a,0.004,0.01,30,A_b,A_t,Z_b,Z_t\right) = 2.03\times10^8$ 5MJ T-lean case

We have already estimated the radial expansion of plasma in the beam channel (see Eq 77 page 29) , from which we can infer an ablation plasma electron temperature due to beam heating:

$$Tea_k := \frac{0.5}{2}\cdot m_h\cdot10^{-3}\cdot\left(vaperp_k\right)^2\cdot\frac{10^{-4}}{e} \qquad \text{(eV)} \qquad \text{Eq 95.}$$

See plot on next page, Fig. 34.

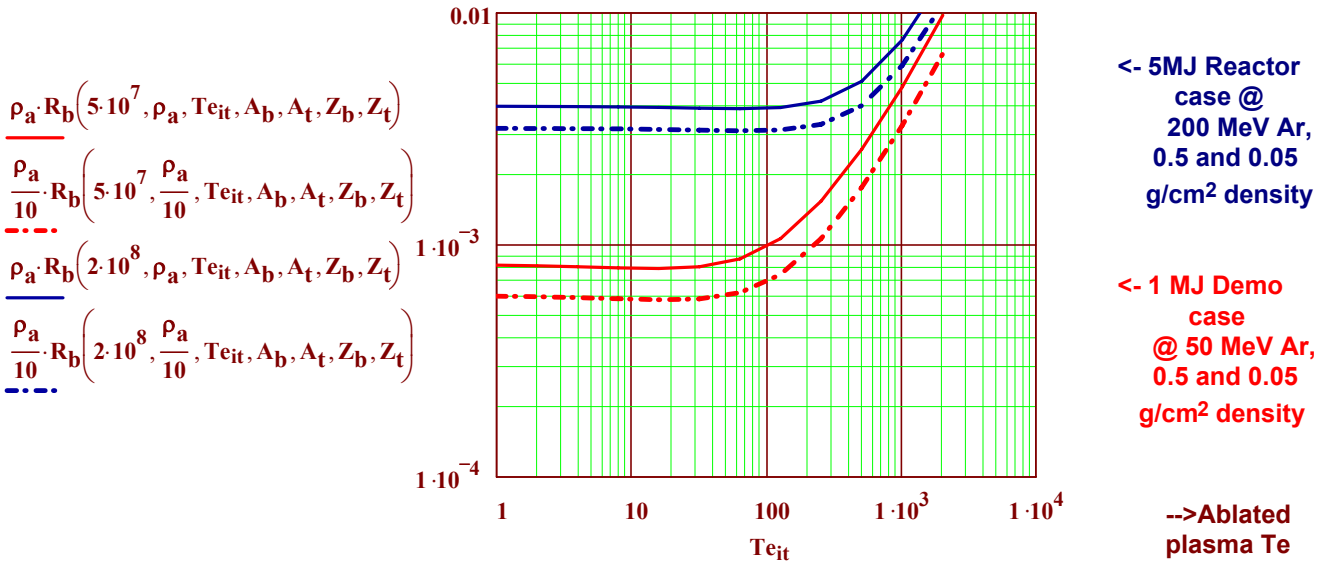

Figure 33: Ion range versus plasma temperature. Note range first shortens slightly as Te goes from 1 eV to 100 eV, and then increases several fold with Te up to 2 keV. There is also a range shortening (20% log λ_D effect) at 10X lower density of ablated plasma, partially offsetting the effect of ablated plasma expansion.

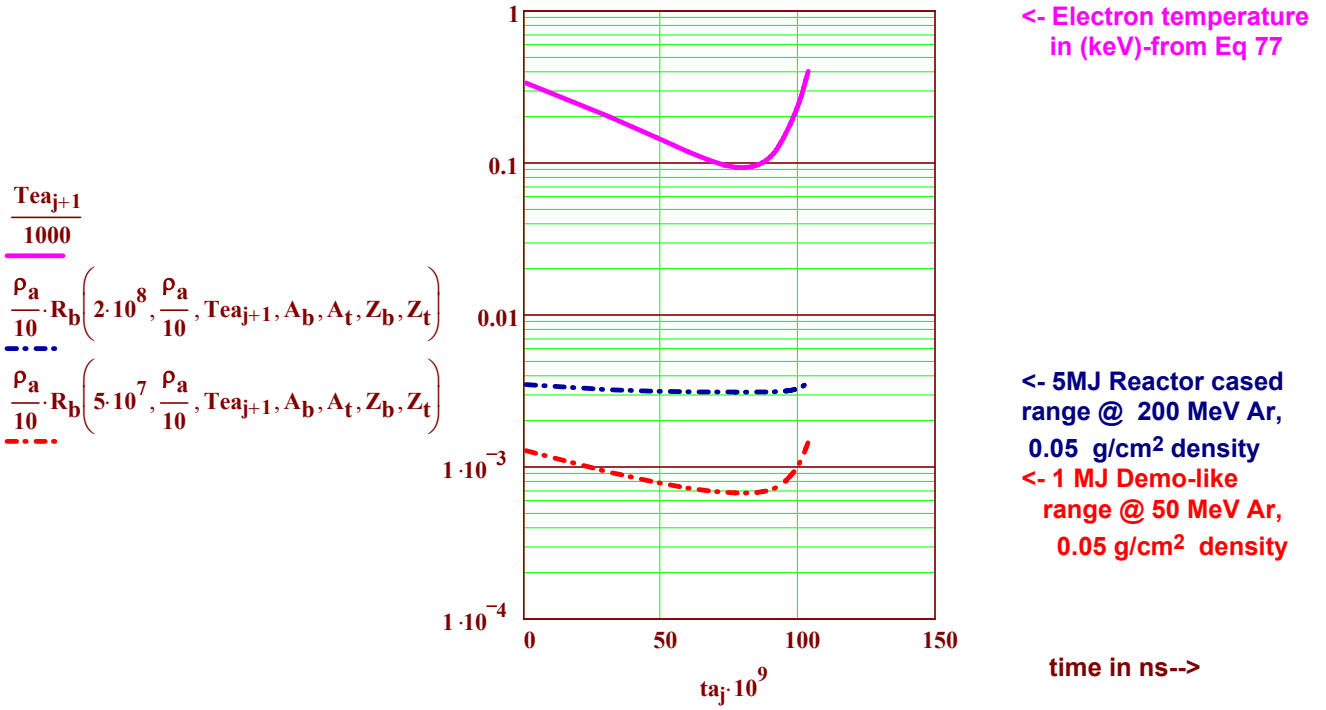

Figure 34: Ion ranges and Te during Case A implosions for ***constant energy*** 200 MeV and 50 MeV Argon ion beams. The beam heating effect on Te and range is most pronounced for the lower velocity 50 MeV beams. Early in time during the foot of the implosion, Te and range both decrease because ablated mass increases faster than beam input to it minus expansion cooling, but then later, net beam input exceeds ablation mass rates (J/g goes up) in the ramp up to peak power, when Te and range again increase. This may explain qualitatively why, in John Perkins implosion calculations, the beam 50% deposition radius first *migrates away* from the imploding shell, up until the big ramp up to peak power begins, after which the 50% absorption point *migrates back* to the dense shell. Quantitatively, this range variation should be larger in John Perkins 1 MJ example than this at lower beam intensity and Te for a 4 MJ case A target.

Ion beam requirements for Case A implosions with polar (two-sided) beam illumination.

With initial ion range set equal to one fourth of the initial ablator ρr, determine required two sided beam input intensity and range at four times t_{js}, when the ablator mass is 1, 3/4, 1/2, and 1/4 of initial mass. Determine beam intensity and range [$I_{bz}(r,t)$ and $\rho r_b(r,t)$] for beam deposition uniform in θ and in J/g (Fig. 32) into 8 polar segments of angles θ_{is} and width π/16. Account for beam attenuation in ablated plasma at each time and θ. Work for Case A power plant (page 25) and then for Case B Demo (page 32).

$is := 1 .. 4$

$is := 1 .. 9$

$\theta_{is} := \left(\frac{\pi}{16}\right)\cdot(is - 1)$

1st quarter ablator mass $\delta MaA_{js} := (115 - 23)\cdot\left(4\cdot 10^{3}\right)^{-1}$ $\delta MaA_1 = 0.023$ g, @ density $\rho aA_1 := \rho_{Ho}$

1st qtr outer radius $raA0 := 0.71$ cm, ablated over time interval $tA_1 := 0$ $\delta tA_1 := 81\cdot 10^{-9}$ s

Ist qtr inner radius $raA_1 := \left[raA0^{3} - \left(\frac{3\cdot\delta MaA_1}{4\cdot\pi\cdot\rho aA_1}\right)\right]^{0.333}$ cm $raA_1 = 0.67$ cm $\delta raA_1 := raA0 - raA_1$

1st qtr layer thickness $\delta raA_1 = 0.038$ cm. Radial KE/exhaust energy efficiency $\eta_{ex}(1.5,1) = 0.61$

1st qtr drive energy $EdA_1 := 0.385\cdot 10^{6}\cdot\eta_{ex}(1.5,1)^{-1}$ $EdA_1 = 6.4\times 10^{5}$ J. Power: $PdA_1 := EdA_1\cdot(\delta tA_1)^{-1}$

$PdA_1\cdot 10^{-12} = 7.85$ TW. 1st qtr energy density $WdA_1 := EdA_1\cdot(\delta MaA_1)^{-1}$ $WdA_1 = 2.8\times 10^{7}$ J/g

Ist quarter ablation front pressure $WdA_1\cdot\rho aA_1\cdot 10^{6}\cdot 2^{-1}\cdot 10^{-11} = 13.8$ MB $WdA_1\cdot\frac{m_h}{10\cdot e} = 29$ eV equiv.

1st qtr shell volume $\delta VaA_{1,is} := 2\cdot\pi\cdot\left(raA_1 + \frac{\delta raA_1}{2}\right)^{2}\cdot\delta raA_1\cdot\sin\left(\theta_{is} + \frac{\pi}{32}\right)\cdot\frac{\pi}{16}$ cm³

$2\cdot\sum_{is=1}^{8}\delta VaA_{1,is} = 0.229$ cm³ $\frac{4}{3}\cdot\pi\cdot\left[(raA_1 + \delta raA_1)^{3} - (raA_1)^{3}\right] = 0.228$ Shell volume checks OK!

Beam convergence angle $\theta b_{is} := 0.125\cdot\sin(\theta_{is})$ Beam-pathlength-1st qtr $\delta zaA_{1,is} := \frac{\delta raA_1}{\cos(\theta_{is} - \theta b_{is})}$

Beam range $\rho raA_{1,is} := \rho aA_1\cdot\delta zaA_{1,is}$ & energy $Ebo_{1,is} := E_{bf}(\rho aA_1, \rho raA_{1,is}, 0.01, 28, A_b, A_t, Z_b, Z_t)$

Incident beam radius vs polar angle θ $rbA_{1,is} := raA_1\cdot\sin\left(\theta_{is} + \frac{\pi}{32}\right)$ $rbA_{1,9} := raA0 + \delta zaA_{1,9}\cdot\theta b_9$

Beam illumination width (cm) per θ increment $\delta rbA_{1,is} := \left(raA_1 + \frac{\delta raA_1}{2}\right)\cdot\sin\left(\theta_{is} + \frac{\pi}{16}\right) - raA_1\cdot\sin(\theta_{is})$

Beam deposition intensity (r_b) $IdA_{1,is} := WdA_1\cdot\delta VaA_{1,is}\cdot\rho aA_1\cdot(\delta tA_1\cdot 2\cdot\pi\cdot rbA_{1,is}\cdot\delta rbA_{1,is})^{-1}$ $IdA_{1,9} := 0$

$Ebo_{1,9} := Ebo_{1,8}$

Table 12: 2-D polar drive requirements for Case A, 1st quarter ablation period.

θ_{is} =	$rbA_{1,is}$ =	$\delta zaA_{1,is}$ =	$\rho raA_{1,is}$ =	$IdA_{1,is}\cdot 10^{-12}$ =	$Ebo_{1,is}\cdot 10^{-6}$ =
0	0.07	0.04	0.0038	1.3	219
0.2	0.2	0.04	0.0039	1.4	222
0.39	0.32	0.04	0.004	1.4	229
0.59	0.43	0.04	0.0044	1.6	243
0.79	0.52	0.05	0.005	1.8	265
0.98	0.59	0.06	0.006	2.3	301
1.18	0.64	0.08	0.0078	3.2	362
1.37	0.67	0.12	0.0121	5.7	483
1.57	0.75	0.31	0.0305	0	483
Polar angle (rad)	Beam radius(cm)	Shell z depth (cm)	Beam range g/cm²	Beam Intensity TW/cm²	Argon Beam Energy (MeV)

$\sum_{is=1}^{8} \delta rbA_{1,is} = 0.778$ cm $2\cdot\sum_{is=1}^{8}\left(WdA_1\cdot\delta VaA_{1,is}\cdot\rho aA_1\right) = 6.3\times10^{5}$ J-Energy Checks-OK!

$\sum_{is=1}^{8}\left[2\cdot\pi\cdot\left(rbA_{1,is}\right)\cdot\delta rbA_{1,is}\right] = 1.77$ cm^2 $\pi\cdot raA0^2 = 1.58$ cm^2. OK as converging beam sees > 2π

Now lets correct for ablation plasma in this first quarter mass ablation period of $\frac{\delta tA_1}{10^{-9}} = 81$ ns
The first quarter ablated plasma mass expands in this time interval to a radius

$uimpA_1 := 2\cdot10^{6}$ cm/s $rpA_1 := raA0 + \left(u_{ex}(1.5,1) - uimpA_1\right)\cdot\delta tA_1$ cm $rpA_1 = 2.03$ cm
average expansion velocity

and to a mass density $\rho pA_1 := \delta MaA_1\cdot\left[\frac{4}{3}\cdot\pi\cdot\left[\left(rpA_1\right)^3 - raA0^3\right]\right]^{-1}$ $\rho pA_1 = 6.8\times10^{-4}$ g/cm3

and to a rho-r $\rho rpA_1 := \rho pA_1\cdot\left(rpA_1 - raA0\right)$ $\rho rpA_1 = 9.03\times10^{-4}$ g/cm^2, ~20% of the ave first quarter beam range.

(Henceforth, to avoid confusion. we switch to subscript "p" to denote ablated plasma quantities, leaving the subscript "a" to apply to the dense remaining ablator shell.

$Eb = 3\times10^{8}$ $A_b = 40$ $Z_b = 18$ $A_t = 1$ $Z_t = 1$ $n_p := \rho pA_1\cdot m_h^{-1}$ $n_p = 4.09\times10^{20}$ protons/cm3

$\tau_p := 6.4\cdot10^{17}\cdot0.1^{1.5}\cdot\left(4\cdot10^{26}\cdot7\right)^{-1}$ $\tau_p = 7.23\times10^{-12}$ s.-->ablation plasma is very collisional

Now lets solve for the initial incident beam energy, which first slows down partially in the ablation plasma to an intermediate energy Eb_p, then enters the dense remaining dense ablator shell where it gives up its remaining energy wihtin the specified shell $\rho_a\Delta r_a$

$$Eb_p\left(Ebo,\rho r_p,\rho_p,T_p,A_b,A_t,Z_b,Z_t\right) := root\left(\rho r_p - \int_{Ebo}^{Eb} dE_{d\rho x}\left(\rho_p,E,T_p,A_b,A_t,Z_b,Z_t\right)^{-1}dE,\ Eb\right)$$ eV

Required ion range neglecting ablation plasma: $Eb_p\left(5\cdot10^{8},\rho rpA_1,\rho pA_1,30,A_b,A_t,Z_b,Z_t\right) = 4.69\times10^{8}$
Required ion range with ablation plasma

Initial guess $Eb := 10^{9}$

$$E_{bo}\left(\rho r_p,\rho r_a,\rho_p,\rho_a,T_p,T_a,A_b,A_t,Z_b,Z_t\right) := root\left(\rho r_a - \int_{Eb_p\left(Eb,\rho r_p,\rho_p,T_p,A_b,A_t,Z_b,Z_t\right)}^{0.02\cdot Eb} dE_{d\rho x}\left(\rho_a,E,T_a,A_b,A_t,\right.\right.$$

Table 13: required incident beam energies, Case A, 1st qtr ablation

With ablation plasma loss (1st qtr) assuming T_p = 80 eV

$E_{bo}(\rho rpA_1, \rho raA_{1,is}, \rho pA_1, \rho aA_1, 80, 30, A_b, A_t, Z_b, Z_t) =$

$2.7 \cdot 10^8$
$2.73 \cdot 10^8$
$2.79 \cdot 10^8$
$2.91 \cdot 10^8$
$3.12 \cdot 10^8$
$3.44 \cdot 10^8$
$4.01 \cdot 10^8$
$5.16 \cdot 10^8$
$8.8 \cdot 10^8$

Without ablation plasma (1st qtr)

$Ebo_{1,is} =$

$2.19 \cdot 10^8$
$2.22 \cdot 10^8$
$2.29 \cdot 10^8$
$2.43 \cdot 10^8$
$2.65 \cdot 10^8$
$3.01 \cdot 10^8$
$3.62 \cdot 10^8$
$4.83 \cdot 10^8$
$4.83 \cdot 10^8$

More exact beam energy after passing through ablation plasma (very close to the simpler form of Ebo):

$Eb_p(E_{bo}(\rho rpA_1, \rho raA_{1,is}, \rho pA_1, \rho aA_1, 80, 30, A_b, A_t, Z_b, Z_t), \rho rpA_1, \rho pA_1, 30, A_b, A_t, Z_b, Z_t) =$

$2.22 \cdot 10^8$
$2.24 \cdot 10^8$
$2.32 \cdot 10^8$
$2.45 \cdot 10^8$
$2.68 \cdot 10^8$
$3.04 \cdot 10^8$
$3.65 \cdot 10^8$
$4.86 \cdot 10^8$
$8.6 \cdot 10^8$

Lets make a first order correction to the exhaust plasma temperature, assuming half of the incremental beam energy deposited into the ablation plasma mass within the beam channel

$$\Delta EbpA_{1,is} := \left(E_{bo}(\rho rpA_1, \rho raA_{1,is}, \rho pA_1, \rho aA_1, 80, 30, A_b, A_t, Z_b, Z_t) - Ebo_{1,is}\right) \cdot \left(Ebo_{1,is}\right)^{-1}$$

goes into increased hydro motion (both radial and transverse), the other half into incremental thermal energy $3\Delta T_p$, and for the moment lets assume the ablated plasma density does not change; then we have

$$TpA_{1,is} := \frac{IdA_{1,is} \cdot \delta tA_1 \cdot \Delta EbpA_{1,is}}{\rho rpA_1} \cdot \frac{m_h}{6 \cdot e} \ldots + T_{ex}(1.5, 1)$$

Table 14: Effects of beam heating of ablation plasma as a funtion of polar angle θ in the beam channel

$TpA_{1,is} =$	$\frac{TpA_{1,is}}{T_{ex}(1.5,1)} =$	$\Delta EbpA_{1,is} =$	$\frac{\rho raA_{1,is}}{\rho rpA_1} =$
75	2.9	0.233	4
75	2.9	0.229	4
75	2.9	0.219	4
76	2.9	0.2	5
76	2.9	0.176	5
78	3	0.145	7
81	3.1	0.109	9
88	3.4	0.07	13
26	1	0.823	34

One can see in this table that the ablation plasma is substantially heated (Te increases several-fold) during the 1st qtr of the pulse, but not enough to significantly increase ion range with ve>vi.

The next question to ask is, does the heating (pressurization) cause significant enhanced expansion in the shorter transverse to the beam channel (polar axis) direction? One estimate is the fractional radial expansion of ablated plasma possible in the 1st qtr time of δtA, following eq77:

$$vperpA_{1,is} := 10^2 \cdot \sqrt{\frac{5 \cdot \left[\left(TpA_{1,is}\right) - T_{ex}(1.5,1)\right] \cdot e}{3 \cdot m_h \cdot 10^{-3}}} \quad \text{cm/s}$$

Table 15: Displacement of ablated plasma by beam heating

$vperpA_{1,is}$	$\frac{vperpA_{1,is} \cdot \delta tA_1}{\delta rbA_{1,is}}$	$\frac{vperpA_{1,is} \cdot \delta tA_1}{raA0}$
$8.84 \cdot 10^6$	5.31	1.01
$8.82 \cdot 10^6$	5.36	1.01
$8.83 \cdot 10^6$	5.64	1.01
$8.86 \cdot 10^6$	6.23	1.01
$8.94 \cdot 10^6$	7.28	1.02
$9.07 \cdot 10^6$	9.22	1.03
$9.31 \cdot 10^6$	13.25	1.06
$9.94 \cdot 10^6$	25.19	1.13
0	0	0

Table 15 showing vperp*δt/δrb >>1 means that beam heating of ablation plasma will reach pressure equilibrium locally within the beam channel very quickly, and vperp*δt/ ra ~ 1 means significant expansion transverse to the polar axis over the whole channel, justifying allocating half the incremental beam energy input going into hydro motion. The first effect of local pressure balance means the local ablation plasma density will be depressed inversely with the local increase in beam temperature. The second effect will reduce the overall pressure withing the beam channel by roughly a factor of (1+ vperp*δt /r a)^-1 (The net T_p will stay roughly the same as beam energy dE/dx transfer as "per electron"remains rougly the same. Using "pressure balance" and channel expansion factors, the corrected ablation plasma densities and associated rho-r's are reduced by beam heating are estimated by

$$\rho pA_{1,is} := \rho pA_1 \cdot \left(\frac{TpA_{1,1}}{TpA_{1,is}}\right) \cdot \left(1 + \frac{vperpA_{1,is} \cdot \delta tA_1}{raA0}\right)^{-2} \qquad \rho pA_{1,9} := \rho pA_1$$

and $$\rho rpA_{1,is} := \rho rpA_1 \cdot \left(\frac{TpA_{1,1}}{TpA_{1,is}}\right) \cdot \left(1 + \frac{vperpA_{1,is} \cdot \delta tA_1}{raA0}\right)^{-2} \qquad \rho rpA_{1,9} := \rho rpA_1$$

We can now plot all these adjusted beam requirements versus beam radius in the next Figure 35. The corrected incident beam energy requirement adjusted for heated ablation plasma loss is

$$EbcA_{1,is} := E_{bo}\left(\rho rpA_{1,is}, \rho raA_{1,is}, \rho pA_{1,is}, \rho aA_1, TpA_{1,is}, T_{ex}(1.5,1), A_b, A_t, Z_b, Z_t\right)$$

$$EbcA_{1,9} := EbcA_{1,8}$$

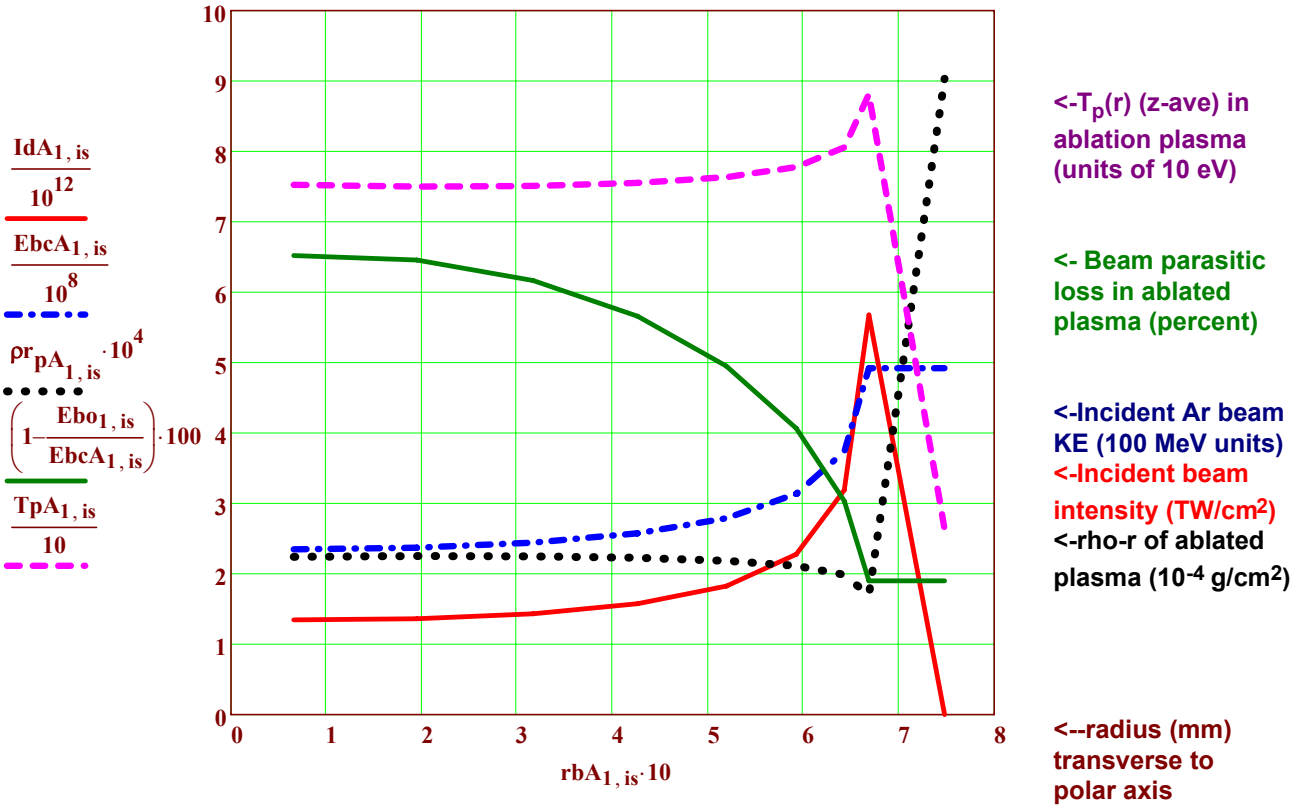

Figure 35: Plots of polar beam drive intensity (TW/cm^2, one of two sides), incident Ar beam energy (in 100 MeV units), rho-r of ablated plasma column density (10^{-4} g/cm^2 units) (dotted black line), percent beam loss in ablated plasma, and the temperature T_p of the ablation plasma(units of 10 eV), as functions of radius in the beam channel, transverse to the polar axis near the target, during the first quarter of the ablation drive pulse, (the foot part of the pulse) for the large T-lean target case A (see Figs 19 to 23 above for case A details). Note required beam intensity is sharply higher (peak is ~ 4X intensity on axis) in the beam channel "rim", as expected due to the polar drive geometry shown in Fig. 32. Also, note the local ablation temperature ($T_p(r_b)$ increases with the beam intensity, resulting in pressurization digging a "hole" in ablated plasma rho-r *just in the annulus through which most beam energy is delivered,* reducing parasitic beam loss. This beneficial effect will increase later in the drive.

1st qtr beam input inc loss on ablation plasma $EdcA_1 := \sum_{is=1}^{8}\left[\frac{EbcA_{1,is}}{Ebo_{1,is}}\cdot 2\cdot\left(WdA_1\cdot\delta VaA_{1,is}\cdot\rho aA_1\right)\right]$ $EdcA_1 = 6.6\times 10^5$ J

Neglecting beam ablation loss $EdA_1 = 6.36\times 10^5$ -->fractional loss $\left(EdcA_1 - EdA_1\right)\cdot\left(EdcA_1\right)^{-1} = 0.037$

Fig. 35 shows a key feature of polar drive geometry-the local peaking of beam intensity and locally higher beam ion energy in the "rim" of the beam channel driving the limb of the ablator shell. This ideal beam variation provides symmetric ablation drive for a spheical implosion, but may prove difficult to achieve in practice, and so further work will explore ways to relax the locally-sharp, beam intensity "rim":
(a) Most important, add appropriate Δra (θ) capsule ablator shimming to accept a more uniform beam profile;
(b) Allow 20% low mode-P2 asymmetries at large rho-r fuel (Steve Slutz at San Ramon IFE meeting);
(c) Possibly in conjuction with (a), overdrive the foot intensity at the rim for early 5 to 20 % P2 prolate asymmetry with beam spill beyond the limb (small drive energy penalty, and then under-drive the rim later;
(d) If ignition still fails in a too-asymmetric implosion, then add a powerful late shock.

Polar drive parameters for Case A, 2nd quarter of ablation drive

2nd quarter ablator mass $\delta MaA_2 = 0.023$ $tA_2 := \delta tA_1$ $tA_2 = 8.1 \times 10^{-8}$ g, @ density $\rho aA_2 := 3 \cdot \rho_{Ho}$

2nd qtr outer radius $raA1 := 0.61$ cm, ablated over time interval $\delta tA_2 := 11.95 \cdot 10^{-9}$ s

2nd qtr inner radius $raA_2 := \left[raA1^3 - \left(\frac{3 \cdot \delta MaA_2}{4 \cdot \pi \cdot \rho aA_2} \right) \right]^{0.333}$ $raA_2 = 0.59$ $\delta raA_2 := raA1 - raA_2$

2nd qtr layer thickness $\delta raA_2 = 0.017$ cm. Radial KE/exhaust energy efficiency $\eta_{ex}(1.5, 1) = 0.61$

2nd qtr drive energy $EdA_2 := 0.385 \cdot 10^6 \cdot \eta_{ex}(1.5, 1)^{-1}$ $EdA_2 = 6.36 \times 10^5$ J. Power: $PdA_2 := EdA_2 \cdot (\delta tA_2)^{-1}$

$PdA_2 \cdot 10^{-12} = 53$ TW. 2nd qtr energy density $WdA_2 := EdA_2 \cdot (\delta MaA_2)^{-1}$ $WdA_2 = 2.77 \times 10^7$ J/g

2nd quarter ablation front pressure $WdA_2 \cdot \rho aA_2 \cdot 10^6 \cdot 2^{-1} \cdot 10^{-11} = 41.5$ MB $WdA_2 \cdot \frac{m_h}{10 \cdot e} = 29$ eV equiv.

2nd qtr shell volume $\delta VaA_{2,is} := 2 \cdot \pi \cdot \left(raA_2 + \frac{\delta raA_2}{2} \right)^2 \cdot \delta raA_2 \cdot \sin\left(\theta_{is} + \frac{\pi}{32} \right) \cdot \frac{\pi}{16}$ cm³

$2 \cdot \sum_{is=1}^{8} \delta VaA_{2,is} = 0.075$ cm³ $\frac{4}{3} \cdot \pi \cdot \left[(raA_2 + \delta raA_2)^3 - (raA_2)^3 \right] = 0.075$ Shell volume checks OK!

Beam convergence angle $\theta b_{is} := 0.125 \cdot \sin(\theta_{is})$ Beam-pathlength-2nd qtr $\delta zaA_{2,is} := \frac{\delta raA_2}{\cos(\theta_{is} - \theta b_{is})}$

Beam range $\rho raA_{2,is} := \rho aA_2 \cdot \delta zaA_{2,is}$ & energy $Ebo_{2,is} := E_{bf}(\rho aA_2, \rho raA_{2,is}, 0.01, 29, A_b, A_t, Z_b, Z_t)$

Incident beam radius vs polar angle θ $rbA_{2,is} := raA_2 \cdot \sin\left(\theta_{is} + \frac{\pi}{32} \right)$ $rbA_{2,9} := raA1 + \delta zaA_{2,9} \cdot \theta b_9$

Beam illumination width (cm) per θ increment $\delta rbA_{2,is} := \left(raA_2 + \frac{\delta raA_2}{2} \right) \cdot \sin\left(\theta_{is} + \frac{\pi}{16} \right) - raA_2 \cdot \sin(\theta_{is})$

Beam deposition intensity (r_b) $IdA_{2,is} := WdA_2 \cdot \delta VaA_{2,is} \cdot \rho aA_2 \cdot (\delta tA_2 \cdot 2 \cdot \pi \cdot rbA_{2,is} \cdot \delta rbA_{2,is})^{-1}$ $IdA_{2,9} := 0$

$Ebo_{2,9} := Ebo_{2,8}$

Table 16: 2-D polar drive requirements for Case A, 2nd quarter ablation period.

θ_{is} =	$rbA_{2,is}$ =	$\delta zaA_{2,is}$ =	$\rho raA_{2,is}$ =	$IdA_{2,is} \cdot 10^{-12}$ =	$Ebo_{2,is} \cdot 10^{-6}$ =
0	0.06	0.02	0.005	12	247
0.2	0.17	0.02	0.005	12	250
0.39	0.28	0.02	0.0053	13	258
0.59	0.38	0.02	0.0057	14	273
0.79	0.46	0.02	0.0065	17	298
0.98	0.52	0.03	0.0078	22	338
1.18	0.57	0.03	0.0102	33	406
1.37	0.59	0.05	0.0158	70	541
1.57	0.63	0.13	0.0398	0	541

Polar angle (rad) | Beam radius(cm) | Shell z depth (cm) | Beam range g/cm² | Beam Intensity TW/cm² | Argon Beam Energy (MeV) (No parasitic ablation plasma loss)

Now lets correct for ablation plasma in this ablation period of $\frac{\delta tA_2}{10^{-9}} = 11.95$ ns

The second quarter ablated plasma mass expands in this time interval to a radius

$u_{ave2} := 0.7 \cdot 10^7$ $\quad rpA_2 := raA1 + \left(u_{ex}(1.5,1) - u_{ave2}\right) \cdot \delta tA_2$ $\quad rpA_2 = 0.7$ cm

and to a mass density $\rho pA_2 := \delta MaA_2 \cdot \left[\frac{4}{3} \cdot \pi \cdot \left[(rpA_2)^3 - raA1^3\right]\right]^{-1}$ $\quad \rho pA_2 = 0.029$ g/cm3

and to a rho-r $\rho rpA_{2,is} := \rho pA_2 \cdot (rpA_2 - raA1) + \rho r_{pA_{1,is}}$ $\quad \rho rpA_{2,8} = 0.0041$ g/cm^2, now ~ 50% of the ave 2nd qtr ablator range.

(Note we add ablation rho-r from the first qtr!)

Lets make a first order correction to the exhaust plasma temperature, assuming input goes both to hydro

$$\Delta EbpA_{2,is} := \left(E_{bo}\left(\rho rpA_{2,is}, \rho raA_{2,is}, \rho pA_2, \rho aA_2, 190, 29, A_b, A_t, Z_b, Z_t\right) - Ebo_{2,is}\right) \cdot \left(Ebo_{2,is}\right)^{-1}$$

and into incremental thermal energy $3\Delta T_p$, and for the moment lets assume the ablated plasma density does not change; then we have, adding the last qtr beam input to heating on top:

$$TpA_{2,is} := \frac{IdA_{2,is} \cdot \delta tA_2 \cdot \Delta EbpA_{2,is}}{\rho rpA_{2,is}} \cdot \frac{m_h}{6 \cdot e} \ldots + TpA_{1,is}$$

$T_{ex}(1.5,1) = 26.3$

$TpA_{2,is} =$	$\frac{TpA_{2,is}}{T_{ex}(1.5,1)} =$	$\Delta EbpA_{2,is} =$	$Ebo_{2,is} =$
112	4.3	0.632	$2.47 \cdot 10^8$
112	4.3	0.622	$2.5 \cdot 10^8$
113	4.3	0.594	$2.58 \cdot 10^8$
114	4.4	0.546	$2.73 \cdot 10^8$
117	4.4	0.481	$2.98 \cdot 10^8$
121	4.6	0.399	$3.38 \cdot 10^8$
130	4.9	0.301	$4.06 \cdot 10^8$
155	5.9	0.191	$5.41 \cdot 10^8$
26	1	0.922	$5.41 \cdot 10^8$

One can see in this table that the ablation plasma is substantially heated (Te increases 10X) (more in the 2nd qtr of the pulse). Check if heating (pressurization) can still cause significant enhanced expansion in the shorter transverse to the beam channel (polar axis) direction in the shorter time δtA_2:

$$vperpA_{2,is} := 10^2 \cdot \sqrt{\frac{5 \cdot \left[\left(TpA_{2,is}\right) - T_{ex}(1.5,1)\right] \cdot e}{3 \cdot m_h \cdot 10^{-3}}}$$ cm/s

$$\rho_{pA_{2,is}} := \rho pA_2 \cdot \left(\frac{TpA_{2,1}}{TpA_{2,is}}\right) \cdot \left(1 + \frac{vperpA_{2,is} \cdot \delta tA_2}{raA_2}\right)^{-2}$$

$$\rho_{pA_{2,9}} := \rho pA_2$$

and

$$\rho r_{pA_{2,is}} := \rho rpA_{2,is} \cdot \left(\frac{TpA_{2,1}}{TpA_{2,is}}\right) \cdot \left(1 + \frac{vperpA_{2,is} \cdot \delta tA_2}{raA_2}\right)^{-2}$$

$$\rho r_{pA_{2,9}} := \rho rpA_{2,9}$$

$vperpA_{2,is} =$	$\frac{vperpA_{2,is} \cdot \delta tA_2}{\delta rbA_{2,is}}$	$\frac{vperpA_{2,is} \cdot \delta tA_2}{raA_2} =$
$1.17 \cdot 10^7$	1.19	0.24
$1.17 \cdot 10^7$	1.22	0.24
$1.18 \cdot 10^7$	1.31	0.24
$1.19 \cdot 10^7$	1.48	0.24
$1.2 \cdot 10^7$	1.78	0.24
$1.23 \cdot 10^7$	2.36	0.25
$1.29 \cdot 10^7$	3.67	0.26
$1.44 \cdot 10^7$	8.71	0.29
0	0	0

The corrected incident beam energy requirement adjusted for heated ablation plasma loss is

$$EbcA_{2,is} := E_{bo}\left(\rho r_{pA_{2,is}}, \rho raA_{2,is}, \rho_{pA_{2,is}}, \rho aA_2, TpA_{2,is}, 29, A_b, A_t, Z_b, Z_t\right) \qquad EbcA_{2,9} := EbcA_{2,8}$$

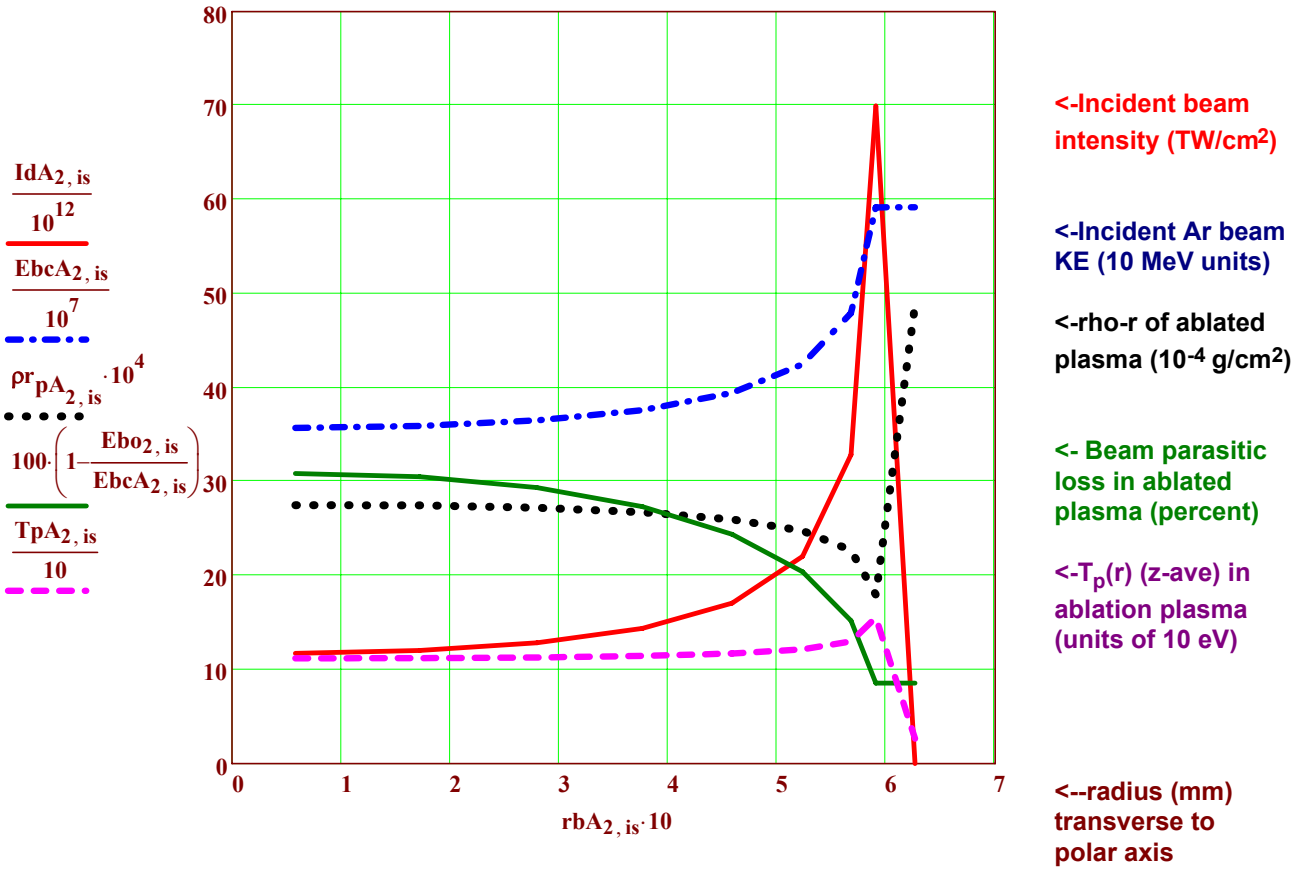

Figure 36: Plots of polar beam drive intensity (TW/cm^2, one of two sides), incident Ar beam energy (in 10 MeV units), rho-r of ablated plasma column density (10^{-4} g/cm^2 units) (dotted black line), percent beam loss in ablated plasma, and the temperature T_p of the ablation plasma (in 10 eV units), as functions of radius in the beam channel, transverse to the polar axis near the target, during the second quarter of the ablation drive pulse for the large T-lean target case A. Note beam intensity peak is now ~ 6X intensity on axis, and percent beam loss on ablated plasma is higher. Also, note the local ablation temperature ($T_p(r_b)$ has increased with the beam intensity, and a greater beam heating effect digging a hole in the density at the beam rim position, compared to the 1st quarter ablation period.

2nd qtr beam input inc loss on ablation plasma $EdcA_2 := \sum_{is=1}^{8} \left[\frac{EbcA_{2,is}}{Ebo_{2,is}} \cdot 2 \cdot \left(WdA_2 \cdot \delta VaA_{2,is} \cdot \rho aA_2\right)\right]$ $EdcA_2 = 7.91 \times 10^5$ J

Neglecting beam ablation loss $EdA_2 = 6.36 \times 10^5$ -->fractional loss $\left(EdcA_2 - EdA_2\right) \cdot \left(EdcA_2\right)^{-1} = 0.2$

Polar drive parameters for Case A, 3rd quarter of ablation drive $tA_3 := \delta tA_1 + \delta tA_2$

3rd quarter ablator mass $\delta MaA_3 = 0.023$ g $tA_3 = 9.295 \times 10^{-8}$ s @ density $\rho aA_3 := 5 \cdot \rho_{Ho}$

3rd qtr outer radius $raA2 := 0.54$ cm, δMaA_3 ablated over time interval $\delta tA_3 := 6 \cdot 10^{-9}$ s

3rd qtr inner radius $raA_3 := \left[raA2^3 - \left(\frac{3 \cdot \delta MaA_3}{4 \cdot \pi \cdot \rho aA_3} \right) \right]^{0.333}$ $raA_3 = 0.53$ $\delta raA_3 := raA2 - raA_3$

3rd qtr layer thickness $\delta raA_3 = 0.013$ cm. Radial KE/exhaust energy efficiency $\eta_{ex}(1.5, 1) = 0.61$

3rd qtr drive energy $EdA_3 := 0.385 \cdot 10^6 \cdot \eta_{ex}(1.5, 1)^{-1}$ $EdA_3 = 6.36 \times 10^5$ J. Power: $PdA_3 := EdA_3 \cdot (\delta tA_3)^{-1}$

$PdA_3 \cdot 10^{-12} = 106$ TW. 3rd qtr energy density $WdA_3 := EdA_3 \cdot (\delta MaA_3)^{-1}$ $WdA_3 = 2.77 \times 10^7$ J/g

3rd quarter ablation front pressure $WdA_3 \cdot \rho aA_3 \cdot 10^6 \cdot 2^{-1} \cdot 10^{-11} = 69$ MB $WdA_3 \cdot \frac{m_h}{10 \cdot e} = 29$ eV equiv.

3rd qtr shell volume $\delta VaA_{3,is} := 2 \cdot \pi \cdot \left(raA_3 + \frac{\delta raA_3}{2} \right)^2 \cdot \delta raA_3 \cdot \sin\left(\theta_{is} + \frac{\pi}{32} \right) \cdot \frac{\pi}{16}$ cm³

$2 \cdot \sum_{is=1}^{8} \delta VaA_{3,is} = 0.045$ cm³ $\frac{4}{3} \cdot \pi \cdot \left[(raA_3 + \delta raA_3)^3 - (raA_3)^3 \right] = 0.045$ Shell volume checks OK!

Beam convergence angle $\theta b_{is} := 0.125 \cdot \sin(\theta_{is})$ Beam-pathlength-3rd qtr $\delta zaA_{3,is} := \frac{\delta raA_3}{\cos(\theta_{is} - \theta b_{is})}$

Beam range $\rho raA_{3,is} := \rho aA_3 \cdot \delta zaA_{3,is}$ & energy $Ebo_{3,is} := E_{bf}(\rho aA_3, \rho raA_{3,is}, 0.01, 28, A_b, A_t, Z_b, Z_t)$

Incident beam radius vs polar angle θ $rbA_{3,is} := raA_3 \cdot \sin\left(\theta_{is} + \frac{\pi}{32} \right)$ $rbA_{3,9} := raA2 + \delta zaA_{3,9} \cdot \theta b_9$

Beam illumination width (cm) per θ increment $\delta rbA_{3,is} := \left(raA_3 + \frac{\delta raA_3}{2} \right) \cdot \sin\left(\theta_{is} + \frac{\pi}{16} \right) - raA_3 \cdot \sin(\theta_{is})$

Beam deposition intensity (r_b) $IdA_{3,is} := WdA_3 \cdot \delta VaA_{3,is} \cdot \rho aA_3 \cdot (\delta tA_3 \cdot 2 \cdot \pi \cdot rbA_{3,is} \cdot \delta rbA_{3,is})^{-1}$ $IdA_{3,9} := 0$

$Ebo_{3,9} := Ebo_{3,8}$

Table 17: 2-D polar drive requirements for Case A, 3rd quarter ablation period.

θ_{is} =	$rbA_{3,is}$ =	$\delta zaA_{3,is}$ =	$\rho raA_{3,is}$ =	$IdA_{3,is} \cdot 10^{-12}$ =	$Ebo_{3,is} \cdot 10^{-6}$ =
0	0.05	0.013	0.0063	29	281
0.2	0.15	0.013	0.0064	30	284
0.39	0.25	0.013	0.0067	32	294
0.59	0.33	0.014	0.0072	36	311
0.79	0.41	0.016	0.0082	43	339
0.98	0.47	0.02	0.0098	56	384
1.18	0.5	0.026	0.0129	85	460
1.37	0.52	0.04	0.02	187	610
1.57	0.55	0.1	0.0502	0	610
Polar angle (rad)	Beam radius(cm)	Shell z depth (cm)	Beam range g/cm²	Beam Intensity TW/cm²	Argon Beam Energy (MeV) (Neglect parasitic ablation plasma loss)

Now lets correct for ablation plasma in this ablation period of $\frac{\delta tA_3}{10^{-9}} = 6$ ns

The third quarter ablated plasma mass expands in this time interval to a radius

$u_{ave3} := 1.3 \cdot 10^7$ $rpA_3 := raA2 + \left(u_{ex}(1.5,1) - u_{ave3}\right) \cdot \delta tA_3$ $rpA_3 = 0.6$ cm

and to a mass density $\rho pA_3 := \delta MaA_3 \cdot \left[\frac{4}{3} \cdot \pi \cdot \left[(rpA_3)^3 - raA2^3\right]\right]^{-1}$ $\rho pA_3 = 0.185$ g/cm3

and to a rho-r $\rho rpA_{3,is} := \rho pA_3 \cdot (rpA_3 - raA2) + \rho r_{pA_{2,is}}$ $\rho rpA_{3,8} = 0.0077$ g/cm^2, now ~ 95% of the ave 3rd qtr ablator range.

(Note we add in ablation rho-r from the 2nd qtr!)

Lets make a first order correction to the exhaust plasma temperature, assuming all beam energy deposited into the ablation plasma mass within the beam channel

$$\Delta EbpA_{3,is} := \left(E_{bo}\left(\rho rpA_{3,is}, \rho raA_{3,is}, \rho pA_3, \rho aA_3, 300, 29, A_b, A_t, Z_b, Z_t\right) - Ebo_{3,is}\right) \cdot \left(Ebo_{3,is}\right)^{-1}$$

goes into incremental thermal energy $3\Delta T_p$, and for the moment lets assume the ablated plasma density does not change; then we have, adding the last qtr beam input to heating on top:

$$TpA_{3,is} := \frac{IdA_{3,is} \cdot \delta tA_3 \cdot \Delta EbpA_{3,is}}{\rho rpA_{3,is}} \cdot \frac{m_h}{6 \cdot e} \ldots + TpA_{2,is}$$

$T_{ex}(1.5,1) = 26.3$

$TpA_{3,is}$ =	$\frac{TpA_{3,is}}{T_{ex}(1.5,1)}$ =	$\Delta EbpA_{3,is}$ =	$Ebo_{3,is}$ =
143	5.4	0.873	$2.81 \cdot 10^8$
143	5.4	0.86	$2.84 \cdot 10^8$
145	5.5	0.821	$2.94 \cdot 10^8$
148	5.6	0.754	$3.11 \cdot 10^8$
152	5.8	0.662	$3.39 \cdot 10^8$
160	6.1	0.546	$3.84 \cdot 10^8$
174	6.6	0.408	$4.6 \cdot 10^8$
218	8.3	0.25	$6.1 \cdot 10^8$
26	1	0.997	$6.1 \cdot 10^8$

One can see in this table that the ablation plasma is substantially heated (Te increases 10X) (more in the 3rd qtr of the pulse). Check if heating (pressurization) can still cause significant enhanced expansion in the shorter transverse to the beam channel (polar axis) direction in the shorter time δtA_3:

$$vperpA_{3,is} := 10^2 \cdot \sqrt{\frac{5 \cdot \left[\left(TpA_{3,is}\right) - T_{ex}(1.5,1)\right] \cdot e}{3 \cdot m_h \cdot 10^{-3}}}$$ cm/s

$$\rho_{pA_{3,is}} := \rho pA_3 \cdot \left(\frac{TpA_{3,1}}{TpA_{3,is}}\right) \cdot \left(1 + \frac{vperpA_{3,is} \cdot \delta tA_3}{raA_3}\right)^{-2}$$

and $\rho_{pA_{3,9}} := \rho pA_3$

$$\rho r_{pA_{3,is}} := \rho rpA_{3,is} \cdot \left(\frac{TpA_{3,1}}{TpA_{3,is}}\right) \cdot \left(1 + \frac{vperpA_{3,is} \cdot \delta tA_3}{raA_3}\right)^{-2}$$

$\rho r_{pA_{3,9}} := \rho rpA_{3,9}$

$vperpA_{3,is}$ =	$\frac{vperpA_{3,is} \cdot \delta tA_3}{\delta rbA_{3,is}}$	$\frac{vperpA_{3,is} \cdot \delta tA_3}{raA_3}$ =
$1.36 \cdot 10^7$	0.79	0.16
$1.37 \cdot 10^7$	0.81	0.16
$1.38 \cdot 10^7$	0.87	0.16
$1.39 \cdot 10^7$	0.99	0.16
$1.42 \cdot 10^7$	1.2	0.16
$1.46 \cdot 10^7$	1.6	0.17
$1.54 \cdot 10^7$	2.55	0.17
$1.75 \cdot 10^7$	6.41	0.2
0	0	0

The corrected incident beam energy requirement adjusted for heated ablation plasma loss is

$$EbcA_{3,is} := E_{bo}\left(\rho r_{pA_{3,is}}, \rho raA_{3,is}, \rho_{pA_{3,is}}, \rho aA_3, TpA_{3,is}, 29, A_b, A_t, Z_b, Z_t\right)$$ $EbcA_{3,9} := EbcA_{3,8}$

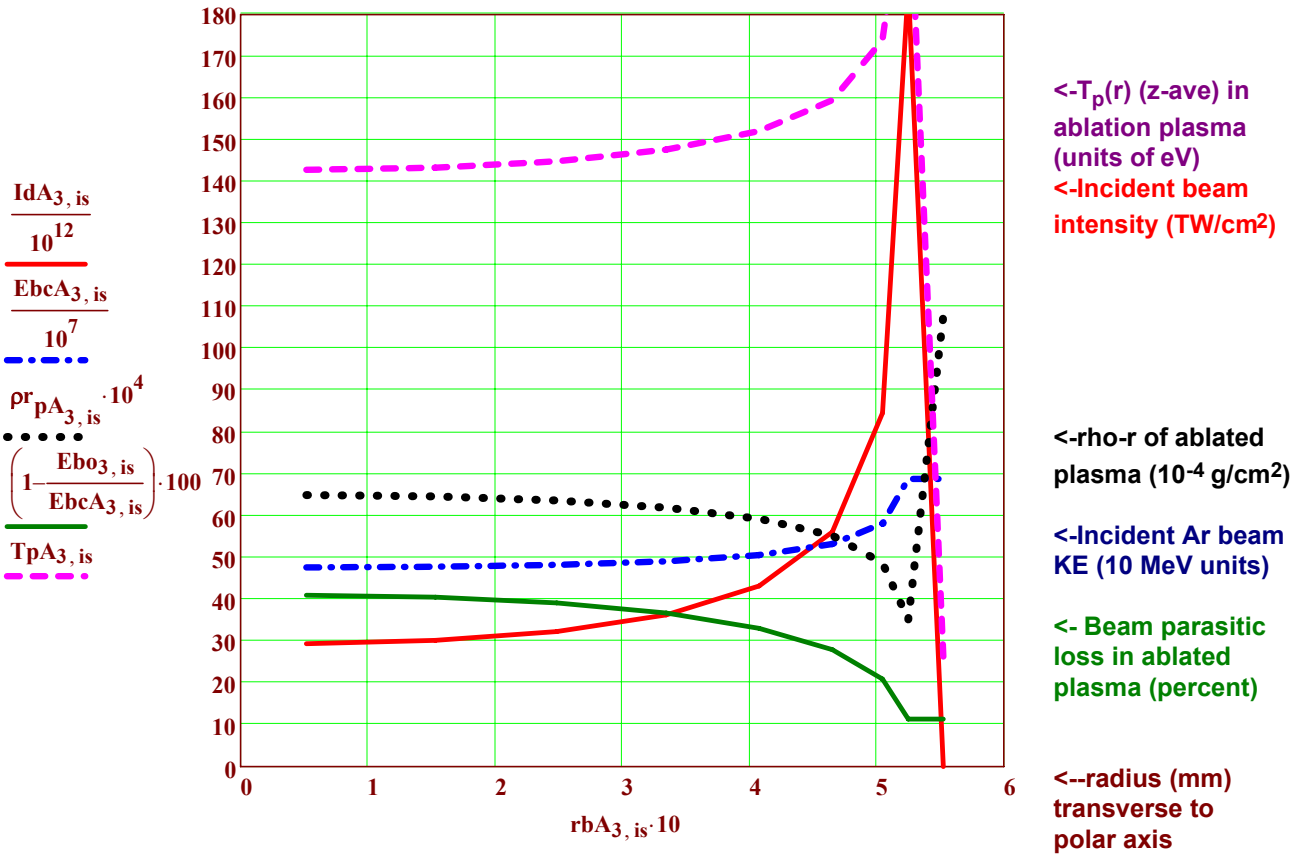

Figure 37: Plots of polar beam drive intensity (TW/cm^2, one of two sides), incident Ar beam energy (in 10 MeV units), rho-r of ablated plasma column density (10^{-4} g/cm^2 units) (dotted black line), percent beam loss in ablated plasma, and the temperature T_p of the ablation plasma (in eV units), as functions of radius in the beam channel, transverse to the polar axis near the target, during the third quarter of the ablation drive pulse for the large T-lean target case A. Note the ablation cloud rho-r is now comparable to the 3rd quarter shell rho-r, essentially doubling the required ion range on axis. However, the beam losses on ablation plasma over the whole profile, while larger than in the 2nd quarter, are greatly mitigated compared to what they would have been without taking hole-boring into account, especially because of 2-D polar drive and beam heating effects included.

3rd qtr beam input inc loss on ablation plasma $EdcA_3 := \sum_{is=1}^{8}\left[\frac{EbcA_{3,is}}{Ebo_{3,is}}\cdot 2\cdot\left(WdA_3\cdot\delta VaA_{3,is}\cdot\rho aA_3\right)\right]$ $EdcA_3 = 8.69\times 10^{5}$ J

Neglecting beam ablation loss $EdA_3 = 6.36\times 10^{5}$ -->fractional loss $\left(EdcA_3 - EdA_3\right)\cdot\left(EdcA_3\right)^{-1} = 0.27$

Polar drive parameters for Case A, 4th quarter of ablation drive $tA_4 := \delta tA_1 + \delta tA_2 + \delta tA_3$

4th quarter ablator mass $\delta MaA_4 = 0.023$ g $tA_4 = 9.9 \times 10^{-8}$ s, @ density $paA_4 := 12 \cdot \rho_{Ho}$

4th qtr outer radius $raA3 := 0.445$ cm, ablated over time interval $\delta tA_4 := 6 \cdot 10^{-9}$ s

4th qtr inner radius $raA_4 := \left[raA3^3 - \left(\frac{3 \cdot \delta MaA_4}{4 \cdot \pi \cdot paA_4} \right) \right]^{0.333}$ $raA_4 = 0.44$ $\delta raA_4 := raA3 - raA_4$

4th qtr layer thickness $\delta raA_4 = 0.007$ cm. Radial KE/exhaust energy efficiency $\eta_{ex}(1.5, 1) = 0.61$

4th qtr drive energy $EdA_4 := 0.385 \cdot 10^6 \cdot \eta_{ex}(1.5, 1)^{-1}$ $EdA_4 = 6.36 \times 10^5$ J. Power*: $PdA_4 := EdA_4 \cdot (\delta tA_4)^{-1}$

$PdA_4 \cdot 10^{-12} = 106$ TW. 4th qtr energy density $WdA_4 := EdA_4 \cdot (\delta MaA_4)^{-1}$ $WdA_4 = 2.77 \times 10^7$ J/g

4th quarter ablation front pressure $WdA_4 \cdot paA_4 \cdot 10^6 \cdot 3^{-1} \cdot 10^{-11} = 111$ MB $WdA_4 \cdot \frac{m_h}{10 \cdot e} = 29$ eV equiv.

4th qtr shell volume $\delta VaA_{4,is} := 2 \cdot \pi \cdot \left(raA_4 + \frac{\delta raA_4}{2} \right)^2 \cdot \delta raA_4 \cdot \sin\left(\theta_{is} + \frac{\pi}{32} \right) \cdot \frac{\pi}{16}$ cm³

$2 \cdot \sum_{is=1}^{8} \delta VaA_{4,is} = 0.018$ cm³ $\frac{4}{3} \cdot \pi \cdot \left[(raA_4 + \delta raA_4)^3 - (raA_4)^3 \right] = 0.018$ Shell volume checks OK!

Beam convergence angle $\theta b_{is} := 0.125 \cdot \sin(\theta_{is})$ Beam-pathlength-4th qtr $\delta zaA_{4,is} := \frac{\delta raA_4}{\cos(\theta_{is} - \theta b_{is})}$

Beam range $\rho raA_{4,is} := paA_4 \cdot \delta zaA_{4,is}$ & energy* $Ebo_{4,is} := E_{bf}(paA_4, \rho raA_{4,is}, 0.01, 29, A_b, A_t, Z_b, Z_t)$

Incident beam radius vs polar angle θ $rbA_{4,is} := raA_4 \cdot \sin\left(\theta_{is} + \frac{\pi}{32} \right)$ $rbA_{4,9} := raA3 + \delta zaA_{4,9} \cdot \theta b_9$

Beam illumination width (cm) per θ increment $\delta rbA_{4,is} := \left(raA_4 + \frac{\delta raA_4}{2} \right) \cdot \sin\left(\theta_{is} + \frac{\pi}{16} \right) - raA_4 \cdot \sin(\theta_{is})$

Beam deposition intensity (r_b) $IdA_{4,is} := WdA_4 \cdot \delta VaA_{4,is} \cdot paA_4 \cdot (\delta tA_4 \cdot 2 \cdot \pi \cdot rbA_{4,is} \cdot \delta rbA_{4,is})^{-1}$ $IdA_{4,9} := 0$

*Beam power, energy before taking beam losses into account

$Ebo_{4,9} := Ebo_{4,8}$

Table 18: 2-D polar drive requirements for Case A, 4th quarter ablation period.

θ_{is} =	$rbA_{4,is}$ =	$\delta zaA_{4,is}$ =	$\rho raA_{4,is}$ =	$IdA_{4,is} \cdot 10^{-12}$ =	$Ebo_{4,is} \cdot 10^{-6}$ =
0	0.04	0.01	0.009	42	341
0.2	0.13	0.01	0.0091	43	344
0.39	0.21	0.01	0.0095	47	355
0.59	0.28	0.01	0.0103	52	376
0.79	0.34	0.01	0.0117	63	409
0.98	0.39	0.01	0.014	82	462
1.18	0.42	0.02	0.0184	127	552
1.37	0.44	0.02	0.0286	298	730
1.57	0.45	0.06	0.072	0	730
Polar angle (rad)	Beam radius(cm)	Shell z depth (cm)	Beam range g/cm²	Beam Intensity TW/cm²	Argon Beam Energy (MeV) (No parasitic ablation plasma loss)

Now lets correct for ablation plasma in this ablation period of $\frac{\delta tA_4}{10^{-9}} = 6$ ns

The fourth quarter ablated plasma mass expands in this time interval to a radius

$u_{ave4} := 2.4 \cdot 10^7$ $rpA_4 := raA3 + \left(u_{ex}(1.5, 1) - u_{ave4}\right) \cdot \delta tA_4$ $rpA_4 = 0.4$ cm $raA4 := raA3 - u_{ave4} \cdot \delta tA_4$

and to a mass density $ppA_4 := \delta MaA_4 \cdot \left[\frac{4}{3} \cdot \pi \cdot \left[(rpA_4)^3 - raA4^3\right]\right]^{-1}$ $ppA_4 = 0.13$ g/cm3

and to a rho-r $\rho rpA_{4,is} := ppA_4 \cdot (rpA_4 - raA4) + \rho r_{pA_{3,is}}$ $\rho rpA_{4,8} = 0.018$ g/cm^2, now ~equal to the ave 4th qtr ablator range.

(Note we add ablation rho-r's accumulated up through the third qtr!)

Lets make a first order correction to the exhaust plasma temperature, assuming all beam energy deposited into the ablation plasma mass within the beam channel

$$\Delta EbpA_{4,is} := \left(E_{bo}\left(\rho rpA_{4,is}, \rho raA_{4,is}, ppA_4, \rho aA_4, 250, 29, A_b, A_t, Z_b, Z_t\right) - Ebo_{4,is}\right) \cdot \left(Ebo_{4,is}\right)^{-1}$$

goes into incremental thermal energy $3\Delta T_p$, and for the moment lets assume the ablated plasma density does not change; then we have, adding the last qtr beam input to heating on top :

$$TpA_{4,is} := \frac{IdA_{4,is} \cdot \delta tA_4 \cdot \Delta EbpA_{4,is}}{\rho rpA_{4,is}} \cdot \frac{m_h}{6 \cdot e} \ldots + TpA_{3,is}$$

$T_{ex}(1.5, 1) = 26.3$

$TpA_{4,is}$	$\frac{TpA_{4,is}}{T_{ex}(1.5,1)}$	$\Delta EbpA_{4,is}$	$Ebo_{4,is}$
172	6.5	1.381	$3.41 \cdot 10^8$
173	6.6	1.36	$3.44 \cdot 10^8$
175	6.7	1.299	$3.55 \cdot 10^8$
180	6.8	1.197	$3.76 \cdot 10^8$
186	7.1	1.055	$4.09 \cdot 10^8$
197	7.5	0.875	$4.62 \cdot 10^8$
219	8.3	0.658	$5.52 \cdot 10^8$
289	11	0.406	$7.3 \cdot 10^8$
26	1	1.141	$7.3 \cdot 10^8$

One can see in this table that the ablation plasma is substantially heated (Te increases 10-17X) (most in this 4th qtr of the pulse). Check if heating (pressurization) can still cause significant enhanced expansion in the shorter transverse to the beam channel (polar axis) direction in the shorter time δtA_4:

$$vperpA_{4,is} := 10^2 \cdot \sqrt{\frac{5 \cdot \left[(TpA_{4,is}) - T_{ex}(1.5, 1)\right] \cdot e}{3 \cdot m_h \cdot 10^{-3}}}$$ cm/s

$$\rho_{pA_{4,is}} := ppA_4 \cdot \left(\frac{TpA_{4,1}}{TpA_{4,is}}\right) \cdot \left(1 + \frac{vperpA_{4,is} \cdot \delta tA_4}{raA_4}\right)^{-2}$$

and $\rho_{pA_{4,9}} := ppA_4$

$$\rho r_{pA_{4,is}} := \rho rpA_{4,is} \cdot \left(\frac{TpA_{4,1}}{TpA_{4,is}}\right) \cdot \left(1 + \frac{vperpA_{4,is} \cdot \delta tA_4}{raA_4}\right)^{-2}$$

$\rho r_{pA_{4,9}} := \rho rpA_{4,9}$

$vperpA_{4,is}$	$\frac{vperpA_{4,is} \cdot \delta tA_4}{\delta rbA_{4,is}}$	$\frac{vperpA_{4,is} \cdot \delta tA_4}{raA_4}$
$1.52 \cdot 10^7$	1.06	0.21
$1.53 \cdot 10^7$	1.1	0.21
$1.54 \cdot 10^7$	1.19	0.21
$1.56 \cdot 10^7$	1.36	0.21
$1.6 \cdot 10^7$	1.67	0.22
$1.65 \cdot 10^7$	2.26	0.23
$1.75 \cdot 10^7$	3.69	0.24
$2.05 \cdot 10^7$	10.12	0.28
0	0	0

The corrected incident beam energy requirement adjusted for heated ablation plasma loss is

$$EbcA_{4,is} := E_{bo}\left(\rho r_{pA_{4,is}}, \rho raA_{4,is}, \rho_{pA_{4,is}}, \rho aA_4, TpA_{4,is}, 29, A_b, A_t, Z_b, Z_t\right) \qquad EbcA_{4,9} := EbcA_{4,8}$$

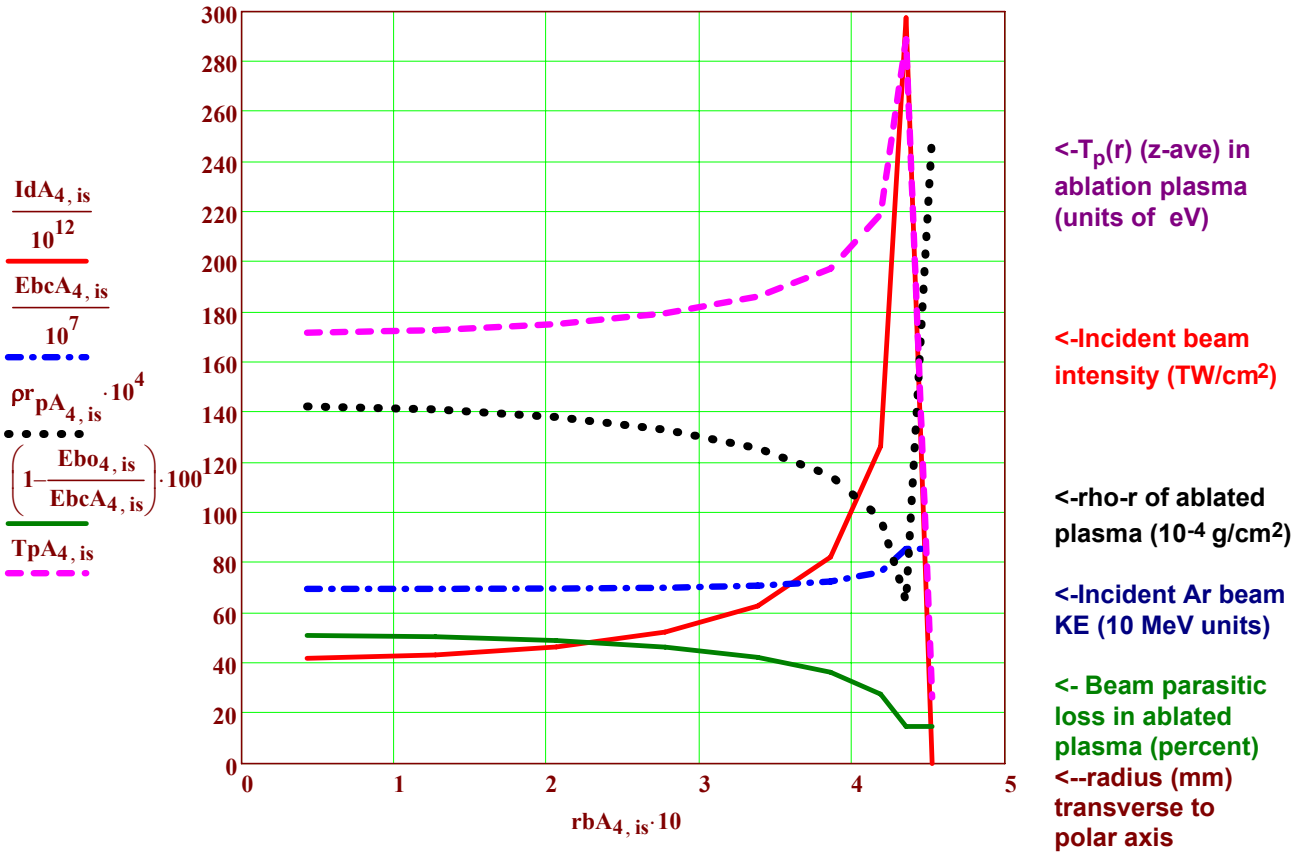

Figure 38: Plots of polar beam drive intensity (TW/cm^2, one of two sides), incident Ar beam energy (in 10 MeV units), rho-r of ablated plasma column density (10^{-4} g/cm^2 units) (dotted black line), percent beam loss in ablated plasma, and the temperature T_p of the ablation plasma (in eV units), as functions of radius in the beam channel, transverse to the polar axis near the target, during the fourth quarter of the ablation drive pulse for the large T-lean target case A.

4th qtr beam input inc loss on ablation plasma $EdcA_4 := \sum_{is=1}^{8}\left[\frac{EbcA_{4,is}}{Ebo_{4,is}}\cdot 2\cdot\left(WdA_4\cdot\delta VaA_{4,is}\cdot\rho aA_4\right)\right]$ $EdcA_4 = 9.68\times 10^5$ J

Neglecting beam ablation loss $EdA_4 = 6.36\times 10^5$ -->fractional loss $\left(EdcA_4 - EdA_4\right)\cdot\left(EdcA_4\right)^{-1} = 0.34$

$EdriveA_{tot} := \sum_{js=1}^{4} EdcA_{js}$ $EdriveA_{tot} = 3.29\times 10^6$ J

Compressed fuel energy $E_{fuelA} := 1\cdot 10^6$

Overall coupling efficiency $\eta_{dbAc} := \frac{E_{fuelA}}{EdriveA_{tot}}$ $\eta_{dbAc} = 0.304$

(a new record > three times laser direct drive (if it holds up)

This increased overall coupling efficiency of 30 % for a complete modelling of *2-D beam interaction with 2-D ablation plasma expansion*, compares to 19% estimated for spherically-symmetric beam losses on ablation plasma (page 27), or compares to 25% taking 2-D effects only in expansion of ablation plasma (page 30). The highest ablation plasma temperatures (300 eV) late in the drive pulse for the large targets (Case A) (Fig 38 above) is not high enough to cause significant range increase in for the 700 MeV Ar beams (in view of Fig. 33), so all of the improvements in coupling efficiency in 2-D is due to beam geometry and plasma expansion alone.

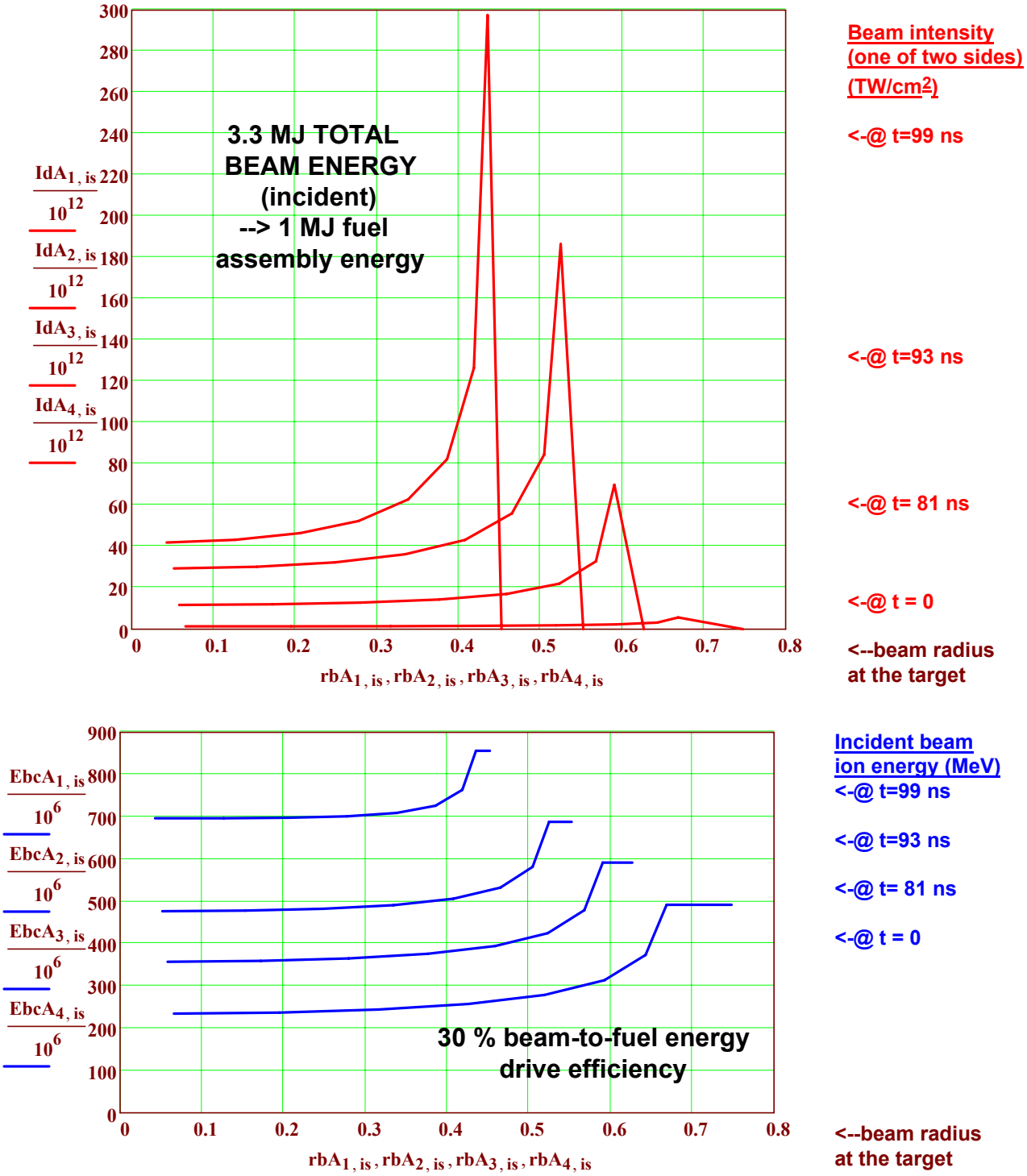

Figure 39. Beam intensity profiles (TW/cm2) (one of two sides) (red curves-top) and beam ion energies for Argon (in MeV) (blue curves-bottom) vs radius for the large Case A reactor T-Lean DD target required for symmetric polar (two sided) drive with spherically symmetric ablators, at each time the H2 ablator loses 1/4 of its initial mass. Beam losses in ablated plasma are accounted for in a 2-D model including heating Tp and "hole-boring" effects. Future work will seek use of P2 variations of ablator thickness Δra(θ) [shims] to enable time-dependent symmetry using beams with less-peaked rims.

Beam requirements for DEMO Case B implosions with polar beam illumination

We now repeat the 2-D calculations that we did for Case A for the small DEMO example (Case B).
Will more beam intensity at lower ion energies--> more range shortening (higher T_p, lower ρ_p)?

1st quarter ablator mass $\delta MaB_{js} := (16.7 - 3.3)\cdot\left(4\cdot 10^{3}\right)^{-1}$ $\delta MaB_1 = 0.003$ g, @ density $\rho aB_1 := \rho_{Ho}$

1st qtr outer radius $raB0 := 0.371$ cm, ablated over time interval $tB_1 := 0$ $\delta tB_1 := 32\cdot 10^{-9}$ s

Ist qtr inner radius $raB_1 := \left[raB0^{3} - \left(\frac{3\cdot\delta MaB_1}{4\cdot\pi\cdot\rho aB_1}\right)\right]^{0.333}$ cm $raB_1 = 0.35$ cm $\delta raB_1 := raB0 - raB_1$

1st qtr layer thickness $\delta raA_1 = 0.038$ cm. Radial KE/exhaust energy efficiency $\eta_{ex}(1.5, 0.2) = 0.63$

1st qtr drive energy $EdB_1 := 7.75\cdot 10^{4}\cdot\eta_{ex}(1.5, 0.2)^{-1}$ $EdB_1 = 1.2\times 10^{5}$ J. Power: $PdB_1 := EdB_1\cdot\left(\delta tB_1\right)^{-1}$

$PdB_1\cdot 10^{-12} = 3.87$ TW. 1st qtr energy density $WdB_1 := EdB_1\cdot\left(\delta MaB_1\right)^{-1}$ $WdB_1 = 3.7\times 10^{7}$ J/g

Ist quarter ablation front pressure $WdB_1\cdot\rho aB_1\cdot 10^{6}\cdot 2^{-1}\cdot 10^{-11} = 18.5$ MB $WdB_1\cdot\frac{m_h}{10\cdot e} = 39$ eV equiv.

1st qtr shell volume $\delta VaB_{1,is} := 2\cdot\pi\cdot\left(raB_1 + \frac{\delta raB_1}{2}\right)^{2}\cdot\delta raB_1\cdot\sin\left(\theta_{is} + \frac{\pi}{32}\right)\cdot\frac{\pi}{16}$ cm3

$2\cdot\sum_{is=1}^{8}\delta VaB_{1,is} = 0.033$ cm3 $\frac{4}{3}\cdot\pi\cdot\left[\left(raB_1 + \delta raB_1\right)^{3} - \left(raB_1\right)^{3}\right] = 0.033$ Shell volume checks OK!

Beam convergence angle $\theta b_{is} := 0.125\cdot\sin\left(\theta_{is}\right)$ Beam-pathlength-1st qtr $\delta zaB_{1,is} := \frac{\delta raB_1}{\cos\left(\theta_{is} - \theta b_{is}\right)}$

Beam range $\rho raB_{1,is} := \rho aB_1\cdot\delta zaB_{1,is}$ & energy $EbB_{1,is} := E_{bf}\left(\rho aB_1, \rho raB_{1,is}, 0.01, 39, A_b, A_t, Z_b, Z_t\right)$

Incident beam radius vs polar angle θ $rbB_{1,is} := raB_1\cdot\sin\left(\theta_{is} + \frac{\pi}{32}\right)$ $rbB_{1,9} := raB0 + \delta zaB_{1,9}\cdot\theta b_9$

Beam illumination width (cm) per θ increment $\delta rbB_{1,is} := \left(raB_1 + \frac{\delta raB_1}{2}\right)\cdot\sin\left(\theta_{is} + \frac{\pi}{16}\right) - raB_1\cdot\sin\left(\theta_{is}\right)$

Beam deposition intensity (r_b) $IdB_{1,is} := WdB_1\cdot\delta VaB_{1,is}\cdot\rho aB_1\cdot\left(\delta tB_1\cdot 2\cdot\pi\cdot rbB_{1,is}\cdot\delta rbB_{1,is}\right)^{-1}$ $IdB_{1,9} := 0$

Table 19: 2-D polar drive requirements for DEMO Case B, 1st quarter ablation period. $EbB_{1,9} := EbB_{1,8}$

θ_{is} =	$rbB_{1,is}$ =	$\delta zaB_{1,is}$ =	$\rho raB_{1,is}$ =	$IdB_{1,is}\cdot 10^{-12}$ =	$EbB_{1,is}\cdot 10^{-6}$ =
0	0.03	0.02	0.002	2.4	136
0.2	0.1	0.02	0.002	2.4	137
0.39	0.17	0.02	0.0021	2.6	142
0.59	0.22	0.02	0.0023	2.8	152
0.79	0.27	0.03	0.0026	3.3	167
0.98	0.31	0.03	0.0031	4.1	191
1.18	0.34	0.04	0.0041	5.7	233
1.37	0.35	0.06	0.0064	10.1	317
1.57	0.39	0.16	0.0161	0	317

Polar angle (rad) | Beam radius(cm) | Shell z depth (cm) | Beam range g/cm² | Beam Intensity TW/cm² | Argon Beam Energy (MeV)

$\sum_{is=1}^{8} \delta rbB1_{is} = 0.407$ cm $2\cdot \sum_{is=1}^{8} \left(WdB1\cdot \delta VaB1_{is}\cdot \rho aB1\right) = 1.2\times 10^{5}$ J-Energy Checks-OK!

$\sum_{is=1}^{8} \left[2\cdot\pi\cdot\left(rbB1_{is}\right)\cdot \delta rbB1_{is}\right] = 0.48$ cm^2 $\pi\cdot raB0^2 = 0.43$ cm^2. OK as converging beam sees > 2π

Now lets correct for ablation plasma in this ablation period of $\frac{\delta tB1}{10^{-9}} = 32$ ns

The first quarter ablated plasma mass expands in this time interval to a radius

$uimpB1 := 2.6\cdot 10^{6}$ cm/s

average expansion velocity $rpB1 := raB0 + \left(u_{ex}(1.5, 0.2) - uimpB1\right)\cdot \delta tB1$ cm $rpB1 = 0.98$ cm

and to a mass density $\rho pB1 := \delta MaB1\cdot\left[\frac{4}{3}\cdot\pi\cdot\left[\left(rpB1\right)^3 - raB0^3\right]\right]^{-1}$ $\rho pB1 = 9.1\times 10^{-4}$ g/cm3

and to a rho-r $\rho rpB1 := \rho pB1\cdot\left(rpB1 - raB0\right)$ $\rho rpB1 = 5.51\times 10^{-4}$ g/cm^2, ~8 % of the ave first quarter beam range.

Lets make a first order correction to the exhaust plasma temperature, assuming half of the incremental beam energy deposited into the ablation plasma mass within the beam channel

$\Delta EbpB1_{is} := \left(E_{bo}\left(\rho rpB1, \rho raB1_{is}, \rho pB1, \rho aB1, 150, 39, A_b, A_t, Z_b, Z_t\right) - EbB1_{is}\right)\cdot\left(EbB1_{is}\right)^{-1}$

goes into increased hydro motion (both radial and transverse), the other half into incremental thermal energy $3\Delta T_p$, and for the moment lets assume the ablated plasma density does not change; then we have

$$TpB1_{is} := \frac{IdB1_{is}\cdot \delta tB1\cdot \Delta EbpB1_{is}}{\rho rpB1}\cdot\frac{m_h}{6\cdot e} \ldots + T_{ex}(1.5, 0.2)$$

Table 20: Effects of beam heating of ablation plasma as a funtion of polar angle θ in the beam channel

$TpB1_{is}$	$\frac{TpB1_{is}}{T_{ex}(1.5,0.2)}$	$\Delta EbpB1_{is}$	$\frac{\rho raB1_{is}}{\rho rpB1}$
108	3	0.295	4
107	3	0.29	4
107	3	0.276	4
108	3	0.252	4
108	3	0.22	5
110	3	0.18	6
113	3.1	0.134	8
122	3.4	0.084	12
36	1	0.888	29

One can see in this table that the ablation plasma is substantially heated (Te increases several-fold) during the 1st qtr of the pulse.

The next question to ask is, does the heating (pressurization) cause significant enhanced expansion in the shorter transverse to the beam channel (polar axis) direction? One estimate is the fractional radial expansion of ablated plasma possible in the 1st qtr time of δtB, following eq77:

$$vperpB_{1,is} := 10^2 \cdot \sqrt{\frac{5 \cdot \left[\left(TpB_{1,is} \right) - T_{ex}(1.5, 0.2) \right] \cdot e}{3 \cdot m_h \cdot 10^{-3}}} \quad \text{cm/s}$$

Table 21: Displacement of ablated plasma by beam heating

$vperpB_{1,is}$ =	$\frac{vperpB_{1,is} \cdot \delta tB_1}{\delta rbB_{1,is}}$ =	$\frac{vperpB_{1,is} \cdot \delta tB_1}{raB0}$ =
$1.07 \cdot 10^7$	4.86	0.92
$1.07 \cdot 10^7$	4.9	0.92
$1.07 \cdot 10^7$	5.15	0.92
$1.07 \cdot 10^7$	5.67	0.92
$1.07 \cdot 10^7$	6.61	0.93
$1.08 \cdot 10^7$	8.32	0.94
$1.11 \cdot 10^7$	11.88	0.96
$1.17 \cdot 10^7$	22.31	1.01
0	0	0

Table 15 showing vperp*δt/δrb >>1 means that beam heating of ablation plasma will reach pressure equilibrium locally within the beam channel very quickly, and vperp*δt/ ra ~ 1 means significant expansion transverse to the polar axis over the whole channel, justifying allocating half the incremental beam energy input going into hydro motion. The first effect of local pressure balance means the local ablation plasma density will be depressed inversely with the local increase in beam temperature. The second effect will reduce the overall pressure withing the beam channel by roughly a factor of (1+ vperp*δt /r a)^-1 (The net T_p will stay roughly the same as beam energy dE/dx transfer as "per electron"remains rougly the same. Using "pressure balance" and channel expansion factors, the corrected ablation plasma densities and associated rho-r's are reduced by beam heating are estimated by

$$\rho pB_{1,is} := \rho pB_1 \cdot \left(\frac{TpB_{1,1}}{TpB_{1,is}} \right) \cdot \left(1 + \frac{vperpB_{1,is} \cdot \delta tB_1}{raB0} \right)^{-2} \qquad \rho pB_{1,9} := \rho pB_1$$

and $$\rho rpB_{1,is} := \rho rpB_1 \cdot \left(\frac{TpB_{1,1}}{TpB_{1,is}} \right) \cdot \left(1 + \frac{vperpB_{1,is} \cdot \delta tB_1}{raB0} \right)^{-2} \qquad \rho rpB_{1,9} := \rho rpB_1$$

We can now plot all these adjusted beam requirements versus beam radius in the next Figure 35. The corrected incident beam energy requirement adjusted for heated ablation plasma loss is

$$EbcB_{1,is} := E_{bo}\left(\rho rpB_{1,is}, \rho raB_{1,is}, \rho pB_{1,is}, \rho aB_1, TpB_{1,is}, T_{ex}(1.5, 0.2), A_b, A_t, Z_b, Z_t \right)$$

$$EbcB_{1,9} := EbcB_{1,8}$$

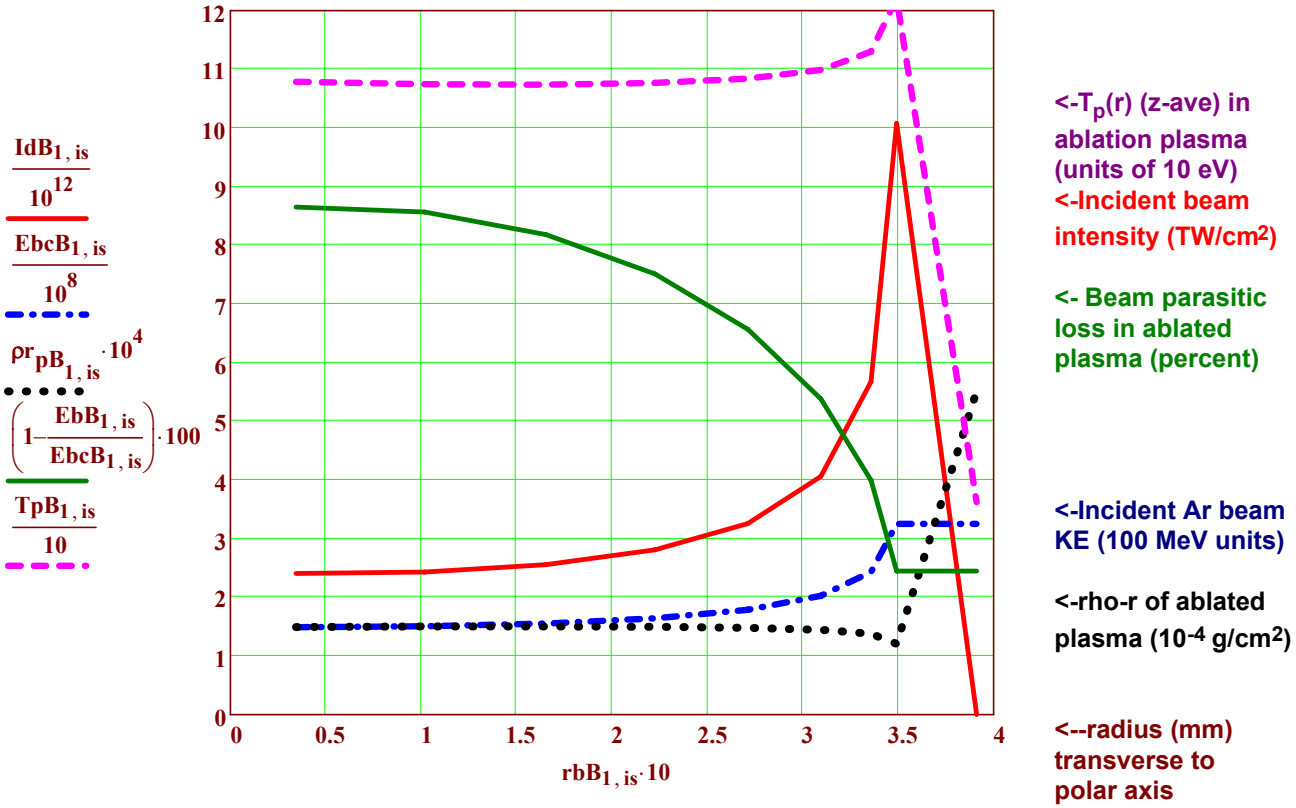

Figure 40: Plots of polar beam drive intensity (TW/cm^2, one of two sides), incident Ar beam energy (in 100 MeV units), rho-r of ablated plasma column density (10^{-4} g/cm^2 units) (dotted black line), percent beam loss in ablated plasma, and the temperature T_p of the ablation plasma(units of 10 eV), as functions of radius in the beam channel, transverse to the polar axis near the target, during the first quarter of the ablation drive pulse, (the foot part of the pulse) for the DEMO case B (see Figs 25 to 27 above for case B details). Note required beam intensity is sharply higher (peak is ~ 4X intensity on axis) in the beam channel "rim", as expected due to the polar drive geometry shown in Fig. 32. Also, note the local ablation temperature ($T_p(r_b)$ increases with the beam intensity, resulting in pressurization digging a "hole" in ablated plasma rho-r *just in the annulus through which most beam energy is delivered,* reducing parasitic beam loss. This beneficial effect will increase later in the drive.

1st qtr beam input inc loss on ablation plasma $EdcB_1 := \sum_{is=1}^{8}\left[\frac{EbcB_{1,is}}{EbB_{1,is}}\cdot 2\cdot\left(WdB_1\cdot\delta VaB_{1,is}\cdot\rho aB_1\right)\right]$ $EdcB_1 = 1.29\times 10^5$ J

Neglecting beam ablation loss $EdB_1 = 1.24\times 10^5$ -->fractional loss $\left(EdcB_1 - EdB_1\right)\cdot\left(EdcB_1\right)^{-1} = 0.04$

Fig. 40 shows a key feature of polar drive geometry-the local peaking of beam intensity and locally higher beam ion energy in the "rim" of the beam channel driving the limb of the ablator shell. This ideal beam variation provides symmetric ablation drive for a spheical implosion, but may prove difficult to achieve in practice, and so further work will explore ways to relax the locally-sharp, beam intensity "rim":
(a) Most important, add appropriate Δra (θ) capsule ablator shimming to accept a more uniform beam profile;
(b) Allow 20% low mode-P2 asymmetries at large rho-r fuel (Steve Slutz at San Ramon IFE meeting);
(c) Possibly in conjuction with (a), overdrive the foot intensity at the rim for early 5 to 20 % P2 prolate asymmetry with beam spill beyond the limb (small drive energy penalty, and then under-drive the rim later;
(d) If ignition still fails in a too-asymmetric implosion, then add a powerful late shock.

Polar drive parameters for Case B, 2nd quarter of ablation drive

2nd quarter ablator mass $\delta MaB_2 := 0.003$ $tB_2 := \delta tB_1$ $tB_2 = 3.2 \times 10^{-8}$ g, @ density $\rho aB_2 := 3 \cdot \rho_{Ho}$

2nd qtr outer radius $raB1 := 0.325$ cm, ablated over time interval $\delta tB_2 := 4.9 \cdot 10^{-9}$ s

2nd qtr inner radius $raB_2 := \left[raB1^3 - \left(\frac{3 \cdot \delta MaB_2}{4 \cdot \pi \cdot \rho aB_2} \right) \right]^{0.333}$ $raB_2 = 0.317$ $\delta raB_2 := raB1 - raB_2$

2nd qtr layer thickness $\delta raB_2 = 0.008$ cm. Radial KE/exhaust energy efficiency $\eta_{ex}(1.5, 0.2) = 0.63$

2nd qtr drive energy $EdB_2 := 7.75 \cdot 10^4 \cdot \eta_{ex}(1.5, 0.2)^{-1}$ $EdB_2 = 1.24 \times 10^5$ J. Power: $PdB_2 := EdB_2 \cdot (\delta tB_2)^{-1}$

$PdB_2 \cdot 10^{-12} = 25$ TW. 2nd qtr energy density $WdB_2 := EdB_2 \cdot (\delta MaB_2)^{-1}$ $WdB_2 = 3.69 \times 10^7$ J/g

2nd quarter ablation front pressure $WdB_2 \cdot \rho aB_2 \cdot 10^6 \cdot 2^{-1} \cdot 10^{-11} = 55.4$ MB $WdB_2 \cdot \frac{m_h}{10 \cdot e} = 39$ eV equiv.

2nd qtr shell volume $\delta VaB_{2,is} := 2 \cdot \pi \cdot \left(raB_2 + \frac{\delta raB_2}{2} \right)^2 \cdot \delta raB_2 \cdot \sin\left(\theta_{is} + \frac{\pi}{32} \right) \cdot \frac{\pi}{16}$ cm³

$2 \cdot \sum_{is=1}^{8} \delta VaB_{2,is} = 0.011$ cm³ $\frac{4}{3} \cdot \pi \cdot \left[(raB_2 + \delta raB_2)^3 - (raB_2)^3 \right] = 0.011$ Shell volume checks OK!

Beam convergence angle $\theta b_{is} := 0.125 \cdot \sin(\theta_{is})$ Beam-pathlength-2nd qtr $\delta zaB_{2,is} := \frac{\delta raB_2}{\cos(\theta_{is} - \theta b_{is})}$

Beam range $\rho raB_{2,is} := \rho aB_2 \cdot \delta zaB_{2,is}$ & energy $EbB_{2,is} := E_{bf}(\rho aB_2, \rho raB_{2,is}, 0.01, 39, A_b, A_t, Z_b, Z_t)$

Incident beam radius vs polar angle θ $rbB_{2,is} := raB_2 \cdot \sin\left(\theta_{is} + \frac{\pi}{32} \right)$ $rbB_{2,9} := raB1 + \delta zaB_{2,9} \cdot \theta b_9$

Beam illumination width (cm) per θ increment $\delta rbB_{2,is} := \left(raB_2 + \frac{\delta raB_2}{2} \right) \cdot \sin\left(\theta_{is} + \frac{\pi}{16} \right) - raB_2 \cdot \sin(\theta_{is})$

Beam deposition intensity (r_b) $IdB_{2,is} := WdB_2 \cdot \delta VaB_{2,is} \cdot \rho aB_2 \cdot (\delta tB_2 \cdot 2 \cdot \pi \cdot rbB_{2,is} \cdot \delta rbB_{2,is})^{-1}$ $IdB_{2,9} := 0$

$EbB_{2,9} := EbB_{2,8}$

Table 22: 2-D polar drive requirements for Case B, 2nd quarter ablation period.

θ_{is} =	$rbB_{2,is}$ =	$\delta zaB_{2,is}$ =	$\rho raB_{2,is}$ =	$IdB_{2,is} \cdot 10^{-12}$ =	$EbB_{2,is} \cdot 10^{-6}$ =
0	0.03	0.008	0.0025	19	147
0.2	0.09	0.008	0.0025	20	148
0.39	0.15	0.009	0.0026	21	154
0.59	0.2	0.01	0.0029	23	164
0.79	0.24	0.011	0.0032	28	180
0.98	0.28	0.013	0.0039	36	207
1.18	0.3	0.017	0.0051	54	252
1.37	0.32	0.026	0.0079	117	343
1.57	0.33	0.066	0.0199	0	343
Polar angle (rad)	Beam radius(cm)	Shell z depth (cm)	Beam range g/cm²	Beam Intensity TW/cm²	Argon Beam Energy (MeV) (No parasitic ablation plasma loss)

Now lets correct for ablation plasma in this ablation period of $\frac{\delta tB_2}{10^{-9}} = 4.9$ ns

The second quarter ablated plasma mass expands in this time interval to a radius

$u_{aveB2} := 0.8 \cdot 10^7$ $rpB_2 := raB1 + \left(u_{ex}(1.5, 0.2) - u_{aveB2}\right) \cdot \delta tB_2$ $rpB_2 = 0.4$ cm

and to a mass density $\rho pB_2 := \delta MaB_2 \cdot \left[\frac{4}{3} \cdot \pi \cdot \left[(rpB_2)^3 - raB1^3\right]\right]^{-1}$ $\rho pB_2 = 0.031$ g/cm3

and to a rho-r $\rho rpB_{2,is} := \rho pB_2 \cdot (rpB_2 - raB1) + \rho r_{pB_{1,is}}$ $\rho rpA_{2,8} = 0.0041$ g/cm^2, now ~ 80% of the ave 2nd qtr ablator range.

(Note we add ablation rho-r from the first qtr!)

Lets make a first order correction to the exhaust plasma temperature, assuming input goes both to hydro

$$\Delta EbpB_{2,is} := \left(E_{bo}(\rho rpB_{2,is}, \rho raB_{2,is}, \rho pB_2, \rho aB_2, 190, 39, A_b, A_t, Z_b, Z_t) - EbB_{2,is}\right) \cdot (EbB_{2,is})^{-1}$$

and into incremental thermal energy $3\Delta T_p$, and for the moment lets assume the ablated plasma density does not change; then we have, adding the last qtr beam input to heating on top:

$$TpB_{2,is} := \frac{IdB_{2,is} \cdot \delta tB_2 \cdot \Delta EbpB_{2,is}}{\rho rpB_{2,is}} \cdot \frac{m_h}{6 \cdot e} \ldots + TpB_{1,is}$$

$T_{ex}(1.5, 0.2) = 36.18$

$TpB_{2,is}$	$\frac{TpB_{2,is}}{T_{ex}(1.5,0.2)}$	$\Delta EbpB_{2,is}$	$Ebo_{2,is}$
163	4.5	0.751	$2.47 \cdot 10^8$
163	4.5	0.739	$2.5 \cdot 10^8$
164	4.5	0.704	$2.58 \cdot 10^8$
166	4.6	0.645	$2.73 \cdot 10^8$
169	4.7	0.565	$2.98 \cdot 10^8$
174	4.8	0.465	$3.38 \cdot 10^8$
185	5.1	0.347	$4.06 \cdot 10^8$
221	6.1	0.217	$5.41 \cdot 10^8$
36	1	1.006	$5.41 \cdot 10^8$

One can see in this table that the ablation plasma is substantially heated (Te increases 6X) (more in the 2nd qtr of the pulse). Check if heating (pressurization) can still cause significant enhanced expansion in the shorter transverse to the beam channel (polar axis) direction in the shorter time δtB_2:

$$vperpB_{2,is} := 10^2 \cdot \sqrt{\frac{5 \cdot \left[(TpB_{2,is}) - T_{ex}(1.5, 0.2)\right] \cdot e}{3 \cdot m_h \cdot 10^{-3}}}$$ cm/s

$$\rho_{pB_{2,is}} := \rho pB_2 \cdot \left(\frac{TpB_{2,1}}{TpB_{2,is}}\right) \cdot \left(1 + \frac{vperpB_{2,is} \cdot \delta tB_2}{raB_2}\right)^{-2}$$

$\rho_{pB_{2,9}} := \rho pB_2$

and

$$\rho r_{pB_{2,is}} := \rho rpB_{2,is} \cdot \left(\frac{TpB_{2,1}}{TpB_{2,is}}\right) \cdot \left(1 + \frac{vperpB_{2,is} \cdot \delta tB_2}{raB_2}\right)^{-2}$$

$\rho r_{pB_{2,9}} := \rho rpB_{2,9}$

$vperpB_{2,is}$	$\frac{vperpB_{2,is} \cdot \delta tB_2}{\delta rbB_{2,is}}$	$\frac{vperpB_{2,is} \cdot \delta tB_2}{raB_2}$
$1.42 \cdot 10^7$	1.11	0.22
$1.42 \cdot 10^7$	1.14	0.22
$1.43 \cdot 10^7$	1.23	0.22
$1.44 \cdot 10^7$	1.38	0.22
$1.46 \cdot 10^7$	1.67	0.23
$1.49 \cdot 10^7$	2.2	0.23
$1.54 \cdot 10^7$	3.43	0.24
$1.72 \cdot 10^7$	8.23	0.27
0	0	0

The corrected incident beam energy requirement adjusted for heated ablation plasma loss is

$$EbcB_{2,is} := E_{bo}\left(\rho r_{pB_{2,is}}, \rho raB_{2,is}, \rho_{pB_{2,is}}, \rho aB_2, TpB_{2,is}, 39, A_b, A_t, Z_b, Z_t\right) \qquad EbcB_{2,9} := EbcB_{2,8}$$

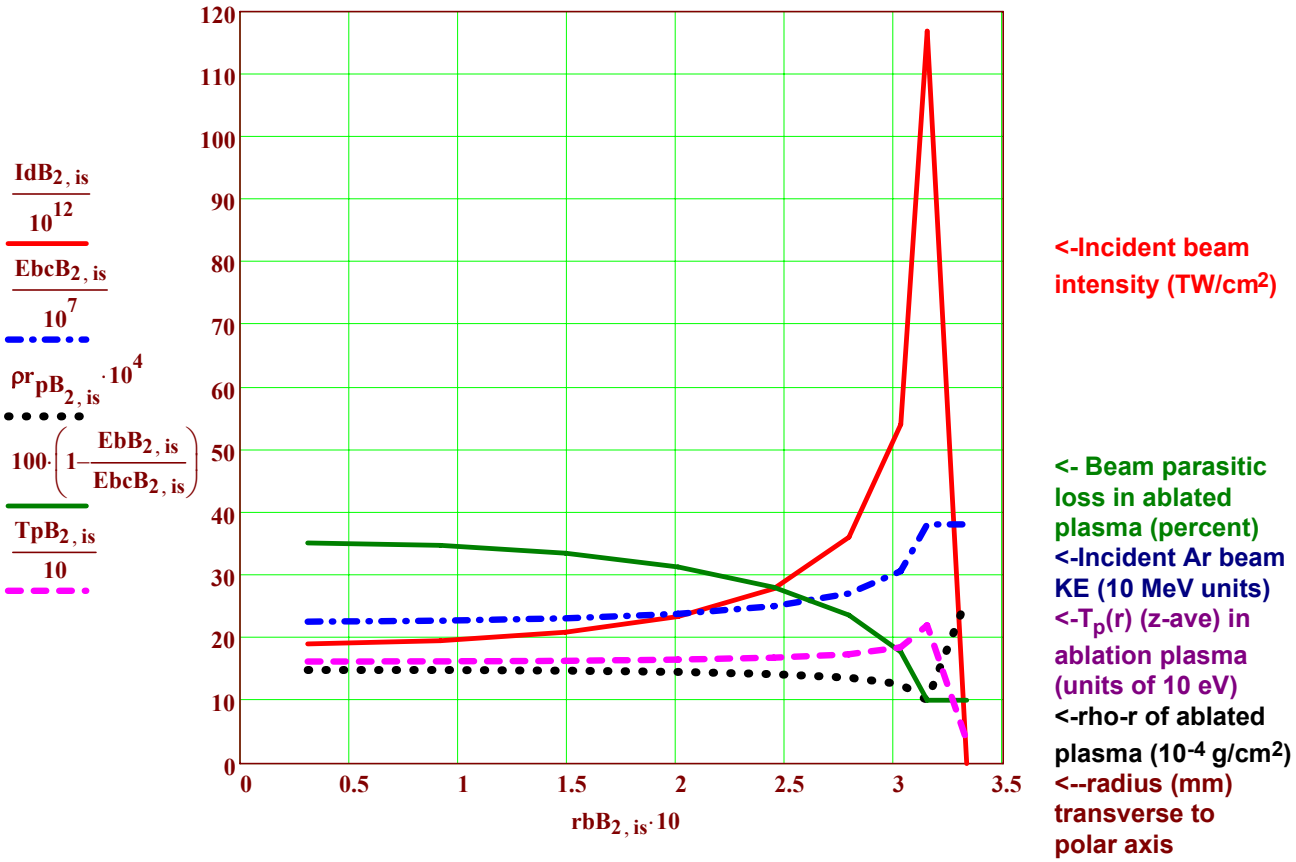

Figure 41: Plots of polar beam drive intensity (TW/cm^2, one of two sides), incident Ar beam energy (in 10 MeV units), rho-r of ablated plasma column density (10^{-4} g/cm^2 units) (dotted black line), percent beam loss in ablated plasma, and the temperature T_p of the ablation plasma (in 10 eV units), as functions of radius in the beam channel, transverse to the polar axis near the target, during the second quarter of the ablation drive pulse for the DEMO case B. Note beam intensity peak is now ~ 6X intensity on axis, and percent beam loss on ablated plasma is higher. Also, note the local ablation temperature ($T_p(r_b)$ has increased with the beam intensity, and a greater beam heating effect digging a hole in the density at the beam rim position, compared to the 1st quarter ablation period.

2nd qtr beam input inc loss on ablation plasma $EdcB_2 := \sum_{is=1}^{8} \left[\frac{EbcB_{2,is}}{EbB_{2,is}} \cdot 2 \cdot \left(WdB_2 \cdot \delta VaB_{2,is} \cdot \rho aB_2\right)\right]$ $EdcB_2 = 1.57 \times 10^5$ J

Neglecting beam ablation loss $EdB_2 = 1.24 \times 10^5$ -->fractional loss $\left(EdcB_2 - EdB_2\right) \cdot \left(EdcB_2\right)^{-1} = 0.21$

Polar drive parameters for Case B, 3rd quarter of ablation drive $tB_3 := \delta tB_1 + \delta tB_2$

3rd quarter ablator mass $\delta MaB_3 = 0.0034$ g $tB_3 = 3.69 \times 10^{-8}$ s @ density $\rho aB_3 := 5 \cdot \rho_{Ho}$

3rd qtr outer radius $raB2 := 0.296$ cm, δMaA_3 ablated over time interval $\delta tB_3 := 2.4 \cdot 10^{-9}$ s

3rd qtr inner radius $raB_3 := \left[raB2^3 - \left(\frac{3 \cdot \delta MaB_3}{4 \cdot \pi \cdot \rho aB_3} \right) \right]^{0.333}$ $raB_3 = 0.29$ $\delta raB_3 := raB2 - raB_3$

3rd qtr layer thickness $\delta raB_3 = 0.006$ cm. Radial KE/exhaust energy efficiency $\eta_{ex}(1.5, 0.2) = 0.63$

3rd qtr drive energy $EdB_3 := 7.75 \cdot 10^4 \cdot \eta_{ex}(1.5, 0.2)^{-1}$ $EdB_3 = 1.24 \times 10^5$ J. Power: $PdB_3 := EdB_3 \cdot (\delta tB_3)^{-1}$

$PdB_3 \cdot 10^{-12} = 52$ TW. 3rd qtr energy density $WdB_3 := EdB_3 \cdot (\delta MaB_3)^{-1}$ $WdB_3 = 3.69 \times 10^7$ J/g

3rd quarter ablation front pressure $WdB_3 \cdot \rho aB_3 \cdot 10^6 \cdot 2^{-1} \cdot 10^{-11} = 92$ MB $WdB_3 \cdot \frac{m_h}{10 \cdot e} = 39$ eV equiv.

3rd qtr shell volume $\delta VaB_{3,is} := 2 \cdot \pi \cdot \left(raB_3 + \frac{\delta raB_3}{2} \right)^2 \cdot \delta raB_3 \cdot \sin\left(\theta_{is} + \frac{\pi}{32} \right) \cdot \frac{\pi}{16}$ cm³

$2 \cdot \sum_{is=1}^{8} \delta VaB_{3,is} = 0.006$ cm³ $\frac{4}{3} \cdot \pi \cdot \left[(raB_3 + \delta raB_3)^3 - (raB_3)^3 \right] = 0.006$ Shell volume checks OK!

Beam convergence angle $\theta b_{is} := 0.125 \cdot \sin(\theta_{is})$ Beam-pathlength-3rd qtr $\delta zaB_{3,is} := \frac{\delta raB_3}{\cos(\theta_{is} - \theta b_{is})}$

Beam range $\rho raB_{3,is} := \rho aB_3 \cdot \delta zaB_{3,is}$ & energy $EbB_{3,is} := E_{bf}(\rho aB_3, \rho raB_{3,is}, 0.01, 38, A_b, A_t, Z_b, Z_t)$

Incident beam radius vs polar angle θ $rbB_{3,is} := raB_3 \cdot \sin\left(\theta_{is} + \frac{\pi}{32} \right)$ $rbB_{3,9} := raB2 + \delta zaB_{3,9} \cdot \theta b_9$

Beam illumination width (cm) per θ increment $\delta rbB_{3,is} := \left(raB_3 + \frac{\delta raB_3}{2} \right) \cdot \sin\left(\theta_{is} + \frac{\pi}{16} \right) - raB_3 \cdot \sin(\theta_{is})$

Beam deposition intensity (r_b) $IdB_{3,is} := WdB_3 \cdot \delta VaB_{3,is} \cdot \rho aB_3 \cdot (\delta tB_3 \cdot 2 \cdot \pi \cdot rbB_{3,is} \cdot \delta rbB_{3,is})^{-1}$ $IdB_{3,9} := 0$

$EbB_{3,9} := EbB_{3,8}$

Table 23: 2-D polar drive requirements for Case B, 3rd quarter ablation period.

θ_{is} =	$rbB_{3,is}$ =	$\delta zaB_{3,is}$ =	$\rho raB_{3,is}$ =	$IdB_{3,is} \cdot 10^{-12}$ =	$EbB_{3,is} \cdot 10^{-6}$ =
0	0.03	0.006	0.0029	46	160
0.2	0.08	0.006	0.003	47	162
0.39	0.14	0.006	0.0031	51	168
0.59	0.18	0.007	0.0034	57	179
0.79	0.22	0.008	0.0038	68	196
0.98	0.26	0.009	0.0046	89	225
1.18	0.28	0.012	0.006	135	274
1.37	0.29	0.019	0.0093	308	372
1.57	0.3	0.047	0.0235	0	372
Polar angle (rad)	Beam radius(cm)	Shell z depth (cm)	Beam range g/cm²	Beam Intensity TW/cm²	Argon Beam Energy (MeV) (Neglect parasitic ablation plasma loss)

Now lets correct for ablation plasma in this ablation period of $\frac{\delta tB_3}{10^{-9}} = 2.4$ ns

The third quarter ablated plasma mass expands in this time interval to a radius

$u_{aveB3} := 1.55 \cdot 10^7$ $\quad rpB_3 := raB2 + \left(u_{ex}(1.5, 0.2) - u_{aveB3}\right) \cdot \delta tB_3$ $\quad rpB_3 = 0.3$ cm

and to a mass density $\rho pB_3 := \delta MaB_3 \cdot \left[\frac{4}{3} \cdot \pi \cdot \left[(rpB_3)^3 - raB2^3\right]\right]^{-1}$ $\quad \rho pB_3 = 0.201$ g/cm3

and to a rho-r $\rho rpB_{3,is} := \rho pB_3 \cdot (rpB_3 - raB2) + \rho r_{pB_{2,is}}$ $\quad \rho rpB_{3,8} = 0.0039$ g/cm^2, now ~ 95% of the ave 3rd qtr ablator range.

(Note we add in ablation rho-r from the 2nd qtr!)

Lets make a first order correction to the exhaust plasma temperature, assuming all beam energy deposited into the ablation plasma mass within the beam channel

$$\Delta EbpB_{3,is} := \left(E_{bo}\left(\rho rpB_{3,is}, \rho raB_{3,is}, \rho pB_3, \rho aB_3, 200, 36, A_b, A_t, Z_b, Z_t\right) - EbB_{3,is}\right) \cdot \left(EbB_{3,is}\right)^{-1}$$

goes into incremental thermal energy $3\Delta T_p$, and for the moment lets assume the ablated plasma density does not change; then we have, adding the last qtr beam input to heating on top :

$$TpB_{3,is} := \frac{IdB_{3,is} \cdot \delta tB_3 \cdot \Delta EbpB_{3,is}}{\rho rpA_{3,is}} \cdot \frac{m_h}{6 \cdot e} \ldots + TpB_{2,is}$$

$T_{ex}(1.5, 0.2) = 36.18$

$TpA_{3,is}$	$\frac{TpB_{3,is}}{T_{ex}(1.5,1)}$	$\Delta EbpA_{3,is}$	$EbB_{3,is}$
143	7.1	0.873	$1.6 \cdot 10^8$
143	7.1	0.86	$1.62 \cdot 10^8$
145	7.2	0.821	$1.68 \cdot 10^8$
148	7.3	0.754	$1.79 \cdot 10^8$
152	7.4	0.662	$1.96 \cdot 10^8$
160	7.7	0.546	$2.25 \cdot 10^8$
174	8.3	0.408	$2.74 \cdot 10^8$
218	10.2	0.25	$3.72 \cdot 10^8$
26	1.4	0.997	$3.72 \cdot 10^8$

One can see in this table that the ablation plasma is substantially heated (Te increases 10X) (more in the 3rd qtr of the pulse). Check if heating (pressurization) can still cause significant enhanced expansion in the shorter transverse to the beam channel (polar axis) direction in the shorter time δtB_3:

$$vperpB_{3,is} := 10^2 \cdot \sqrt{\frac{5 \cdot \left[\left(TpB_{3,is}\right) - T_{ex}(1.5, 0.2)\right] \cdot e}{3 \cdot m_h \cdot 10^{-3}}}$$ cm/s

$$\rho_{pB_{3,is}} := \rho pB_3 \cdot \left(\frac{TpB_{3,1}}{TpB_{3,is}}\right) \cdot \left(1 + \frac{vperpB_{3,is} \cdot \delta tB_3}{raB_3}\right)^{-2}$$

and $\rho_{pB_{3,9}} := \rho pB_3$

$$\rho r_{pB_{3,is}} := \rho rpB_{3,is} \cdot \left(\frac{TpB_{3,1}}{TpB_{3,is}}\right) \cdot \left(1 + \frac{vperpB_{3,is} \cdot \delta tB_3}{raB_3}\right)^{-2}$$

$\rho r_{pB_{3,9}} := \rho rpB_{3,9}$

$vperpB_{3,is}$	$\frac{vperpB_{3,is} \cdot \delta tB_3}{\delta rbB_{3,is}}$	$\frac{vperpB_{3,is} \cdot \delta tB_3}{raB_3}$
$1.55 \cdot 10^7$	0.65	0.13
$1.55 \cdot 10^7$	0.67	0.13
$1.56 \cdot 10^7$	0.72	0.13
$1.57 \cdot 10^7$	0.82	0.13
$1.59 \cdot 10^7$	0.99	0.13
$1.63 \cdot 10^7$	1.33	0.14
$1.71 \cdot 10^7$	2.11	0.14
$1.93 \cdot 10^7$	5.44	0.16
0	0	0

The corrected incident beam energy requirement adjusted for heated ablation plasma loss is

$$EbcB_{3,is} := E_{bo}\left(\rho r_{pB_{3,is}}, \rho raB_{3,is}, \rho_{pB_{3,is}}, \rho aB_3, TpB_{3,is}, 36, A_b, A_t, Z_b, Z_t\right) \quad EbcB_{3,9} := EbcB_{3,8}$$

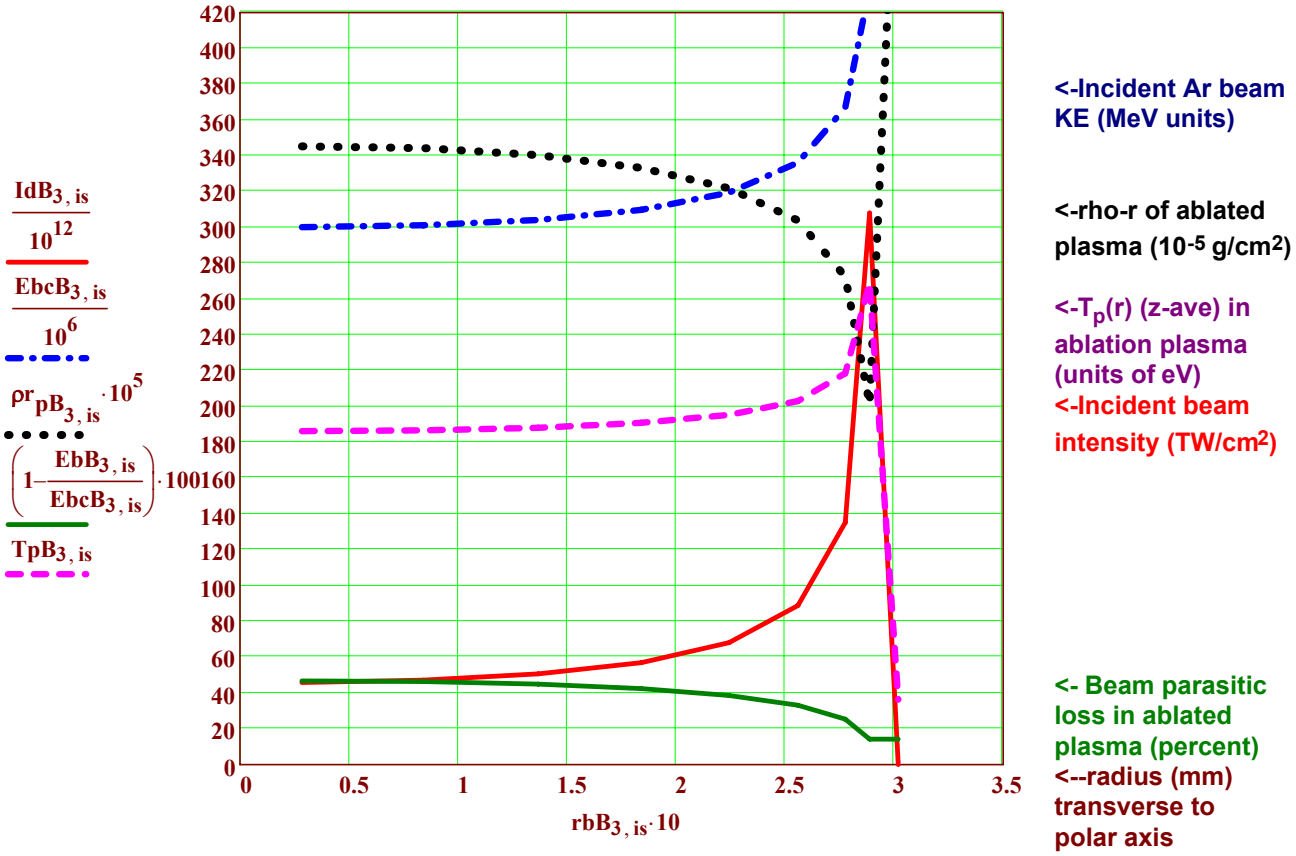

Figure 42: Plots of polar beam drive intensity (TW/cm^2, one of two sides), incident Ar beam energy (in MeV units), rho-r of ablated plasma column density (10^{-5} g/cm^2 units) (dotted black line), percent beam loss in ablated plasma, and the temperature T_p of the ablation plasma (in eV units), as functions of radius in the beam channel, transverse to the polar axis near the target, during the third quarter of the ablation drive pulse for the DEMO case B.

3rd qtr beam input inc loss on ablation plasma $EdcB3 := \sum_{is=1}^{8} \left[\frac{EbcB3_{,is}}{EbB3_{,is}} \cdot 2 \cdot \left(WdB3 \cdot \delta VaB3_{,is} \cdot \rho aB3\right)\right]$ $EdcB3 = 1.76 \times 10^{5}$ J

Neglecting beam ablation loss $EdB3 = 1.24 \times 10^{5}$ -->fractional loss $\left(EdcB3 - EdB3\right)\cdot\left(EdcB3\right)^{-1} = 0.3$

Polar drive parameters for Case B, 4th quarter of ablation drive $tB_4 := \delta tB_1 + \delta tB_2 + \delta tB_3$

4th quarter ablator mass $\delta MaB_4 = 0.003$ g $tB_4 = 3.93 \times 10^{-8}$ s, @ density $\rho aB_4 := 12 \cdot \rho_{Ho}$

4th qtr outer radius $raB3 := 0.25$ cm, ablated over time interval $\delta tB_4 := 2.4 \cdot 10^{-9}$ s

4th qtr inner radius $raB_4 := \left[raB3^3 - \left(\frac{3 \cdot \delta MaB_4}{4 \cdot \pi \cdot \rho aB_4} \right) \right]^{0.333}$ $raB_4 = 0.25$ $\delta raB_4 := raB3 - raB_4$

4th qtr layer thickness $\delta raB_4 = 0.003$ cm. Radial KE/exhaust energy efficiency $\eta_{ex}(1.5, 0.2) = 0.63$

4th qtr drive energy $EdB_4 := 7.75 \cdot 10^4 \cdot \eta_{ex}(1.5, 0.2)^{-1}$ $EdB_4 = 1.24 \times 10^5$ J. Power*: $PdB_4 := EdB_4 \cdot (\delta tB_4)^{-1}$

$PdB_4 \cdot 10^{-12} = 52$ TW. 4th qtr energy density $WdB_4 := EdB_4 \cdot (\delta MaB_4)^{-1}$ $WdB_4 = 3.69 \times 10^7$ J/g

4th quarter ablation front pressure $WdB_4 \cdot \rho aB_4 \cdot 10^6 \cdot 3^{-1} \cdot 10^{-11} = 148$ MB $WdB_4 \cdot \frac{m_h}{10 \cdot e} = 39$ eV equiv.

4th qtr shell volume $\delta VaB_{4,is} := 2 \cdot \pi \cdot \left(raB_4 + \frac{\delta raB_4}{2} \right)^2 \cdot \delta raB_4 \cdot \sin\left(\theta_{is} + \frac{\pi}{32} \right) \cdot \frac{\pi}{16}$ cm³

$2 \cdot \sum_{is=1}^{8} \delta VaB_{4,is} = 0.003$ cm³ $\frac{4}{3} \cdot \pi \cdot \left[(raB_4 + \delta raB_4)^3 - (raB_4)^3 \right] = 0.003$ Shell volume checks OK!

Beam convergence angle $\theta b_{is} := 0.125 \cdot \sin(\theta_{is})$ Beam-pathlength-4th qtr $\delta zaB_{4,is} := \frac{\delta raB_4}{\cos(\theta_{is} - \theta b_{is})}$

Beam range $\rho raB_{4,is} := \rho aB_4 \cdot \delta zaB_{4,is}$ & energy* $EbB_{4,is} := E_{bf}(\rho aB_4, \rho raB_{4,is}, 0.01, 39, A_b, A_t, Z_b, Z_t)$

Incident beam radius vs polar angle θ $rbB_{4,is} := raB_4 \cdot \sin\left(\theta_{is} + \frac{\pi}{32} \right)$ $rbB_{4,9} := raB3 + \delta zaB_{4,9} \cdot \theta b_9$

Beam illumination width (cm) per θ increment $\delta rbB_{4,is} := \left(raB_4 + \frac{\delta raB_4}{2} \right) \cdot \sin\left(\theta_{is} + \frac{\pi}{16} \right) - raB_4 \cdot \sin(\theta_{is})$

Beam deposition intensity (r_b) $IdB_{4,is} := WdB_4 \cdot \delta VaB_{4,is} \cdot \rho aB_4 \cdot (\delta tB_4 \cdot 2 \cdot \pi \cdot rbB_{4,is} \cdot \delta rbB_{4,is})^{-1}$ $IdB_{4,9} := 0$

*Beam power, energy before taking beam losses into account

$EbB_{4,9} := EbB_{4,8}$

Table 24: 2-D polar drive requirements for Case B, 4th quarter ablation period.

θ_{is} =	$rbB_{4,is}$ =	$\delta zaB_{4,is}$ =	$\rho raB_{4,is}$ =	$IdB_{4,is} \cdot 10^{-12}$ =	$EbB_{4,is} \cdot 10^{-6}$ =
0	0.02	0.003	0.0039	61	185
0.2	0.07	0.003	0.004	63	188
0.39	0.12	0.003	0.0042	68	194
0.59	0.16	0.004	0.0045	77	207
0.79	0.19	0.004	0.0051	92	227
0.98	0.22	0.005	0.0061	122	260
1.18	0.24	0.007	0.008	189	316
1.37	0.25	0.01	0.0125	464	428
1.57	0.25	0.026	0.0314	0	428
Polar angle (rad)	Beam radius(cm)	Shell z depth (cm)	Beam range g/cm²	Beam Intensity TW/cm²	Argon Beam Energy (MeV) (No parasitic ablation plasma loss)

Now lets correct for ablation plasma in this ablation period of $\frac{\delta tB_4}{10^{-9}} = 2.4$ ns

The fourth quarter ablated plasma mass expands in this time interval to a radius

$u_{aveB4} := 2.9 \cdot 10^7$ $rpB_4 := raB3 + \left(u_{ex}(1.5, 0.2) - u_{aveB4}\right) \cdot \delta tB_4$ $rpB_4 = 0.2$ cm $raB4 := raB3 - u_{aveB4} \cdot \delta tB_4$

and to a mass density $\rho pB_4 := \delta MaB_4 \cdot \left[\frac{4}{3} \cdot \pi \cdot \left[(rpB_4)^3 - raB4^3\right]\right]^{-1}$ $\rho pB_4 = 0.121$ g/cm3

and to a rho-r $\rho rpB_{4,is} := \rho pB_4 \cdot (rpB_4 - raB4) + \rho r_{pB_{3,is}}$ $\rho rpB_{4,8} = 0.008$ g/cm^2, now ~equal to the ave 4th qtr ablator range.

(Note we add ablation rho-r's accumulated up through the third qtr!)

Lets make a first order correction to the exhaust plasma temperature, assuming all beam energy deposited into the ablation plasma mass within the beam channel

$$\Delta EbpB_{4,is} := \left(E_{bo}\left(\rho rpB_{4,is}, \rho raB_{4,is}, \rho pB_4, \rho aB_4, 250, 39, A_b, A_t, Z_b, Z_t\right) - EbB_{4,is}\right) \cdot \left(EbB_{4,is}\right)^{-1}$$

goes into incremental thermal energy $3\Delta T_p$, and for the moment lets assume the ablated plasma density does not change; then we have, adding the last qtr beam input to heating on top:

$$TpB_{4,is} := \frac{IdB_{4,is} \cdot \delta tB_4 \cdot \Delta EbpB_{4,is}}{\rho rpB_{4,is}} \cdot \frac{m_h}{6 \cdot e} \ldots + TpB_{3,is}$$

$T_{ex}(1.5, 0.2) = 36.18$

Note that Tp with higher intensities with lower beam range for the DEMO Case B is still only enough for a very slight beam range increases as ve is still ~ < vbeam! (see Fig. 33)

$TpB_{4,is}$	$\frac{TpB_{4,is}}{T_{ex}(1.5,0.2)}$	$\Delta EbpB_{4,is}$	$EbB_{4,is}$
231	6.4	1.699	$1.85 \cdot 10^8$
232	6.4	1.673	$1.88 \cdot 10^8$
235	6.5	1.594	$1.94 \cdot 10^8$
240	6.6	1.463	$2.07 \cdot 10^8$
248	6.8	1.282	$2.27 \cdot 10^8$
261	7.2	1.054	$2.6 \cdot 10^8$
287	7.9	0.782	$3.16 \cdot 10^8$
379	10.5	0.47	$4.28 \cdot 10^8$
36	1	1.273	$4.28 \cdot 10^8$

One can see in this table that the ablation plasma is substantially heated (Te increases 5-8X) (most in this 4th qtr of the pulse). Check if heating (pressurization) can still cause significant enhanced expansion in the shorter transverse to the beam channel (polar axis) direction in the shorter time δtB_4:

$$vperpB_{4,is} := 10^2 \cdot \sqrt{\frac{5 \cdot \left[\left(TpB_{4,is}\right) - T_{ex}(1.5, 0.2)\right] \cdot e}{3 \cdot m_h \cdot 10^{-3}}}$$ cm/s

$$\rho_{pB_{4,is}} := \rho pB_4 \cdot \left(\frac{TpB_{4,1}}{TpB_{4,is}}\right) \cdot \left(1 + \frac{vperpB_{4,is} \cdot \delta tB_4}{raB_4}\right)^{-2}$$

and $\rho_{pB_{4,9}} := \rho pB_4$

$$\rho r_{pB_{4,is}} := \rho rpB_{4,is} \cdot \left(\frac{TpB_{4,1}}{TpB_{4,is}}\right) \cdot \left(1 + \frac{vperpB_{4,is} \cdot \delta tB_4}{raB_4}\right)^{-2}$$

$\rho r_{pB_{4,9}} := \rho rpB_{4,9}$

$vperpB_{4,is}$	$\frac{vperpB_{4,is} \cdot \delta tB_4}{\delta rbB_{4,is}}$	$\frac{vperpB_{4,is} \cdot \delta tB_4}{raB_4}$
$1.76 \cdot 10^7$	0.87	0.17
$1.77 \cdot 10^7$	0.9	0.17
$1.78 \cdot 10^7$	0.98	0.17
$1.8 \cdot 10^7$	1.12	0.18
$1.84 \cdot 10^7$	1.38	0.18
$1.89 \cdot 10^7$	1.87	0.18
$2 \cdot 10^7$	3.07	0.19
$2.34 \cdot 10^7$	8.82	0.23
0	0	0

The corrected incident beam energy requirement adjusted for heated ablation plasma loss is

$$EbcB_{4,is} := E_{bo}\left(\rho r_{pB_{4,is}}, \rho raB_{4,is}, \rho_{pB_{4,is}}, \rho aB_4, TpB_{4,is}, 39, A_b, A_t, Z_b, Z_t\right) \qquad EbcB_{4,9} := EbcB_{4,8}$$

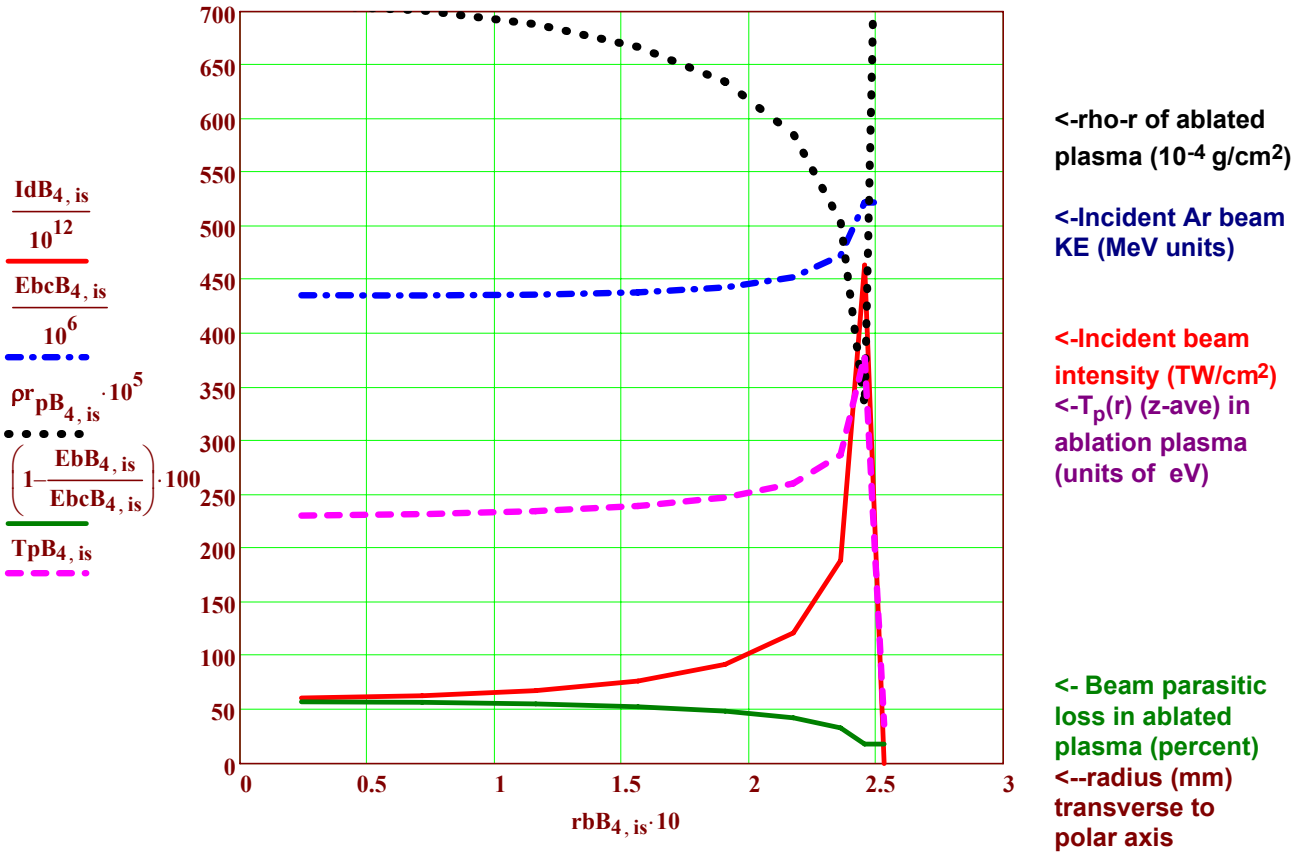

Figure 43: Plots of polar beam drive intensity (TW/cm^2, one of two sides), incident Ar beam energy (in MeV units), rho-r of ablated plasma column density (10^{-5} g/cm^2 units) (dotted black line), percent beam loss in ablated plasma, and the temperature T_p of the ablation plasma (in eV units), as functions of radius in the beam channel, transverse to the polar axis near the target, during the fourth quarter of the ablation drive pulse for the small DEMO case A.

4th qtr beam input inc loss on ablation plasma $EdcB_4 := \sum_{is=1}^{8}\left[\frac{EbcB_{4,is}}{EbB_{4,is}}\cdot 2\cdot\left(WdB_4\cdot\delta VaB_{4,is}\cdot\rho aB_4\right)\right]$ $EdcB_4 = 1.98\times 10^5$ J

Neglecting beam ablation loss $EdB_4 = 1.24\times 10^5$ -->fractional loss $\left(EdcB_4 - EdB_4\right)\cdot\left(EdcB_4\right)^{-1} = 0.37$

$EdriveB_{tot} := \sum_{js=1}^{4} EdcB_{js}$ $EdriveB_{tot} = 6.6\times 10^5$ J

Compressed fuel energy $E_{fuelB} := 2\cdot 10^5$

Overall coupling efficiency $\eta_{dfBc} := \frac{E_{fuelB}}{EdriveB_{tot}}$ $\eta_{dfBc} = 0.303$ (a record > three times laser direct drive (if it holds up)

This increased overall coupling efficiency of 30 % for a complete modelling of *2-D beam interaction with 2-D ablation plasma expansion*, compares to 24% taking 2-D effects only in expansion of ablation plasma (page 35). The highest ablation plasma temperatures (350 eV) late in the drive pulse for the large targets (Case B) (Fig 43 above) is just high enough to cause a slight beam range increase in the 450 MeV Ar beams (in view of Fig. 33), so all of the improvements in coupling efficiency in 2-D is due to beam geometry and plasma expansion alone. *However, M_o/M_f =2 leads to more range lengthening effect (next).*

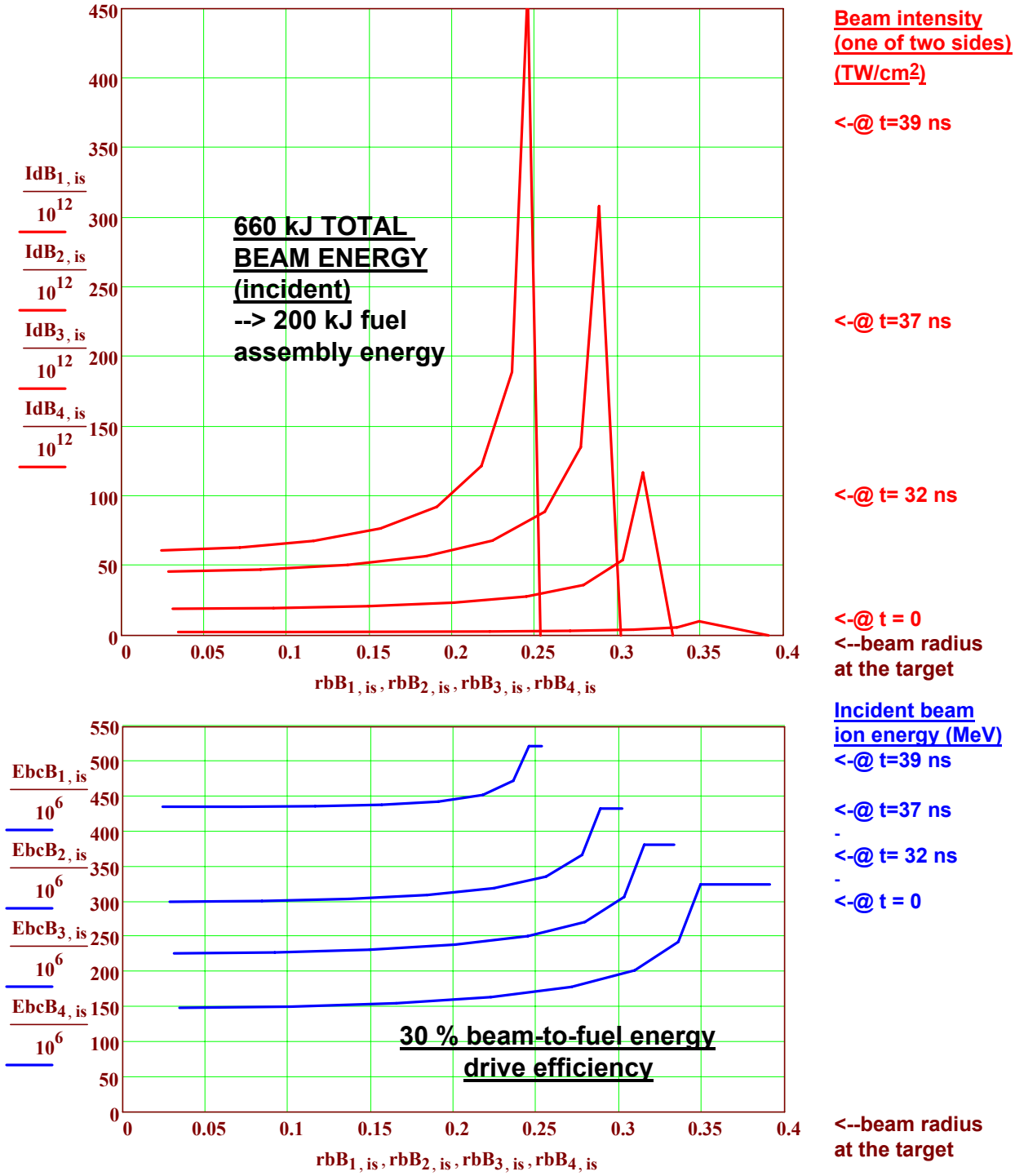

Figure 44. Beam intensity profiles (TW/cm2) (one of two sides) (red curves-top) and beam ion energies for Argon (in MeV) (blue curves-bottom) vs radius for the small Case B DEMO target, required for symmetric polar (two sided) drive with spherically symmetric ablation, at four times during the implosion when the H2 ablator mass is reduced by 1/4 . Beam losses in ablated plasma are accounted for in the 2-D model including density reductions due to heating Tp and "hole-boring" effects. Note that local reduction of abaltion plasma column density in the high intensity beam rim tends to reduce the variation in ion energy (range) between the polar axis and the rim. Future work will seek use of P2 variations of ablator thickness Δra(θ) [shims] to enable time-averaged symmetry using beam profiles with less peaked rims.

Range lengthening estimate for a lower ablator mass DEMO case.

Estimated beam range lengthening effects for the a small DEMO (Ef = 200 kJ) case, but with less ablator mass M_o/M_f = 2 (more laser like case for the small DEMO, and more like John Perkins example, except for hydrogen ablator.). Use same beam-ablation plasma interaction model model as in M_o/M_f = 5. First note that there is four times less ablator mass for the same payload mass:

$\delta MaBc := \frac{\delta MaB_4}{4}$ $\delta MaBc = 8.375 \times 10^{-4}$ g, and so there will also be

one fourth of the ablator shell range for the ion beams as before, still assuming the ion range is a quarter of the initial total ablator mass. Thus the indicent ion beam energy will be reduced to get the required 1/4 ablator range. For the same payload mass and velocity (same implosion time), and same ablator H2 mass density at each stage, a comparison of Case A for M_o/M_f =5 versus Case C for M_o/M_f =2 shows that the required incident ion beam intensity is three times higher, the shell radii are 0.81 times less, while the implosion time is half as long. Thus, roughly, we find:

$IdBc_{4,is} := 3 \cdot IdB_{4,is}$ $IdBc_{4,9} := 0$ $\delta tBc_4 := 0.5 \cdot \delta tB_4$ $rbBc_{4,is} := 0.81 \cdot rbB_{4,is}$

Beam range $\rho raBc_{4,is} := \rho aB_4 \cdot 0.25 \cdot \delta zaB_{4,is}$

Energy (not corrected yet for ablation plasma $EbBc_{4,is} := E_{bf}(\rho aB_4, \rho raBc_{4,is}, 0.01, 100, A_b, A_t, Z_b, Z_t)$ $EbBc_{4,9} := EbBc_{4,8}$

Now lets correct for ablation plasma at the ln5/ln2 faster exhaust velocity The fourth quarter ablated plasma mass expands in this time interval to a radius $\frac{\delta tBc_4}{10^{-9}} = 1.2$ ns

$u_{aveB4} := 2.9 \cdot 10^7$ $rpBc_4 := raB3 + \left(u_{ex}(1.5, 0.2) \cdot \frac{\ln(5)}{\ln(2)} - u_{aveB4}\right) \cdot \delta tBc_4$ $rpBc_4 = 0.28$ cm

$raBc4 := 0.81 \cdot raB3 - u_{aveB4} \cdot \delta tBc_4$ $raBc4 = 0.17$

and to a mass density $\rho pBc_4 := \delta MaBc \cdot \left[\frac{4}{3} \cdot \pi \cdot \left[(rpBc_4)^3 - raBc4^3\right]\right]^{-1}$ $\rho pBc_4 = 0.0124$ g/cm3

and to rho-r $\rho rpBc_{4,is} := \rho pBc_4 \cdot (rpBc_4 - raB4) + 0.25 \cdot \rho r_{pB_{3,is}}$

$\rho rpBc_{4,8} = 0.0017$ g/cm^2, ~equal to the M_o/M_f=2 4th qtr ablator.

Lets make a first order correction to the exhaust plasma temperature, assuming all beam energy deposited into the ablation plasma mass within the beam channel

$\Delta EbpBc_{4,is} := \left(E_{bo}(\rho rpBc_{4,is}, \rho raBc_{4,is}, \rho pBc_4, \rho aB_4, 500, 100, A_b, A_t, Z_b, Z_t) - EbBc_{4,is}\right) \cdot (EbBc_{4,is})^{-1}$

goes into incremental thermal energy $3\Delta T_p$, and for the moment lets assume the ablated plasma density does not change; then we have, adding the last qtr beam input to heating on top:

$TpBc_{4,is} := \frac{IdBc_{4,is} \cdot \delta tBc_4 \cdot \Delta EbpBc_{4,is}}{\rho rpBc_{4,is}} \cdot \frac{m_h}{6 \cdot e} \ldots$
$+ 3 \cdot TpB_{3,is}$

Note that Tp now with much higher intensities with lower beam range for the M_o/M_f=2 lower ablator mass DEMO Case B *is* now high enough for a substantial beam range increase as ve is now > vbeam! (see Fig. 33). Note these dimensions, masses, beam energies and times are roughly comparable to John Perkins 1 MJ example!

Table 25 Ablation plasma for M_o/M_f=2 small DEMO

$TpBc_{4,is}$ =	$\Delta EbpBc_{4,is}$ =	$EbBc_{4,is}$ =
1421	4.601	$3.32 \cdot 10^7$
1402	4.347	$3.49 \cdot 10^7$
1349	3.743	$3.97 \cdot 10^7$
1298	3.033	$4.74 \cdot 10^7$
1270	2.344	$5.86 \cdot 10^7$
1283	1.711	$7.52 \cdot 10^7$
1380	1.136	$1.02 \cdot 10^8$
1857	0.607	$1.53 \cdot 10^8$
109	1.669	$1.53 \cdot 10^8$

Corrected exhaust temperature for the Mo/Mf=2 case $Texc := T_{ex}(1.5, 0.2)\cdot\left(\frac{\ln(5)}{\ln(2)}\right)^2$ $Texc = 195$

$TpBc4_{,9} := 1.01\cdot Texc$

Check if heating (pressurization) can still cause significant enhanced expansion in the shorter transverse to the beam channel (polar axis) direction in the shorter time δtBc_4:

$$vperpBc4_{,is} := 10^2\cdot\sqrt{\frac{5\cdot(TpBc4_{,is} - Texc)\cdot e}{3\cdot m_h\cdot 10^{-3}}} \quad \text{cm/s}$$

Table 26: Ablation plasma expansion parameters for the small M_o/M_f=2 DEMO case (~ Perkins 1 MJ case)

We see in Table 26 that the ~2 x higher exhaust velocites are offest by the shorter ablation times for M_o/M_f =2, such that ablation expansion ratios are about the same as in M_o/M_f=5, even though the plasma Tp and thermal speed is much higher.

$vperpBc4_{,is}$ =	$\frac{vperpB4_{,is}\cdot\delta tBc4}{raBc4}$ =	$\frac{vperpBc4_{,is}\cdot\delta tBc4}{0.81\cdot\delta rbB4_{,is}}$ =
$4.42\cdot10^7$	0.13	1.35
$4.39\cdot10^7$	0.13	1.39
$4.29\cdot10^7$	0.13	1.46
$4.2\cdot10^7$	0.13	1.61
$4.14\cdot10^7$	0.13	1.92
$4.17\cdot10^7$	0.14	2.54
$4.35\cdot10^7$	0.14	4.12
$5.15\cdot10^7$	0.17	11.98
$1.76\cdot10^6$	0	-0.83

Now finish correcting for the rho's and rho-r's:

$$\rho_{pBc4_{,is}} := \rho pBc4\cdot\left(\frac{TpBc4_{,1}}{TpBc4_{,is}}\right)\cdot\left(1 + \frac{vperpBc4_{,is}\cdot\delta tBc4}{raBc4}\right)^{-2}$$

and $\rho_{pBc4_{,9}} := \rho pBc4$

$$\rho r_{pBc4_{,is}} := \rho rpBc4_{,is}\cdot\left(\frac{TpBc4_{,1}}{TpBc4_{,is}}\right)\cdot\left(1 + \frac{vperpBc4_{,is}\cdot\delta tBc4}{raBc4}\right)^{-2}$$

$\rho r_{pBc4_{,9}} := \rho rpBc4_{,9}$

The corrected incident beam energy requirement adjusted for heated ablation plasma loss is

$$EbcBc4_{,is} := E_{bo}\left(\rho r_{pBc4_{,is}}, \rho raBc4_{,is}, \rho_{pBc4_{,is}}, \rho aB4, TpBc4_{,is}, 100, A_b, A_t, Z_b, Z_t\right)$$

$EbcBc4_{,9} := EbcBc4_{,8}$

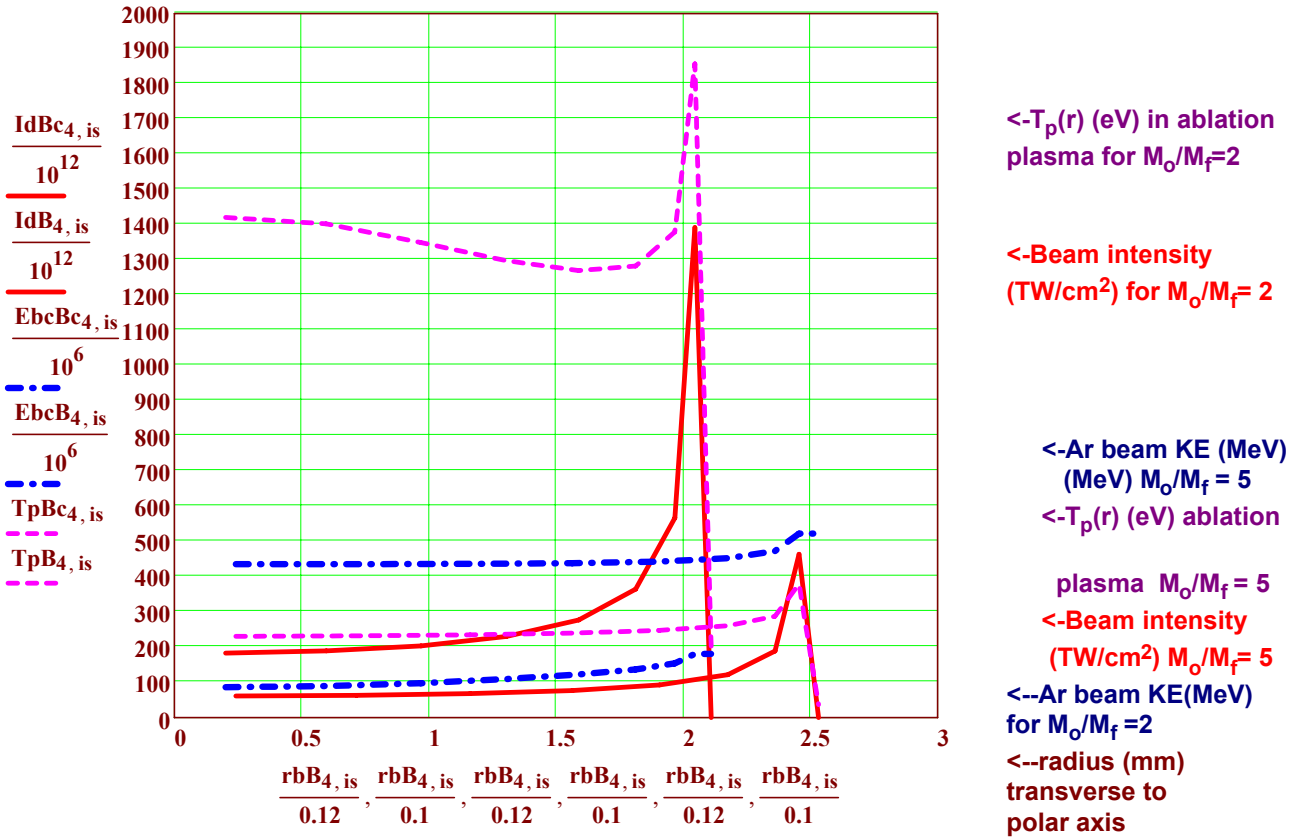

Figure 45: Comparison of polar beam drive intensity (TW/cm^2, one of two sides), incident Ar beam energy (in MeV units), , and the temperature T_p of the ablation plasma (in eV units), as functions of radius in the beam channel, transverse to the polar axis near the target, during the fourth quarter of the ablation drive pulse for the small DEMO case A, for M_o/M_f=2 out to radius 2.15 mm, compared to previous DEMO case (Fig. 43) with more H2 ablator mass for M_o/M_f=5 out to the larger radius of 2.55 mm.

$iso := 1 .. 8$

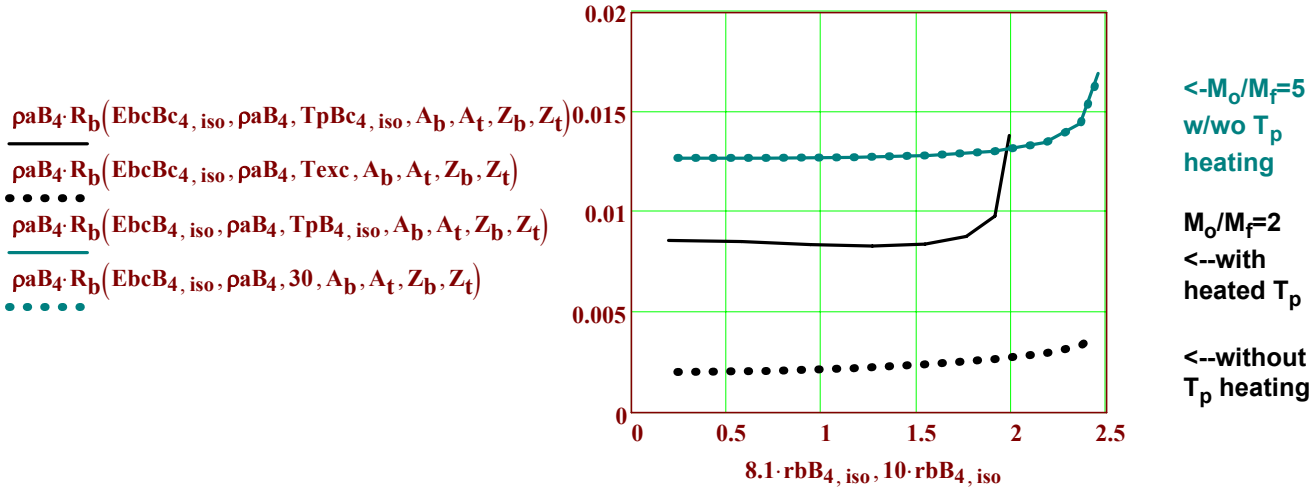

Figure 46: For the lower ablator mass case with M_o/M_f=2, closest to John Perkins 1 MJ example, beam heating vethermal > vbeam increases ion range sufficient to penetrate the lower density ablation cloud layers. John uses a fixed ion energy of 50 MeV Argon, which has even more pronounced effect on Te ("bleaching" like increase of ion range through ablation cloud heating).

Estimating incident beam perveance, assuming no plasma neutralization,

for the total incident drive beam current for Case A and Case B versus implosion time

$$Ibcur_{totA_{js}} := \sum_{is=1}^{8} \left(\frac{IdA_{js,is}}{EbcA_{js,is}} \cdot 2 \cdot \pi \cdot rbA_{js,is} \cdot \delta rbA_{js,is} \right)$$

$$Ibcur_{totB_{js}} := \sum_{is=1}^{8} \left(\frac{IdB_{js,is}}{EbcB_{js,is}} \cdot 2 \cdot \pi \cdot rbB_{js,is} \cdot \delta rbB_{js,is} \right)$$

$$I_0 := 3.1 \cdot 10^7$$

(Amps) -constant in beam perveance)

Incident beam perveance if there was no plasma neutralization of beam space charge

and if the beam charge state was $q := 1$

$$K_b(T, A, I, q) := \frac{2 \cdot q \cdot I}{A \cdot I_0 \cdot (\beta(T, A) \cdot \gamma(T, A))^3}$$

$$K_{bA_{js}} := K_b\left(\frac{EbcA_{js,7}}{q}, A_b, Ibcur_{totA_{js}}, q \right) \qquad K_{bB_{js}} := K_b\left(\frac{EbcB_{js,7}}{q}, A_b, Ibcur_{totB_{js}}, q \right)$$

Table 27: Incident beam vacuum perveances for Case A power plant and Case B DEMO examples (assuming there were no local plasma to neutralize the beam space charge).

Case A 3.3 MJ target example			Case B 660 kJ DEMO target example		
$Ibcur_{totA_{js}}$ =	$EbcA_{js,7}$ =	$K_{bA_{js}}$ =	$Ibcur_{totB_{js}}$ =	$EbcB_{js,7}$ =	$K_{bB_{js}}$ =
$1.2 \cdot 10^4$	$3.73 \cdot 10^8$	0.007	$9.4 \cdot 10^3$	$2.43 \cdot 10^8$	0.01
$6 \cdot 10^4$	$4.79 \cdot 10^8$	0.024	$4.4 \cdot 10^4$	$3.07 \cdot 10^8$	0.034
$9.5 \cdot 10^4$	$5.82 \cdot 10^8$	0.028	$7.1 \cdot 10^4$	$3.67 \cdot 10^8$	0.042
$6.8 \cdot 10^4$	$7.64 \cdot 10^8$	0.013	$5.1 \cdot 10^4$	$4.73 \cdot 10^8$	0.02
Amperes	Volts		Amperes	Volts	

Comment: vaccum perveace is a measure of how much Z distance (in beam diameter units) it takes for uncompensated beam space charge to double an iniital beam size if propagating balistically in vacuum. Typically in past heavy ion beam fusion studies, a maximum value of vacuum beam perveance of 10^{-4} was required to focus beams at all, and 10^{-5} to 10^{-6} was generally necessary to get the minimum focal spots sizes set by beam emittance (micro-divergence). The values in Table 27 are too high for vacuum focusing by more than two to three orders of magnitude, as a result of constraining the ranges for ablative direct drive. Since beam currents for fixed range and power scale as A^{-1} (and thus $K \sim A^{-2}$), one could reduce K by a factor of 10 using Xenon at the expense of higher linac voltage, length and cost, for example, but doing so would still not enable vacuum focusing. Thus, neutralized beam compression and focusing within pre-established background plasma, such as has been demonstrated in the NDCX experiment is a requirement for ablative direct drive HIF. A benefit of using such a technique with ablative direct drive is much lower linac accelerator volyage, length, and cost, and the velocity chirp used in NDCX to longitudinally compress the ion pulses in plasma give rise to a natryally increasing ion energy incident on the target, which is synergistic with the requirment we find for increasing the ion range during the imploasion to minimise parasistic beam losses through the ablation plasma corona.

Summary of main points learned so far:

1. This findings of this analytic work and first Lasnex results by John Perkins (LLNL, June 2007) indicate a *potential* for very high beam-to-compressed-fuel-energy coupling efficiencies (15 to 30%) using heavy ions in the ablative rocket regime, higher than any hohlraum or laser IFE direct drive. Like fast ignition, much more detailed work is required before this ion direct drive potential can be counted on, but results so far are sufficient to justify and guide further detailed 2-D implosion calculations needed to benchmark and refine the physics that is unique to heavy-ion coupling in ablative direct drive implosions.
2. There is likely to be a good practical middle ground between opposing constraints on ion range: the ion range cannot be too large with respect to the ablator thickness, or ability to shape drive pulses for low adiabat implosions would be lost, and the ion range cannot be too small compared to the ablator thickness, lest ablation plasma clouds late in the pulse absorb too much of the incident beam energy. A beam range = 1/4 of the initial ablator thickness, with the ion energy increasing a factor or 2 during the implosion, appears to support good performance, but more work is needed to find the optimum.
3. This analysis indicates that neutralized beam drift compression and final focusing in neutralizing background plasma such as employed in NDCX will be required for ablative direct drive HIF. because of neutralization, the velocity chirp used to compress the beam pulse must be compensated with active time dependant upstream transverse beam modulations on the 100 ns time scale, to compensate for the beam chromatic focusing errors. Such a technique is planned to be tested in NDCX by 2009. By employing such time-dependent corrections, one also gains the ability to zoom the focus on target with time, which is synergistic with the zooming implied in the two-sided direct drive geometry analyzed here.
4. Two-D Beam requirements on intensity $I_b(\theta)$ and ion energy $Eb(\theta)$ derived for symmetric implosions with desired two-sided polar drive geometry are calculated to give even higher coupling efficiencies compared to spherically symmetric beam drive because of local reductions in ablated plasma density in the beam channels (a 'hole-boring" effect which reduces parasitic beam loss on ablation plasma clouds). However, these "ideal" incident beam intensity profiles exhibit very high and narrow peaks illuminating the rim of the target ablator, which may prove difficult to deliver in practice. Use of less "rim-peaked" beam profiles implies a departure from the ideal spherically uniform ablator deposition calculated here, and that implies time-dependant asymmetries would arise.

What is most needed to be learned next:

Two-D hydro calculations for two-sided polar ion drive are needed to evaluate time-dependant asymmetry amplitudes as functions of the degree of departure of "real" beam profiles from the ideal ones calculated here. Mitigation of resulting hot spot uniformities need to be studied by controlling the time-dependent zoom of various hollow beam profiles, so as to achieve the lowest *time-averaged* asymmetry. Assuming hot spot ignition needs to be made more robust to work with the residual asymmetries found, then pursue two recovery schemes (a) increase the implosion velocity (at the expense of increased drive energy and lower gain (there is enough gain to "burn" to allow this); or (b) add a powerful late shock, as John Perkins has already found in an ion beam driven example, to "kick-start" the central burn wave.

The prize for success in this effort may be a high performance IFE target more attractive than fast ignition.